The Role of Ekman Ocean Heat Transport in the Northern Hemisphere Response to ENSO

Michael A. Alexander
NOAA/Earth System Research Laboratory, Boulder, Colorado, USA

James D. Scott
CIRES, University of Colorado, and NOAA/ Earth System Research Laboratory, Boulder, Colorado.

Submitted to the Journal of Climate December 2007
Revised April 2008

Corresponding Author
Michael Alexander
NOAA/Earth System Research Laboratory
Physical Science Division
R/PSD1
325 Broadway
Boulder, Colorado 80305
Michael.Alexander@noaa.gov

Abstract

The influence of oceanic Ekman heat transport (Q_{ek}) on air-sea variability associated with ENSO teleconnections is examined via a pair of atmospheric general circulation model (AGCM) experiments. In the "MLM" experiment, observed sea surface temperatures (SSTs) for the years 1950-1999 are specified over the tropical Pacific, while a grid of mixed layer models is coupled to the AGCM elsewhere over the global oceans. The same experimental design was used in the "EKM" experiment with the addition of Q_{ek} in the mixed layer ocean temperature equation. The ENSO signal was evaluated using differences between composites of El Niño and La Niña events averaged over the 16 ensemble members in each experiment.

In both experiments the Aleutian Low deepened and the resulting surface heat fluxes cooled the central North Pacific and warmed the northeast Pacific during boreal winter in El Niño relative to La Niña events. Including Q_{ek} amplified the ENSO-related SSTs by ~1/3 in the central and northeast North Pacific, producing anomalies comparable to those in nature. Differences between the ENSO-induced atmospheric circulation anomalies in the EKM and MLM experiments were not significant over the North Pacific. The sea level pressure (SLP) and SST response to ENSO over the Atlantic strongly projects on the North Atlantic Oscillation (NAO) and the SST tripole pattern in observations and both model experiments. The La Niña anomalies, which are stronger than during El Niño, include high pressure and positive SSTs in the central North Atlantic. Including Ekman transport enhanced the Atlantic SST anomalies, which in contrast to the Pacific, appeared to strengthen the overlying atmospheric circulation.

1. Introduction

Even though the wind-driven Ekman transport is confined to a thin surface layer in the ocean, it plays a critical role in the global heat balance. Ekman transport is responsible for a large fraction of the mean ocean heat transport within ~25º of the equator (Kraus and Levitus 1986; Levitus 1987). It is especially effective in the tropics due to the strong trade winds, low value of the Coriolis parameter and the large difference between the surface temperature and the temperature of the return flow at depth (when one considers the ocean column as a whole). The transport exhibits significant interannual and decadal variability (Adamec et al. 1993, Dong and Sutton 2001; Sato et al. 2002) where the former is tied to fluctuations in large-scale climate variability including the North Atlantic Oscillation (NAO) and El Niño/Southern Oscillation (ENSO).

In contrast to the column integrated heat budget, the greatest impact of Ekman transport (Q_{ek}) on sea surface temperature (SST) anomalies occurs in midlatitudes, where strong and variable winds coupled with large temperature gradients can generate large SST anomalies (e.g. Frankignoul and Reynolds 1983; Frankignoul 1985). The surface currents respond nearly instantaneously to the winds, and thus Ekman heat transport can influence SSTs on sub-monthly time scales. Early studies of the extratropical ocean heat budget found that Q_{ek}, and specifically the anomalous meridional advection across the mean temperature gradient, was the dominant term in the formation of seasonal midlatitude SST anomalies (Namias 1959, 1965, 1972; Jacob 1967; Adem 1970, 1975; Clark 1972). These initial studies may have overestimated the impact of Q_{ek} on SSTs as they used the value for the Ekman current at the surface, which is substantially larger

than the transport averaged over the well-mixed surface layer (Frankignoul 1985). More recent analyses suggest that while anomalous Ekman heat transport is important for interannual extratropical SST variability, its contribution is generally smaller than the forcing associated with the net surface heat fluxes (Q_{net}; Frankignoul and Reynolds 1983; Haney 1985; Luksch and von Storch 1992; Qiu 2000; Sterl and Hazeleger 2003). In midlatitudes, Q_{net} and Q_{ek} often work in tandem to create SST anomalies; stronger westerly winds enhance the upward latent and sensible heat flux and the equatorward advection of cold water by anomalous Ekman currents, thereby cooling the underlying ocean. While the large-scale patterns of SST variability are generally set by the surface fluxes, Ekman heat transport is necessary to obtain the detailed structure and correct magnitude of these patterns (Luksch 1996; Seager et al. 2000; Haarsma et al. 2005).

Under some circumstances Ekman transport may play a pivotal role in the evolution of SST anomalies. Ocean general circulation models (OGCMs) driven by observed surface observations indicate that the transition from warm to cold conditions in the central North Pacific during the winter of 1976-77 was driven in part by Ekman transport (Haney 1980; Miller et al. 1994). Seager et al. (2001) found that the post 1976 cooling due to Q_{ek} was so strong that even though the wind speed increased, the SST decreased more than the air temperature and thus Q_{net} heated the underlying ocean damping the negative SST anomaly. In addition, the associated wind stress curl changes that began in 1976 over the central Pacific created westward propagating baroclinic Rossby waves that subsequently reduced SSTs in the western Pacific Ocean about 5 years later (e.g. Deser et al. 1999; Schneider and Miller 2001; Seager et al. 2001). Following the Rossby wave

adjustment, Ekman transport enhanced this cooling to the east of Japan, reinforcing the decadal ocean signal (Seager et al. 2001; Kwon and Deser 2007).

Global atmospheric teleconnection patterns associated with SST anomalies in the tropical Pacific influence air-sea heat fluxes and Ekman transport, and thus the atmosphere acts like a "bridge" between the equatorial Pacific and much of the world's oceans during ENSO events (as reviewed by Alexander et al. 2002). In El Niño winters, the enhanced cyclonic circulation around a deepened Aleutian low results in anomalous northwesterly winds that advect relatively cold dry air over the western North Pacific, anomalous southerly winds that advect warm moist air along the west coast of North America, and enhanced surface westerlies over the central North Pacific (Fig. 1). The associated Q_{net} and Q_{ek} anomalies cool the ocean between 30ºN-50ºN west of ~150ºW and warm the ocean in the eastern ~1/3 of the North Pacific (Park et al. 2006; Liu and Alexander 2007). ENSO teleconnections also extend to the North Atlantic where the circulation around the anomalous low in the midlatitudes reduces the trade winds, warming the tropics and enhances the westerlies, which cools the ocean along the east coast of the United States (e.g. Curtis and Hastenrath 1995; Enfield and Mayer 1997; Lau and Nath 2001).

Alexander (1990) used output from an AGCM, with ENSO-related SSTs specified as boundary conditions in the tropical Pacific, to drive a variable-depth ocean mixed layer model (MLM) over the North Pacific, while Alexander (1992a) examined the coupled response of the AGCM-MLM system to ENSO. Both studies established that changes in the near surface circulation associated with El Niño induced a fairly realistic North Pacific SST anomaly pattern during boreal fall and winter. Using model experiments with

a similar design, Lau and Nath (1994, 1996, 2001) found that these bridge-induced SST anomalies could be fairly well simulated by a 50 m slab model driven by surface heat fluxes. Alexander et al. (2002), revisited this issue with a more comprehensive set of AGCM-MLM experiments and found that the ENSO-induced SST anomalies were relatively well simulated by the model, although the amplitude of the North Pacific anomalies were smaller than observed during winter. They suggested that the weaker anomalies could have resulted from the absence of dynamical ocean processes in the model. A potentially important process missing from the aforementioned studies was Ekman heat transport, although Alexander et al. (2002) computed the ENSO-driven Q_{ek} as a diagnostic, i.e. it did not influence SST in the ocean model. The diagnosed Q_{ek} values were generally in phase with Q_{net} but approximately 1/2 as large over the North Pacific Ocean in boreal winter.

Studies using AGCM-mixed layer ocean models have reached different conclusions on the impact of the bridge-related North Pacific and North Atlantic SST anomalies on the atmosphere (Alexander 1992b; Bladé 1999; Lau and Nath 1996, 2001). More recent model experiments suggest that atmosphere-ocean coupling outside of the tropical Pacific modifies the extratropical atmospheric circulation anomalies but these changes are of modest amplitude and depend on the seasonal cycle and air-sea interactions both within and beyond the Northern Hemisphere Oceans (Alexander et al., 2002).

In the Atlantic, Peng et al. (2005) found that imposed tropical SST anomalies induced an extratropical response in late winter in an AGCM coupled to a slab ocean model. The response, consisting of the NAO and the North Atlantic "SST tripole", developed one to two months later in the model than in observations. In a follow-on experiment, Peng et al.

(2006) included Ekman heat transport in the ocean model. Mutual reinforcement between the anomalous Q_{ek} and Q_{net} induced extratropical SST anomalies in early winter that were twice as strong as when no Ekman transport was included. In turn, the larger extratropical SST anomalies led to the development of an NAO response by November-December-January (NDJ). By February-March-April (FMA), the sign of the Q_{net} reversed in the Gulf Stream region so that it opposed the anomalous Q_{ek} and the magnitude of the SST and atmospheric circulation anomalies were similar in the simulations with and without Ekman forcing. Thus, the response developed more rapidly and was also more consistent with the observed evolution of the dominant patterns of atmosphere-ocean variability when Q_{ek} was included in the ocean model.

To what extent does Ekman heat transport impact the ENSO-driven SST anomalies in both the North Pacific and North Atlantic as part of the coupled atmosphere-ocean system? Does Q_{ek} alter the role of surface fluxes in the temperature tendency as suggested by the studies Seager et al. (2001) and Peng et al. (2006)? Do the Ekman-induced SST differences feedback on the atmospheric circulation? We address these questions using an AGCM with specified SSTs in the tropical Pacific and a mixed layer model over the remainder of the global oceans. Experiments are conducted with and without Ekman heat transport added to the SST equation in the ocean model. The experiment design is described in section 2. The results, including the influence of ENSO on SST and mixed layer depth (MLD) anomalies, the role of Q_{ek} and Q_{net} in generating these anomalies and the impact of ENSO plus air-sea feedback on the atmospheric circulation, is presented in section 3. The findings are summarized and discussed in section 4.

2. Experiment design

We have conducted two sets of model experiments to examine how ENSO-related Ekman heat transport anomalies influence the upper ocean, air-sea interaction and the atmospheric circulation. In both experiments, SSTs in the eastern tropical Pacific Ocean (15°S-15°N, 172°E-South American Coast) are prescribed to evolve as observed over the period 1950-1999. In the mixed layer model ("**MLM**") experiment, the ocean model is coupled to the AGCM at gridpoints in ice-free regions that are outside of the tropical east Pacific (Fig. 2). The SST is not smoothed along the boundary between the region with specified SSTs and the MLM. Sea ice is prescribed to repeat the climatological seasonal cycle and the ocean model is not active beneath the ice. The model includes local atmosphere-ocean fluxes, penetrating solar radiation and the turbulent entrainment of water into the mixed layer from below, but not mean vertical motions or horizontal processes. The temperature and salinity in all model layers are damped toward their monthly mean climatological values on a 10-year timescale to crudely represent vertically varying processes, such as the mean geostrophic heat transport, in order to retain a stable density profile.

Due to the absence of ocean currents and errors in the atmosphere and ocean model, surface heat and salt flux corrections are applied to maintain realistic seasonal cycles of SST and surface salinity. The surface heat and salt flux corrections are obtained from a 20-year MLM simulation using surface fluxes from a GFDL AGCM simulation with observed climatological SSTs as boundary conditions. Prior to each time step, the SST is set to the observed climatological value on that day. The MLM is then run for one time step where the difference between the model and observed SST is used to compute the

heat flux correction necessary for the model to match observations at each grid point. A similar method is used to obtain the salt flux correction. This procedure is repeated to obtain 20 years of daily correction values. Long-term monthly mean corrections are computed and then linearly interpolated to daily values, which are added to the temperature and salinity tendency equations. The heat flux corrections primarily compensate for the absence of ocean heat flux convergence and errors in the surface shortwave radiation (Alexander et al. 2000).

While the observed vertical structure of wind-induced currents is more complex than Ekman's original theory, the vertically integrated Ekman heat transport appears to be a more robust quantity (e.g. Weller and Plueddeman 1996). Here we assume that the Ekman heat transport is distributed over the MLD (e.g. see Frankignoul 1985) and its impact on the mixed layer temperature (or equivalently the SST) tendency is given by $Q_{ek}/(\rho C\text{MLD})$, where ρ, the density of seawater, is assumed to have a constant value of 1024.5 kgm^{-3}. The direct effect Ekman pumping on interannual mixed layer temperature, salinity and depth anomalies is generally small compared to turbulent entrainment (White et al. 1980, Frankignoul 1985, Alexander 1992a) and thus is not included here.

The Ekman transport/mixed layer model ("**EKM"**) experiment is identical to the MLM experiment except that Q_{ek} anomalies are added to the mixed layer temperature equation at most ocean model grid points (Fig. 2). Q_{ek} is not added to the ocean model at gridpoints immediately adjacent to the coast and from 6°S - 6°N to avoid singularities and to focus on the direct impact of Q_{ek} on SST rather than on Ekman-driven upwelling along the coast or the equator. The heat flux due to Ekman advection (Wm^{-2}) is computed using

$$Q_{ek} = C/f\left[-\tau_y \frac{\partial SST}{\partial x} + \tau_x \frac{\partial SST}{\partial y}\right], \quad (1)$$

where C is the specific heat capacity of seawater, f the Coriolis parameter, τ_x and τ_y are the zonal and meridional wind stress, and ∂SST/∂x and ∂SST/∂y are the zonal and meridional sea surface temperature gradients. The difference between long-term mean SST in the MLM and EKM experiments is < ±0.2ºC at nearly all model grid points. Likewise, the mean surface winds are nearly identical in the two experiments, with differences of < ±0.25 ms^{-1} at nearly all Northern Hemisphere Ocean grid points. Thus, the climatological Q_{ek} fields, derived using Eq. 1, are very similar in the two experiments.

Q_{ek} anomalies are added to the ocean model in the EKM simulations rather than the total Ekman transport so that the same flux correction could be used in the two experiments while maintaining a similar mean SST state. The Q_{ek} anomalies were obtained as follows. First daily Q_{ek} values in the MLM simulations were computed using Eq. 1. They were subsequently averaged over time and across ensemble members to form long-term monthly means. The monthly means were interpolated to daily Q_{ek} values and then subtracted from the total Ekman transport on the corresponding Julian day in the EKM simulations.

The model integrations have been performed with the GFDL R30 AGCM (Gordon and Stern 1982; Broccoli and Manabe 1992), which has an equivalent horizontal resolution of ~2.25° latitude by 3.75° longitude and 14 vertical sigma levels. The MLM consists of a grid of independent column models that include a bulk mixed layer atop a multi-layer system. The bulk model, based on the formulation of Gaspar (1988),

simulates the mixed layer temperature (equivalent to SST), salinity and depth. Beneath the mixed layer, heat is redistributed via convective overturning, vertical diffusion, and penetrating solar radiation. The bottom of each column is 1000 m or the actual depth of the ocean, which ever is shallower. For open-ocean points there are 31 levels from the surface to 1000 m with 15 layers in the upper 100 m. All layers completely within the mixed layer are set to the bulk model values. The ocean model and the method used to couple it to the R30 AGCM are described in more detail in Alexander et al. (2000).

Both experiments consist of an ensemble of sixteen 50-year simulations, where each member within an experiment is initiated from a different atmospheric state obtained from a long AGCM simulation. The results are presented for the difference between the ensemble average of the MLM and EKM simulations, and the spread among the members is used to assess statistical significance based on the t-test. The findings are presented using composite analyses (e.g. Rasmusson and Carpenter 1982, Harrison and Larkin 1998), which are constructed based on 9 El Niño (warm) events beginning in: 1957, 1965, 1969, 1972, 1976, 1982, 1987, 1991 and 1997 and 9 La Niña (cold) events: 1950, 1954, 1955, 1964, 1970, 1973, 1975, 1988 and 1998. The first 8 El Niño and La Niña events were identified by Trenberth (1997), to which we added the 1997 El Niño and 1998 La Niña events. The year in which ENSO peaks and the following year are designated by (0) and (1), respectively.

We originally planned to use the MLM simulations described in Alexander et al. (2002), which were performed on the GFDL computer system. However, the model's climate was altered when the AGCM was integrated on Earth System Research Laboratory (ESRL) computers, where we performed the EKM simulations. Even after

extensive diagnostic tests the cause of this divergence in climates was unclear, although it was likely due to differences in the compilers.[1] Thus, the MLM simulations used here were performed on ESRL computers, so that differences between the EKM and MLM experiments isolated the impact of Ekman heat transport. The mean differences between the GFDL and ESRL MLM simulations were strongest in high latitudes in the stratosphere, where the latter had a cold bias. The difference between the two systems for ENSO composites reached a maximum of ~20 m at 500 mb, approximately 20% of the overall response to tropical SST anomalies. The Aleutian low was deeper in the ESRL simulations in better agreement with observations.

Several of the model fields are compared to those obtained from the National Center for Environmental Prediction (NCEP) reanalysis (Kalnay et al. 1996; Kistler et al. 2001). Some ("A") variables, such as SLP or geopotential heights, are closer to the true state, than other ("C"), such as the surface wind stress or heat flux, which have greater dependence on the model used in the reanalysis system. The reanalysis and other data-based fields presented here have been interpolated to the R30 AGCM grid.

3. Results

a. SST and MLD

We primarily focus on the atmospheric bridge to the Northern Hemisphere Oceans during boreal winter when the impact of Ekman transport in the model is the most robust. Composite El Niño – La Niña differences, also referred to as anomalies, are indicted by a

[1] The simulations conducted at GFDL were performed on a CRAY computer which is no longer in operation and whose complier was specific to that system. Thus, it was not possible to run the EKM experiments at GFDL or port the CRAY compiler to ESRL's computer systems.

, while the ENSO anomalies in the EKM minus MLM experiments are denoted by a Δ. The SST (°C) composite during January-February-March (JFM) in the year after ENSO peaks (Yr 1) for observations (Smith et al. 1996) and the EKM and MLM experiments are shown in Fig. 3. The observed atmospheric bridge includes negative SST* in the central North Pacific and positive SST* along the coast of North America, both of which exceed 1°C in magnitude. In the Atlantic, negative anomalies on the order of 0.5-1.0°C occur in the Gulf of Mexico and along the east coast of the United States, while positive anomalies of this magnitude are located in the tropics north of the equator. Warming also occurs across the Indian Ocean. Many of these anomalies are well simulated in both the EKM and MLM, although the model values are less than observed along the west coast of the United States, over portions of the Atlantic, and in the equatorial Indian Ocean.

Including Ekman heat transport (diagnosed from the difference between the EKM and MLM experiments) alters the amplitude of several bridge-generated SST signals (Fig. 3d), which generally improves the simulation of SST anomalies over the Northern Hemisphere Oceans. The largest change occurs in the central North Pacific, where including Q_{ek} results in ΔSST of ~-0.4°C, leading to SST* < -1.0°C in the EKM experiment (Fig. 3b), similar to the observed signal (Fig. 3a). Including Q_{ek} further warms the ocean around 45°N in the eastern North Pacific and near 10°N, 150°E. In the Atlantic, the ΔSST field resembles the SST tripole pattern (e.g. Cayan 1992; Venzke et al. 1999; Sutton et al. 2001) with negative values east of Florida flanked by positive values near 15°N and 55°N. The magnitude of these changes reach 0.2°-0.3°C for JFM(1) and amplify the warm ENSO-related SST anomalies in the tropical Atlantic, increase the amplitude and eastward extent of the cold SSTs along the east coast of the United States,

and create small positive anomalies in the subarctic Atlantic where the overall bridge signal is weak. The ΔSST is positive (negative) in the northern (southern) Indian Ocean but of modest amplitude (~ 0.1°C).

The mixed layer depth anomalies (m) during JFM(1) from observations (White 1995), the EKM and MLM experiments and ΔMLD are shown in Fig. 4. The observed MLD, obtained from the Joint Environmental Data Analysis Center (JEDAC 2008), is defined as the depth at which the temperature is 1.0°C cooler than at the surface based on bathythermograph (BT) temperature measurements for the years 1956-1999. The MLD was not estimated by JEDAC at high latitudes where it is primarily controlled by salinity. The MLD in the MLM is computed explicitly from the turbulent kinetic energy equation and depends on both temperature and salinity (see Alexander et al. 2000). Both the EKM and MLM simulations reproduce the general pattern of the observed ENSO-related anomalies with positive values in the central North Pacific ringed by negative values. The maximum MLD*, on the order of 50 m in both experiments, is just slightly less than observed. The model underestimates the MLD* shoaling in the northeast Pacific, although the observed anomalies are likely to be overestimated, since salinity and vertical movements of the halocline, not measured by BTs, regulate MLD in the Gulf of Alaska (Whitney and Freeland 1999; Alexander et al. 2008). Including Q_{ek} increases the MLD* by ~10 m near 30°N, 170°W (significant at the 99% level; Fig. 4d), which enhances the southern portion of the bridge-related signal in the central Pacific.

In the North Atlantic, the mixed layer is observed to be shallower during El Niño than La Niña events (MLD*< 0) in southeast portion of the domain and deeper in midlatitudes, with the separation between the two extending diagonally across the basin

from Florida to Spain (Fig. 4a). This structure is better represented in the EKM than in the MLM simulations, due to the positive ΔMLD located at ~35°N, 70°W, but the MLD anomalies are still much smaller than in observations. The MLD* shoals in the northern North Atlantic in both experiments, but the anomalies have significantly greater amplitude in the EKM experiment. The model and observations also differ in the northeast portion of the basin but it is unclear whether this is due to model error, variability in this region not associated with ENSO, or the difficulty in estimating MLD from BTs. Consistent with previous studies (e.g. Deser et al. 1996), there is a strong inverse relationship between ΔSST (Fig. 3d) and ΔMLD (Fig. 4d) in midlatitudes of the Pacific and Atlantic, since cold dense water enables the mixed layer to penetrate deeper into the ocean.

b. SST forcing and feedback: Q_{ek} and Q_{net} anomalies

When Ekman heat transport is introduced into the coupled model it affects the local SST and MLD, but its full impact depends on the subsequent air-sea interactions (as shown schematically in Fig. 5). In the extreme case of no feedback, Q_{ek} in the EKM experiment would be identical to the value diagnosed (but not applied) in the MLM experiment and there would be no change in Q_{net} between the two. It is possible for Q_{ek} to be balanced by terms other than the net heat flux, such as entrainment at the base of the mixed layer, but these terms tend to be small in winter (Alexander et al. 2000). The response could also consist of a basic thermodynamic feedback, where the Q_{ek} forcing creates an SST anomaly that is damped by the net heat flux without significantly altering the atmospheric circulation. The damping is analogous to its counterpart in the stochastic

model for SST anomalies (e.g. Frankignoul and Hassleman 1977): after high frequency atmospheric forcing creates SST anomalies the "slow" response relaxes the SSTs towards climatology, since positive (negative) SST anomalies lose more (less) heat to the atmosphere. Finally, the air-sea interaction can be dynamic, where the atmospheric circulation changes in response to either local or remote SST anomalies, altering Q_{ek} and/or Q_{net}, which in turn can feed back on the ocean below. We explore the nature of the forcing and feedback by comparing Q_{ek} and Q_{net} in the EKM and MLM simulations.

The anomalous Ekman heat transport during JFM (1) derived from NCEP reanalysis and the EKM experiment are shown in Figs. 6a and 6b, respectively. In both reanalysis and the model, the ENSO signal includes stronger surface westerlies over the central and western North Pacific, resulting in anomalous southward Ekman transport that cools the underlying ocean. The cooling is greatest (Q_{ek}^{*}<-20 Wm^{-2}) in the vicinity of 32°N, 165°W, where the anomalous westerlies are strongest. A secondary maximum occurs along ~40°N from 150°E-170°W where modest westerly winds overlay a strong mean meridional SST gradient (Fig. 1). The amplitude of the negative anomalies are smaller in the EKM, but this may not be solely due to errors in the model: Millif et al. (1999) found that the extratropical winds in reanalysis were stronger than those derived from scatterometer measurements and Q_{ek}^{*} computed from in situ observations (Da Silva 1994) are of similar amplitude to those in the EKM experiment (not shown). Along the west coast of North America, southeasterly winds warm the underlying ocean with a maximum Q_{ek}^{*} of ~10 Wm^{-2} from 40°N-50°N. In the Atlantic, Q_{ek}^{*} indicates warming (cooling) at most locations north (south) of ~40°N in reanalysis and ~45°N in the EKM.

Previous analyses have indicated that Ekman heat transport anomalies are primarily associated with anomalous meridional currents, as given by $c/f\left(\tau_x^{'}\partial\overline{\mathrm{SST}}/\partial y\right)$, where ($\bar{}$) denotes the time mean and ($'$) the departure from the time mean. This is also true in the EKM response to ENSO, where stronger than normal westerlies ($\tau_x^{'} > 0$) and colder temperatures towards the poles ($\partial\overline{\mathrm{SST}}/\partial y < 0$) resulted in cooling ($c/f\left(\tau_x^{'}\partial\overline{\mathrm{SST}}/\partial y\right)^{*} < 0$) of the central North Pacific during El Niño relative to La Niña events. There is a compensating warming by $c/f\left(\bar{\tau}_x\partial\mathrm{SST}'/\partial y\right)^{*}$, as the mean westerlies drive southward Ekman flow across the anomalous negative SST gradient between 35°N-50°N. The magnitude of the latter term is ~1/3 of $c/f\left(\tau_x^{'}\partial\overline{\mathrm{SST}}/\partial y\right)^{*}$. To the south of the SST anomaly, northward advection driven by the mean trade winds also weakly warms the ocean between 20°N-25°N, 180°-140°W. The other components of $\left(Q_{ek}^{'}\right)^{*}$ have a negligible impact on SST*.

Q_{ek}^{*} diagnosed from the winds and SST gradient in the MLM experiment (but not included in the MLM SST equation) are shown in Fig. 6c. The pattern and values of Q_{ek}^{*} in the MLM are very similar to those in the EKM experiment over the Pacific. Allowing Q_{ek} to impact the coupled system (determined by comparing Fig. 6b and 6c) slightly reduces the positive Q_{ek}^{*} values in the northeast Pacific. The difference between Q_{ek}^{*} in the two experiments, however, is < 5 Wm^{-2} at nearly all Pacific grid points (not shown), indicating that air-sea feedback has a modest impact on the surface winds and thus Q_{ek}^{*} over the basin. While the Atlantic Q_{ek}^{*} pattern is similar in the MLM and EKM experiments, the amplitude is greater in the EKM, particularly north of ~40°N where Q_{ek}^{*}

is approximately 2-3 times larger than in the MLM. Thus, allowing Ekman heat transport to impact the coupled system has a positive feedback on Q_{ek}^{*} in the Atlantic.

The anomalous net heat flux (positive into the ocean), obtained from NCEP reanalysis (Fig. 7a) and the EKM experiment (Fig. 7b) are fairly similar over the Northern Hemisphere Oceans in JFM(1). Consistent with previous studies, Q_{net}^{*} strongly cools the central North Pacific and warms the northeast Pacific in reanalysis and the EKM experiment, although the maximum cooling is stronger and further west in reanalysis. However, the pattern of Q_{net}^{*} in the EKM, with the strongest cooling in the central Pacific, is consistent with ship-based estimates (Park et al. 2006). In the Atlantic, $|Q_{net}^{*}| > 30$ Wm^{-2} along the south east coast of the United States, and northeast of Newfoundland (~56°N, 55°W), on par with the ENSO-driven heat fluxes in the North Pacific.

Comparing Figs. 6 and 7 indicates that Q_{ek}^{*} is of relatively large amplitude and coincident with Q_{net}^{*} over the central and northeast Pacific and the subarctic Atlantic enhancing the SST forcing during late winter in these regions. The Q_{ek}^{*} minima in the central Pacific, however, is 50-80% as large and displaced to the southeast of the Q_{net}^{*} minima. In the EKM experiment, Q_{ek}^{*} and Q_{net}^{*} are of opposite sign south of Japan (20°N-30°N, 120°E-140°E), in a small region east of the mid Atlantic states (70°W, 35°N) and in the subtropical Atlantic (20°N-30°N, 30°W-60°W)

Including Ekman transport indirectly affects the surface heat flux as indicated by the difference between the ENSO-related net flux anomalies in the two experiments (ΔQ_{net}, Fig. 7c). ΔQ_{net} is quite small over the Pacific, with positive values on the order of 10 Wm^{-}

[2] centered on 30°N, 160°W, indicative of reduced cooling of the central North Pacific Ocean in the EKM relative to the MLM experiment. Since the EKM-MLM surface circulation changes are negligible over the North Pacific (|ΔSLP| < 0.6 mb at nearly all grid points, not shown), these positive ΔQ_{net} values represent thermodynamic damping of the negative SST anomalies (Fig. 5, bottom left panel). The air-sea interaction is quite different in the Atlantic, where ΔQ_{net} and Q^*_{net} have the same sign over most of the basin indicating a dynamic feedback that acts to amplify the ENSO heat flux signal. This feedback is relatively large, i.e. ΔQ_{net} is on the order of 25% to 50% of Q^*_{net}, but is statistically significant only in small regions to the northeast and southwest of Newfoundland and off the west African coast.

The relationship between Q_{net}, Q_{ek} and SST over the ENSO cycle in the EKM and MLM experiments is explored further in Fig. 8 for the central North Pacific (27°N-37°N, 155°W-175°W), western Atlantic (25°N-32°N, 60°W-78°W) and Subarctic Atlantic (50°N-55°N, 30°W-50°W) regions (boxes in Fig. 3d). For each region, the upper panels show Q^*_{ek} and Q^*_{net} in both experiments, while the bottom panels show ΔSST and the difference in the flux-induced SST tendency, denoted by $\Delta(Q/\mathrm{MLD})$. The latter is given by $([Q_{ek}+Q_{net}+Q_{cor}]/\mathrm{MLD})^*$ in the EKM minus $([Q_{net}+Q_{cor}]/\mathrm{MLD})^*$ in the MLM experiment, since Δ in the other mixed layer heat budget terms, including the entrainment heat flux (Q_{we}), are generally small. The surface heat flux correction, Q_{cor}, is the same in the EKM and MLM experiments but can impact the SST* via differences in MLD between experiments. The anomalous SST tendency is also influenced by the mean seasonal cycle of MLD, which ranges from 20-30 m during summer for all three regions to approximately 70-90 m (105-125 m) in the midlatitude (subarctic) regions during

winter in both experiments (not shown). Thus, SSTs will change more rapidly in summer than in winter for the same forcing.

In the central Pacific (Fig. 8a), Q^*_{ek} is nearly identical in the EKM and as diagnosed from the MLM simulations over the course of the ENSO cycle. Q^*_{net} is also similar in the two experiments, but it is slightly more negative from Aug(0)-Nov(0) and positive from Jan(1)-Jul(1) in the EKM. This difference in Q^*_{net} coincides with slightly warmer ΔSSTs during summer and colder ΔSSTs in the following winter/spring, suggesting weak thermodynamic damping of the ΔSST by the surface fluxes over the full ENSO cycle. In the central Pacific, Δ(Q/MLD) primarily results from the inclusion of Q^*_{ek} and begins to generate negative ΔSST by Dec(0), although ΔQ_{we} also cools the ocean between Aug(0) and Jan(1) (not shown). The general relationship between Q_{ek}, Q_{net}, and SST in the northeast Pacific is similar to the central Pacific in that Q^*_{ek} enhances the ENSO driven SST anomalies that are weakly damped by ΔQ_{net} (not shown).

In the western Atlantic region, Q_{ek} anomalies slightly cool the ocean from Aug(0) – Feb(1) in the EKM experiment, similar to the values diagnosed from the MLM (Fig. 8b). In both experiments, Q^*_{net} warms the ocean in the fall and winter but the heat fluxes are roughly 5 Wm^{-2} lower in the EKM from Nov(0)-Jan (1). So, while air-sea coupling does not greatly alter Q^*_{ek} in the western Atlantic, there is positive feedback between the surface heat flux and SST in fall and winter, as both ΔQ_{net} and ΔSST are negative. The combined cooling of ΔQ_{net} and Q^*_{ek} (Δ[Q/MLD] < 0) result in negative ΔSSTs after October(0) that decrease to ~-0.2°C by Feb(1). In the subarctic Atlantic region, a slight rise in ΔSST in summer and early fall occurs despite negative ΔQ/MLD (Fig. 8c), partly

due to positive ΔQ_{we} from Jul(0) – Sep(0) (not shown). Large differences between experiments occur in this region during winter when ΔQ_{we} is negligible. During Jan(1)-Mar(1) Q^*_{ek} is slightly larger in the EKM than in the MLM experiment while Q^*_{net} is substantially greater in EKM from Nov(0)-Mar(1), resulting in positive ΔQ/MLD in winter and ΔSST of ~0.25°C that persist through spring. The shallower mixed layer in the subarctic Atlantic in the EKM experiment (Fig. 4), decreases the thermal inertia, which increases the positive ΔSST tendency during winter. These findings suggest that changes in the ENSO-driven atmospheric circulation over the North Atlantic induce positive air-sea interaction when Ekman heat transport is included in the coupled system.

c) Atmospheric response

The wintertime atmospheric response to ENSO, indicated by the composite El Niño – La Niña 500 mb geopotential height (z500*), from NCEP reanalysis and the EKM and MLM experiments are shown in Fig. 9. The EKM and MLM model simulations reproduce the observed ENSO signal remarkably well both in terms of the pattern and amplitude of the anomalies (the pattern correlation between both experiments and observations is ~0.8). The two are nearly identical over the Pacific, but the difference between them (Δz500, Fig. 9d), includes a ridge over Canada, trough over the eastern US/West Atlantic and ridge above the subtropical east Atlantic/northwest Africa (all significant at the 95% level). The inclusion of Q_{ek} augments ENSO teleconnections over North America, the North Atlantic and western North Africa by approximately 20% to 40%, as well as improving the correspondence between the model and nature. Indeed, the pattern correlations between z500* in observations with the ensemble mean in the EKM

and MLM over the North America-Atlantic Sector (20°N-90°N, 120°W-0°) are 0.75 and 0.66 respectively, which are significantly different from each other at the 95% level as indicated by a t-test using the spread in the pattern correlations across the 16 MLM and EKM ensemble members. The circulation anomalies have an equivalent barotropic structure where the height anomalies at 200 mb (not shown) are stronger and in the same location as the anomalies at 500 mb.

The atmospheric circulation anomalies during ENSO are explored further in Fig. 10a, which displays the anomalous zonal winds (ms^{-1}) at 200 m (U200*) in the EKM experiment. Anomalous westerlies (U200* > 0) extend across the central North Pacific, the United States and the North Atlantic in midlatitudes. They are flanked by anomalous easterlies in the tropics and high latitudes that are strongest and most extensive in the Pacific sector. The inclusion of Q_{ek} enhances U200 anomalies over most of the Northern Hemisphere, i.e. ΔU200 (Fig. 10b) and U200* have the same sign and pattern. The Ekman induced changes are on the order of 1-2 ms^{-1} over eastern Asia/West Pacific and North America/western Atlantic, significant at 99% and 95% levels, respectively. The former may be in response to the positive ΔSST in the tropical northwest Pacific Ocean and/or the positive (negative) ΔSST to the north (south) of the equator in the Indian Ocean (Fig. 3). Like the ΔSST, the Ekman-induced change in precipitation (ΔP) has a complex structure over the tropical west Pacific and Indian Oceans (not shown), and thus it is difficult to relate the atmospheric circulation changes over Asia to a specific diabatic heat source/sink.

d. Atlantic Air-sea Interaction

Figs. 6-10 indicate that Ekman heat transport significantly enhances air-sea interaction and the response to ENSO over the North Atlantic. To examine these interactions in greater detail, the SST/SLP/$\vec{\tau}$ and 200 mb streamlines/P anomalies are presented for the Atlantic sector in the EKM (Fig. 11 top) and for the EKM-MLM (Fig. 11 bottom). SLP* in the EKM bears a strong resemblance to the negative phase of the NAO, with a low in the central North Atlantic and a high centered over southeast Greenland. High pressure also extends across the tropical Atlantic. The anomalous surface winds oppose the mean trade winds and westerlies at ~20°N and 50°N, respectively, warming the underlying ocean via the surface heat fluxes (Fig. 7) by reducing the wind speed. The anomalous easterlies between 45°N and 60°N also warm the ocean by enhancing the poleward Ekman heat transport (Fig. 6), while anomalous northerly winds advect cold continental air over the Gulf of Mexico and along the east coast of the United States, resulting in negative Q_{net} and SST anomalies. In the upper troposphere, cyclonic circulation in midlatitudes and anticyclonic circulation over the Caribbean are associated with enhanced winds and precipitation extending from Mexico to Western Europe and decreased precipitation over northeastern South America (Fig 11b). Overall, the EKM experiment is consistent with previous observational and modeling studies of the response to ENSO in the Atlantic sector (van Loon and Madden 1981; Van Loon and Rogers 1981; Lau and Nath 2001; Pozo-Vázquez et al., 2001).

The impact of including Q_{ek} resembles the overall response to ENSO over much of the Atlantic (compare top and bottom panels of Fig. 11), including the aforementioned ΔSST tripole with positive (negative) values at 10°N and 50°N (30°N), and a negative NAO-like pattern, although the ΔSLP center in midlatitudes is shifted west relative to the

overall ENSO response. The Ekman-induced increase in the atmospheric circulation can reach 40% of the overall signal, e.g. the ΔSLP is ~1.0 mb, while SLP* is ~2.5 mb in the EKM over Greenland. Likewise including Ekman transport increases the strength of the upper-level circulation and precipitation over the storm track region. While ΔP is negligible over the positive ΔSST in the tropical Atlantic, there are substantial but localized changes over South America, e.g. ΔP > 0 near 0°, 65°W and 8°S, 45°W, and ΔP < 0 further south and west. These precipitation changes appear to influence the circulation over the Amazon (5°S, 40°-70°W) and may impact the broader circulation over the North Atlantic (e.g. Peng et al. 2005).

4. Summary and Discussion

The role of anomalous Ekman heat transport in the ocean on ENSO teleconnections was explored using coupled model experiments. In the MLM experiment, observed SSTs were specified in the tropical Pacific, while a variable depth mixed layer model was employed elsewhere over the global oceans. The same experimental design was used in the EKM simulations with the addition of Q_{ek} in the mixed layer temperature equation. In both the MLM and EKM experiments the ENSO response during winter included a deeper Aleutian Low with the associated cyclonic circulation that cooled the central Pacific and warmed the northeastern Pacific via the surface heat fluxes. In the EKM experiment, including Q_{ek} enhanced the ENSO forcing in the central and northeast North Pacific, increasing the magnitude of the SST anomalies by ~1/3 in these regions. As a result, the amplitude of the SST anomalies exceeded 1.0°C in the central North Pacific in the EKM experiment, on par with the observed ENSO signal. Differences between the

EKM and MLM simulations indicated that Q_{net} weakly opposed the North Pacific SST anomalies in the EKM experiment indicative of thermodynamic damping. This may explain why the ratio of Q_{ek} to Q_{net} was lower in the EKM experiment than as diagnosed from the MLM simulations here and in Alexander et al. (2002). These Ekman-induced changes in Q_{net} did not significantly impact the free troposphere, as only minor differences arose between the atmospheric circulation anomalies in the two experiments over the North Pacific.

While the atmospheric response to ENSO over the Atlantic is weaker than in the Pacific, it appears to be robust. The ENSO teleconnections in the MLM and EKM experiments resemble observations, including low pressure and negative SSTs off the east coast of the United States, similar to negative phase of the NAO and SST tripole patterns (c.f. van Loon and Madden 1981; Pozo-Vázquez et al. 2001). The AGCM experiments of Lau and Nath (2001) also showed that ENSO induced the negative phase of the NAO/SST tripole patterns and that the resulting Atlantic SST anomalies appeared to enhance the local atmospheric circulation. In our study, including Ekman transport further enhanced the Atlantic Ocean temperature anomalies and the overlying atmospheric circulation, including the upper-level height anomalies, jet stream and storm track.

The extent to which the bridge-related Atlantic SST anomalies feed back on the atmosphere is uncertain here as well as in Lau and Nath (2001), since in both studies SST anomalies over the global ocean can impact air-sea interaction in the Atlantic. In our study, the Ekman-induced response over the Atlantic may be caused or augmented by a wavetrain that propagates across eastern Asia, over the pole and into eastern North

America/Western Atlantic (Figs. 9d and 10d). Such features occur in idealized models as atmospheric Rossby waves driven by tropical diabatic heat sources (e.g. Hoskins and Karoly 1981; Ting and Sardeshmukh 1993) and in AGCMs with SST anomalies specified in the Indian and/or West Pacific Oceans (Hoerling et al. 2001b, 2004; Li et al. 2006; Annamalai et al. 2007). However, these studies mainly find that the circulation anomalies develop in the North Pacific as well as the North Atlantic, whereas in our experiments the Ekman-driven response is negligible over most of the North Pacific.

In contrast, Mathieu et al. (2004) concluded that the bridge-related SSTs in the Atlantic influenced the overlying atmospheric circulation based on AGCM experiments during ENSO years with and without Atlantic SST anomalies. In addition, observations (Czaja and Frankignoul 2002; Frankignoul and Kestenare 2005), AGCM experiments with specified Atlantic SST anomalies (Rodwell et al. 1999; Sutton et al. 2001; Peng et al. 2003), AGCM-slab ocean models (Watanabe and Kimoto 2000; Peng et al. 2005) and AGCM-MLM experiments (Cassou et al. 2007) all indicate positive feedback between the NAO and SST tripole during winter.

Why does there appear to be relatively strong air-sea feedback in the Atlantic but not the Pacific, even though the largest Ekman induced SST anomalies occur in the Pacific? The answer may lie in the proximity of the SST anomalies to the storm track. A stronger meridional SST gradient enhances the low-level baroclinicity, which is conducive to cyclogenesis (e.g. Hoskins and Valdez 1990). The Ekman-induced SST anomalies, located between 20°N-30°N in the western half of the Atlantic, enhance the SST gradient slightly south of the mean storm track entrance region. The equatorward position of the anomalous SST gradient relative to the upper-level storm track may lead to positive

feedbacks between the two due to the poleward tilt of baroclinic waves with height (Yin and Battisti 2004). In the Pacific, the largest anomalies are in the eastern half of the basin far from the storm track entrance region. Alternatively, the Ekman-induced changes in diabatic heating over South America (Fig. 11d) may excite a Rossby wave train that emanates into the extratropical Atlantic (Drevillion et al. 2003, Cassou et al. 2004), which may also alter the storm track (Peng et al. 2003, 2005).

Observational analyses indicate that during summer and fall the "North Atlantic horseshoe" SST pattern, which resembles the tripole shifted northeast by roughly 10°-20°, influences the NAO in the subsequent winter (Czaja and Frankignoul 2002; Frankignoul and Kestenare 2005). The EKM-MLM SST difference in summer/fall is similar to the horseshoe pattern, with positive SST centers near Europe and northwest Africa (not shown) and thus may influence the model's NAO in winter. However, it is unclear whether the extratropical horseshoe anomalies influence the atmosphere or are driven by the atmospheric response to SSTs in the tropical Atlantic with little feedback on the atmosphere, as suggested by the modeling studies of Cassou and Terray (2001), Drevillion et al. (2003), and Peng et al. (2005, 2006).

In the present study, we have examined the linear symmetrical response to ENSO by presenting the composite difference between El Niño and La Niña events. The SLP and SSTs for El Niño - neutral years and neutral - La Niña years in the EKM experiment are presented in Fig. 12 (La Niña values were multiplied by -1 to facilitate comparison with El Niño). The El Niño and La Niña anomalies are fairly similar (equal and opposite) over the North Pacific except that the amplitude is somewhat stronger and located ~20° further east during El Niño relative to La Niña events, in general agreement with the data

analyses and AGCM experiments of Hoerling et al. (1997, 2001a). In contrast, the response over the Atlantic is stronger during La Niña than El Niño events, especially when Ekman transport is included (not shown). This asymmetry appears to occur in nature as well, e.g. Pozo-Vázquez et al. (2001) identified the positive phase of the NAO as the response to La Niña but no significant signal during El Niño events. Using cluster analyses, Cassou et al. (2004) found a significant association between La Niña and the "Atlantic Ridge" regime, but no significant link with regimes during El Niño events. However, the Ridge regime, features a high at ~50ºN over the Central North Atlantic, ~15º south of its position found here and by Pozo-Vasquez et al. (2001). In addition, the apparent nonlinear response to ENSO in nature may not be statistical significant over the Atlantic (Sardeshmukh et al. 2000), and may be influenced by decadal fluctuations in the background flow (Deweaver and Nigam 2002). Thus, the asymmetrical response to ENSO, particularly over the Atlantic, warrants further study.

Acknowledgements

We thank Matt Newman, Clara Deser and three anonymous reviewers for their comments and suggestions. This research was supported by NOAA's Climate Variability and Prediction program.

References

Adamec, D., M. M. Rienecker, and J. M. Vukovich, 1993: The time varying characteristics of the meridional Ekman heat transport of the world ocean. *J. Phys. Oceanog.*, **23,** 2704-2716.

Adem, J., 1970: On the prediction of mean monthly ocean temperature. *Tellus*, **22,** 410-430.

Adem, J., 1975: Numerical-thermodynamical prediction of monthly ocean temperature. *Tellus*, **27,** 541-551.

Alexander, M. A., 1990: Simulation of the response of the North Pacific Ocean to the anomalous atmospheric circulation associated with El Niño. *Climate Dyn.*, **5,** 53-65.

Alexander, M. A., 1992a: Midlatitude atmosphere-ocean interaction during El Niño. Part I: the North Pacific Ocean. *J. Climate*, **5,** 944-958.

Alexander, M. A., 1992b: Midlatitude atmosphere-ocean interaction during El Niño. Part II: the Northern Hemisphere atmosphere. *J. Climate*, **5,** 959-972.

Alexander, M. A., J. D. Scott, and C. Deser, 2000: Processes that influence sea surface temperature and ocean mixed layer depth variability in a coupled model. *J. Geophys. Res.*, **105,** 16,823-16,842.

Alexander, M. A., I. Bladé, M. Newman, J. R. Lanzante, N.-C. Lau, and J. D. Scott, 2002: The atmospheric bridge: the influence of ENSO teleconnections on air-sea interaction over the global oceans. *J. Climate*, **15,** 2205-2231.

Alexander, M., A. Capotondi, A. Miller, F. Chai, R. Brodeur and C. Deser, 2008: Decadal variability in the Northeast Pacific in a physical-ecosystem model: The role of mixed layer depth and trophic interactions. *J. Geophys. Res.*, **113**, C02017, doi:10.1029/2007JC004359.

Annamalai, H., H. Okajima, and M. Watanabe, 2007: Possible Impact of the Indian Ocean SST on the Northern Hemisphere Circulation during El Niño**.** *J. Climate*, **20**, 3164–3189.

Bladé, I., 1999: The influence of midlatitude ocean-atmosphere coupling on the low-frequency variability of a GCM. Part II: Interannual variability induced by tropical SST forcing. *J. Climate*, **12,** 21-45.

Broccoli, A. J. and S. Manabe, 1992: The effects of orography on midlatitude Northern Hemisphere dry climates. *J. Climate*, **5,** 1181-1201.

Cassou, C., and L. Terray, 2001: Oceanic forcing of the wintertime low-frequency atmospheric variability in the North Atlantic European sector. A study with the ARPEGE model. *J. Climate*, **14,** 4266-4291.

Cassou, C., C. Deser and M. A. Alexander, 2007: Investigating the impact of reemerging sea surface temperature anomalies on the winter atmospheric circulation over the North Atlantic. *J. Climate*, **20**, 3510-3526.

Cassou, C., C. Deser, L. Terray, J. W. Hurrell, and M. Drévillon, 2004: Summer sea surface temperature conditions in the North Atlantic and their impact upon the atmospheric circulation in early winter. *J. Climate*, **17,** 3349–3363.

Cayan, D. R., 1992: Latent and sensible heat flux anomalies over the northern oceans: the connection to monthly atmospheric circulation. *J. Climate*, **5,** 354-369.

Clark, N. E., 1972: Specification of sea surface temperature anomaly patterns in the

eastern North Pacific. *J. Phys. Oceanogr.*, **2,** 391-404.

Curtis, S. and S. Hastenrath, 1995: Forcing of anomalous sea surface temperature evolution in the tropical Atlantic during Pacific warm events. *J. Geophys. Res.*, **100,** 15835-15847.

Czaja, A. and C. Frankignoul, 2002: Observed impact of Atlantic SST anomalies on the North Atlantic Oscillation. *J. Climate*, **15,** 606-623.

da Silva, A. M., C. C. Young and S. Levitus, 1994: Atlas of Surface Marine Data 1994, Volume 3: Anomalies of Heat and Momentum Fluxes. NOAA Atlas NESDIS 8, U.S. Department of Commerce, NOAA, NESDIS.

Deser, C., M. A. Alexander, and M. S. Timlin, 1996: Upper ocean thermal variations in the North Pacific during 1970 - 1991. *J. Climate*, **9,** 1841-1855.

——, 1999: Evidence for wind-driven intensification of the Kuroshio Current Extension from the 1970s to the 1980s. *J. Climate*, **12,** 1697-1706.

DeWeaver, E., and S. Nigam, 2002: Linearity in ENSO's atmospheric response. *J. Clim.*, **15**, 2446–2461.

Dong, B.-W. and R. T. Sutton, 2001: The dominant mechanism of variability in Atlantic ocean heat transport in a coupled ocean-atmosphere GCM. *Geophys. Res. Lett.*, **28,** 2445-2448.

Drevillon, M., C. Cassou, and L. Terray, 2003: Model study of the North Atlantic region atmospheric response to autumn tropical Atlantic sea-surface-temperature anomalies.

Quart. J. Roy. Meteor. Soc., **129,** 2591-2611.

Enfield, D. B. and D. A. Mayer, 1997: Tropical Atlantic sea surface temperature variability and its relation to El Niño-Southern Oscillation. *J. Geophys. Res.*, **102,** 929-945.

Frankignoul, C., 1985: Sea surface temperature anomalies, planetary waves, and air-sea feedback in the middle latitudes. *Rev. Geophys.*, **23,** 357-390.

Frankignoul, C. and K. Hasselmann, 1977: Stochastic climate models. Part 2. Application to sea-surface temperature variability and thermocline variability. *Tellus*, **29,** 284-305.

Frankignoul, C. and R. W. Reynolds, 1983: Testing a dynamical model for mid-latitude sea surface temperature anomalies. *J. Phys. Oceanogr.*, **13,** 1131-1145.

Frankignoul, C. and E. Kestenare, 2005: Observed Atlantic SST anomaly impact on the NAO: an update. *J. Climate*, **18,** 4089-4094.

Gaspar, P., 1988: Modeling the seasonal cycle of the upper ocean. *J. Phys. Ocean*, **18,** 161-180.

Gordon, C. T. and W. Stern, 1982: A description of the GFDL global spectral model. *Mon. Wea. Rev.*, **110,** 625-644.

Haarsma, R. J., E. J. D. Campos, W. Hazeleger, C. Severijns, A. R. Piola, and F. Molteni, 2005: Dominant modes of variability in the South Atlantic: study with a hierarchy of ocean–atmosphere models. *J. Climate*, **18,** 1719–1735.

Haney, R. L., 1980: A numerical case study of the development of large-scale thermal anomalies in the central North Pacific Ocean. *J. Phys. Oceanogr.*, **10,** 541-556.

——, 1985: Midlatitude sea surface temperature anomalies: a numerical hindcast. *J.Phys. Oceanogr.*, **15,** 787-799.

Harrison, D. E. and N. K. Larkin, 1998: El Niño-Southern Oscillation sea surface temperature and wind anomalies. *Rev. of Geophys.*, **36,** 353-399.

Hoerling, M. P., A. Kumar, and M. Zhong, 1997: El Niño, La Niña, and the nonlinearity of their teleconnections. *J. Clim.*, **10**, 1769–1786.

Hoerling, M. P., A. Kumar, and T.-Y. Xu 2001a: Robustness of the nonlinear atmospheric response to opposite phases of ENSO. *J. Clim.*, **14**, 1277–1293.

Hoerling, M. P., J. W. Hurrell, and T. Xu, 2001b: Tropical origins for recent North Atlantic climate change. *Science*, **292**, 90–92.

Hoerling, M. P., J. W. Hurrell, T. Xu, G.T. Bates, and A.S. Phillips, 2004: Twentieth Century North Atlantic Climate Change. Part II: Understanding the Effect of Indian Ocean Warming. *Climate Dyn.*, **23,** 391-405.

Hoskins, B. J., and D. J. Karoly 1981: The steady linear response of a spherical atmosphere to thermal and orographic forcing, *J. Atmos. Sci*., **38**, 1179 – 1196.

Hoskins, B. J. and P. J. Valdes, 1990: On the existence of storm tracks. *J. Atmos. Sci.*, **47,** 1854-1864.

Jacob, W. J., 1967: Numerical semiprediction of monthly mean sea surface temperature. *J. Geophys. Res.*, **72,** 1681-1689.

JEDAC, cited, 2008: Joint Environmental Data Analysis Center, mixed layer depth. [Available online at http://jedac.ucsd.edu/DATA_IMAGES/index.html].

Kalnay, E. and Coauthors, 1996: The NCEP/NCAR 40-year reanalysis project. *Bull. Amer. Meteor. Soc.*, **77,** 437-471.

Kistler, R., E. Kalnay, W. Collins, S. Saha, G. White, J. Woollen, M. Chelliah, W. Ebisuzaki, M. Canamitsu, V. Kousky, H. van den Dool, R. Jenne, and M. Fiorinio, 2001: The NCEP-NCAR 50-year reanalysis: Monthly Means CD-ROM and documentation. *Bull. Amer. Met. Soc.*, **82,** 247-267.

Kraus, E. B. and S. Levitus, 1986: Annual heat fluctuations across the Tropic Circles. *J. Phys. Oceanog*, **16,** 1479-1486.

Kwon, Y. O. and C. Deser, 2007: North Pacific decadal variability in the Community Climate System Model Version 2. *J. Climate*, **20,** 2416-2433.

Lau, N. C. and M. J. Nath, 1994: A modeling study of the relative roles of tropical and extratropical SST anomalies in the variability of the global atmosphere-ocean system. *J. Climate*, **7,** 1184-1207.

Lau, N.-C. and M. J. Nath, 1996: The role of the 'atmospheric bridge' in linking tropical Pacific ENSO events to extratropical SST anomalies. *J. Climate*, **9,** 2036-2057.

Lau, N.-C. and M. J. Nath, 2001: Impact of ENSO on SST variability in the North

Pacific and North Atlantic: seasonal dependence and role of extratropical air-sea coupling. *J. Climate*, **14,** 2846-2866.

Levitus, S., 1987: Meridional Ekman heat fluxes for the world ocean and individual ocean basins. *J. Phys. Oceanog.*, **17,** 1484-1492.

Li, S., M. P. Hoerling, S. Peng, and K. M. Weickmann, 2006: The Annular Response to Tropical Pacific SST Forcing. *J. Climate*, **19**, 1802-1819.

Liu, Z. and M. A. Alexander, 2007: Atmospheric Bridge, Oceanic Tunnel and Global Climatic Teleconnections. *Rev. Geophys.*, **45,** RG2005, doi:10.1029/2005RG000172.

Luksch, U., 1996: Simulation of North Atlantic low frequency variability. *J. Climate*, **9,** 2083-2092.

Luksch, U. and H. v. Storch, 1992: Modeling the low-frequency sea surface temperature variability in the North Pacific. *J. Climate*, **5,** 893-906.

Mathieu, P.-P., R.T. Sutton, B. Dong, and M. Collins, 2004: Predictability of winter climate over the North Atlantic European region during ENSO events. *J. Climate*, **17,** 1953-1974.

Miller, A. J., D. R. Cayan, T. P. Barnett, N. E. Graham, and J. M. Oberhuber, 1994: Interdecadal variability of the Pacific Ocean: model response to observed heat flux and wind stress anomalies. *Climate Dyn.*, **10,** 287-302.

Millif, R. F., W. G. Large, J. Morzel, G. Danabasoglu, T. M. Chin, 1999: Ocean general circulation model sensitivity to forcing from scatterometer winds. *J.*

Geophys. Res., **104**, 11,337-11,358.

Namias, J., 1959: Recent seasonal interactions between North Pacific waters and the overlying atmospheric circulation. *J. Geophys. Res.*, **64,** 631-646.

Namias, J., 1965: Macroscopic association between mean monthly sea surface temperature and the overlying winds. *J. Geophys. Res.*, **70,** 2307-2318.

Namias, J., 1972: Experiments in objectively predicting some atmospheric and oceanic variables for the winter of 1971-1972. *J. Appl. Meteor.*, **11,** 1164-1174.

Park, S., M. A. Alexander, and C. Deser, 2006: The impact of cloud radiative feedback, remote ENSO forcing, and entrainment on the persistence of North Pacific sea surface temperature anomalies. *J. Climate*, **19,** 6243-6261.

Peng, S., W.A. Robinson, and S. Li, 2003: Mechanisms for the NAO responses to the North Atlantic SST tripole. *J. Climate*, **16,** 1987-2004.

Peng, S., W. A. Robinson, S. Li, and M. P. Hoerling, 2005: Tropical Atlantic SST forcing of coupled North Atlantic seasonal responses. *J. Climate*, **18,** 480-496.

Peng, S., W.A. Robinson, S. Li, and M.A. Alexander, 2006: Effects of Ekman transport on the NAO response to a tropical Atlantic SST anomaly. *J. Climate*, **19,** 4803-4818.

Pozo-Vázquez, D., M. J. Esteban-Parra, F. S. Rodrigo, and Y. Castro-Díez, 2001: The association between ENSO and winter atmospheric circulation and temperature in the North Atlantic region. *J. Climate*, **14,** 3408–3420.

Qiu, Bo, 2000: Interannual variability of the Kuroshio Extension and its impact on the

wintertime SST field. *J. Phys. Oceanogr.*, **30**, 1486-1502.

Rasmusson, E. M. and T. H. Carpenter, 1982: Variations in tropical sea surface temperature and surface wind fields associated with the Southern Oscillation/El Niño. *Mon. Wea. Rev.*, **110,** 354-384.

Rodwell, M. J., D. P. Rowell, and C. K. Folland, 1999: Oceanic forcing of the wintertime North Atlantic Oscillation and European climate. *Nature*, **398,** 320-323.

Sardeshmukh, P. D., G. P. Compo, and C. Penland, 2000: Changes of probability associated with El Niño, *J. Clim.*, **13**, 4268–4286.

Sato, O. T., P. S. Polito, and W. T. Liu, 2002: Intradecadal variability in the Ekman heat flux from scatterometer winds. *Geophys. Res. Lett.*, **29,** 1831, doi:10.1029/2002GL014775.

Schneider, N. and A. J. Miller, 2001: Predicting North Pacific Ocean climate. *J. Climate*, **14,** 3997-4002.

Seager, R., Y. Kushnir, N. H. Naik, M. A. Cane, and J. Miller, 2001: Wind-Driven Shifts in the Latitude of the Kuroshio–Oyashio Extension and Generation of SST Anomalies on Decadal Timescales. *J. Climate*, **14,** 4249–4265.

Seager, R., Y. Kushnir, M. Visbeck, N. Naik, J. Miller, G. Krahmann, and H. Cullen, 2000: Causes of Atlantic Ocean climate variability between 1958 and 1998. *J. Climate*, **13,** 2845-2862.

Smith, T. M., R. W. Reynolds, R. E. Livezey, and D. C. Stokes, 1996: Reconstruction of historical sea surface temperatures using empirical orthogonal functions. *J. Climate*, **9,** 1403-1420.

Sterl, A. and W. Hazeleger, 2003: Coupled variability and air-sea interaction in the South Atlantic Ocean. *Climate Dyn.*, **21,** 559-571.

Sutton, R. T., W. A. Norton, and S. P. Jewson, 2001: The North Atlantic Oscillation - what role for the ocean? *Atmosph. Sci. Let.*, **1,** 89-100.

Ting, M. and P. D. Sardeshmukh, 1993: Factors determining the extratropical response to equatorial diabatic heating anomalies. *J. Atmos. Sci.*, **50,** 907-918.

Trenberth, K. E., 1997: The Definition of El Niño. *Bull. Amer. Meteor. Soc.*, **78,** 2562-2584.

van Loon, H. and R. A. Madden, 1981: The Southern Oscillation. Part I. Global associations with pressure and temperature in northern winter. *Mon. Wea. Rev.*, **109,** 1150-1162.

van Loon, H. and J. C. Rogers, 1981: The Southern Oscillation. Part II: Associations with changes in the middle troposphere in the northern winter. *Mon. Wea. Rev.*, **109,** 1163-1168.

Venzke, S., M. R. Allen, R. T. Sutton, D. P. Rowell, 1999: The atmospheric response over the North Atlantic to decadal sea surface temperature changes. *J. Climate*, **12,** 2562-2584.

Watanabe, M. and M. Kimoto, 2000: On the Persistence of Decadal SST Anomalies in the North Atlantic. *J. Climate*, **13,** 3017-3028.

Weller, R. A. and A. J. Plueddemann, 1996: Observations of the vertical structure of the oceanic boundary layer. *J. Geophys. Res. - Oceans*, **101,** 8789-8806.

White, W., B., R. Bernstein, G. McNally, S. Pazan, and R. Dickson, 1980: The thermocline response to transient atmospheric forcing in the interior midlatitude North Pacific 1976-1978. *J. Phys. Oceanogr.*, **10,** 372-384.

White, W. B., 1995: Design of a global observing system for gyre-scale upper ocean temperature variability. *Prog. Oceanogr.*, **36,** 169-217.

Whitney, F. A. and H. J. Freeland, 1999: Variability in upper-ocean water properties in the NE Pacific Ocean. *Deep-Sea Res Pt II*, **46,** 2351-2370.

Yin, J. H. and D. S. Battisti, 2004: Why do baroclinic waves tilt poleward with height. *J. Atmos. Sci.*, **61,** 1454-1460.

Figure Captions

FIG. 1. The El Niño – La Niña composite of SLP (contours, interval 1 mb), surface wind stress (τ, black vectors, N m^{-2}, scale in upper right corner), and mean SST (color shading, interval 0.5 ˚C) during JFM(1) from the EKM, the model that includes Q_{ek}. Colored vectors indicate the direction of anomalous Ekman heat advection.

FIG. 2. Schematic of the ocean configuration for the MLM and EKM experiments. In both experiments SST anomalies are specified in the equatorial Pacific (yellow) for the years 1950-1999 and the ocean mixed layer model, MLM, is active over the remainder of the ice-free ocean (blue). Anomalous Ekman forcing is added to the MLM poleward of 5˚N-5˚S in ice-free regions of all ocean basins in the EKM simulations.

FIG. 3. The composite El Niño – La Niña (*) SST (˚C) during JFM (Yr 1) for (a) observations over 1950-1999, (b) EKM, (c) MLM, and (d) EKM-MLM (Δ). The shading (contour) interval is 0.25 (0.5) ˚C in (a)-(c). The shading in (d) indicates where the t-test exceeds the 95% and 99% confidence levels for ΔSST (contour interval 0.1˚C). The large box in (b)-(d) indicates the region of prescribed SST forcing and the smaller boxes in (d) indicate the regions used in Fig. 8.

FIG. 4. MLD* (m) during JFM(1) for (a) observations (1956-1999), (b) EKM, (c) MLM, and (d) Δ. The shading (contour) interval is 5 (10) m in (a)-(c). In panel (d), the shading indicates 95% and 99% confidence limits for the ΔMLD (contour interval 5 m).

FIG. 5. Schematic for the possible types of air-sea interaction in the EKM and MLM experiments.

FIG. 6. El Niño-La Niña (Q_{ek}^{*} Wm^{-2}) during JFM(1) for (a) NCEP reanalysis, (b) EKM and (c) MLM (diagnosed from archived values of the winds and SSTs but does not impact the ocean model). The shading (contour) interval is 2.5 (5) Wm^{-2}.

FIG. 7. El Niño-La Niña net surface heat flux (Q_{net}^{*} in W m^{-2}) during JFM(1) for (a)NCEP reanalysis (a) EKM, and (c) EKM-MLM(Δ). The shading (contour) interval in (a) is 5 (10) Wm^{-2}. In panel (b), the shading indicates 95% and 99% confidence limits for the ΔQ_{net} (contour interval 5 W m^{-2}). Positive values indicate ocean warming.

FIG. 8. El Niño – La Niña composite evolution for the (a) central Pacific, (b), western Atlantic, and (c) subarctic Atlantic regions (see FIG. 3d for locations). The top panel for each region shows Q_{ek}^{*} (W m^{-2}) from the MLM (red) and EKM (blue) and Q_{net}^{*} (Wm^{-2}) from the MLM (black) and EKM (green). The bottom panel for each region shows ΔQ/MLD (red; ˚C) and ΔSST (black; ˚C). Note the reduced scale in (b).

FIG. 9. The El Niño – La Niña composite of Z500 (m) during JFM(1) for (a) observed (1950-1999), (b) EKM, (c) MLM, and (d) Δ. The shading (contour) interval is 5 (10) m in (a)-(c). In panel (d), the shading indicates 95% and 99% confidence limits for the ΔZ500 (contour interval 5 m).

FIG. 10. The El Niño – La Niña composite of U200 (ms^{-1}) during JFM(1) for (a) EKM, and (b) Δ. The shading (contour) interval in (a) is 1.5 (3) ms^{-1}. In panel (b), the shading indicates 95% and 99% confidence limits for the ΔU200 (contour interval 0.5 ms^{-1}).

FIG. 11. The El Niño – La Niña composite during JFM(1) for (a) EKM SLP (contour interval 0.25 mb), SST (shading interval 0.05˚C), and surface wind stress (τ, black vectors, N m^{-2}, scale upper right corner), (b) EKM 200mb streamlines and precipiatation (P, shading interval 1 cm/3mo), (c) ΔSLP (contour interval 0.25 mb), ΔSST (shading interval 0.05 ˚K), and Δτ (vectors, N m^{-2}), and (d) 200mb streamlines and ΔP (shading interval 1 cm/3mo).

FIG. 12. The EKM a) El Niño – Neutral and b) La Niña – Neutral composites during JFM(1) of SLP (contour interval 0.5 mb) and SST (shading interval 0.05˚C). The La Niña signal was multiplied by -1 to facilitate the comparison with the El Niño composite.

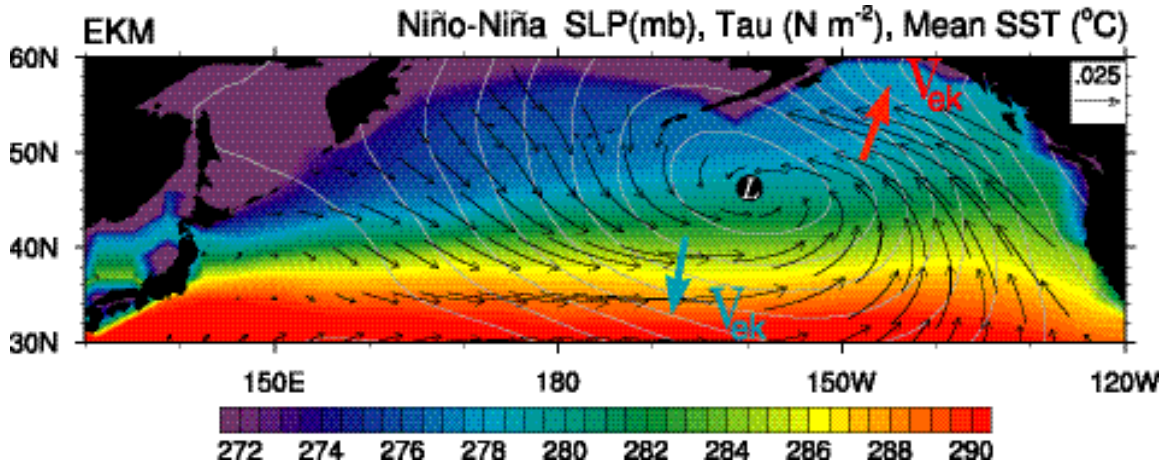

FIG. 1. The El Niño – La Niña composite of SLP (contours, interval 1 mb), surface wind stress (τ, black vectors, N m^{-2}, scale in upper right corner), and mean SST (color shading, interval 0.5 ˚C) during JFM(1) from the EKM, the model that includes Q_{ek}. Colored vectors indicate the direction of anomalous Ekman heat advection.

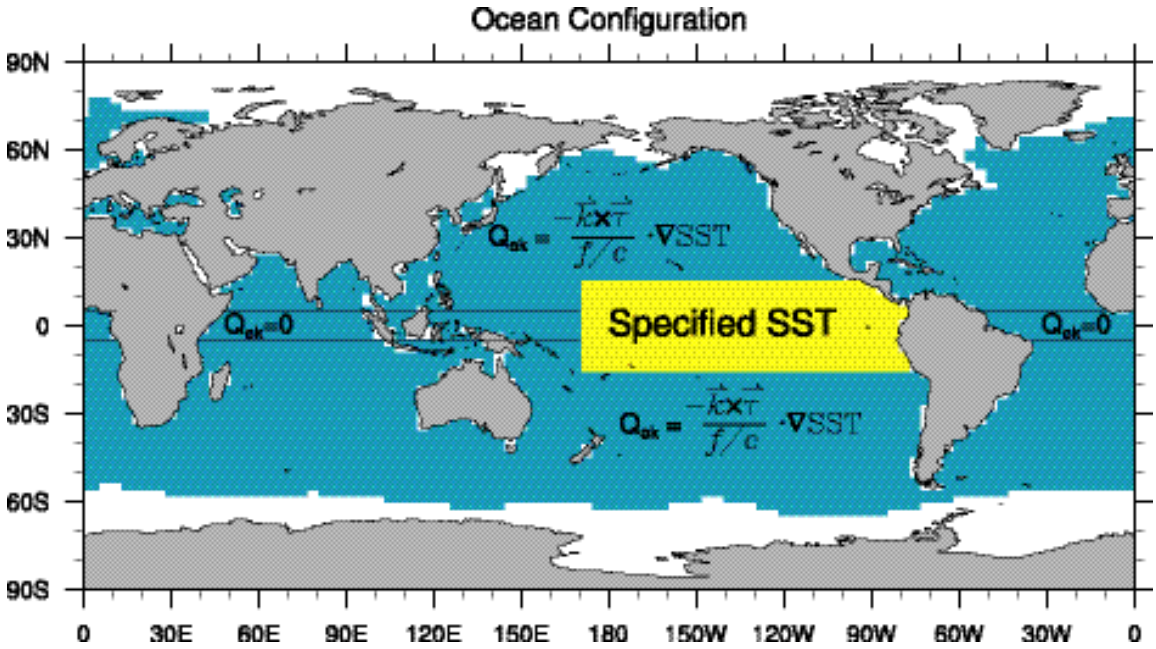

FIG. 2. Schematic of the ocean configuration for the MLM and EKM experiments. In both experiments SST anomalies are specified in the equatorial Pacific (yellow) for the years 1950-1999 and the ocean mixed layer model, MLM, is active over the remainder of the ice-free ocean (blue). Anomalous Ekman forcing is added to the MLM poleward of 5˚N-5˚S in ice-free regions of all ocean basins in the EKM simulations.

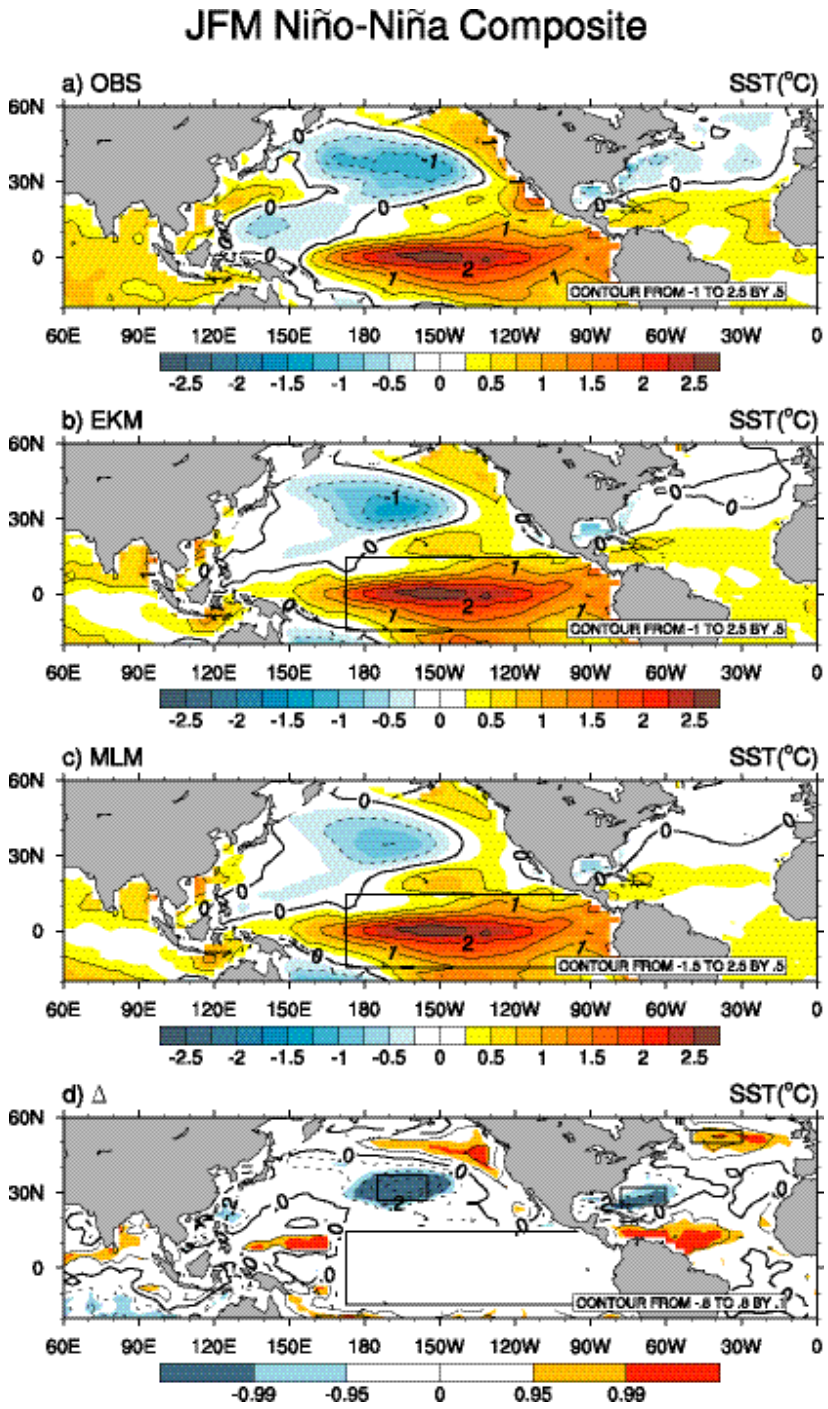

FIG. 3. The composite El Niño – La Niña (*) SST (˚C) during JFM (Yr 1) for (a) observations over 1950-1999, (b) EKM, (c) MLM, and (d) EKM-MLM (Δ). The shading (contour) interval is 0.25 (0.5) ˚C in (a)-(c). The shading in (d) indicates where the t-test exceeds the 95% and 99% confidence levels for ΔSST (contour interval 0.1˚C). The large box in (b)-(d) indicates the region of prescribed SST forcing and the smaller boxes in (d) indicate the regions used in Fig. 8.

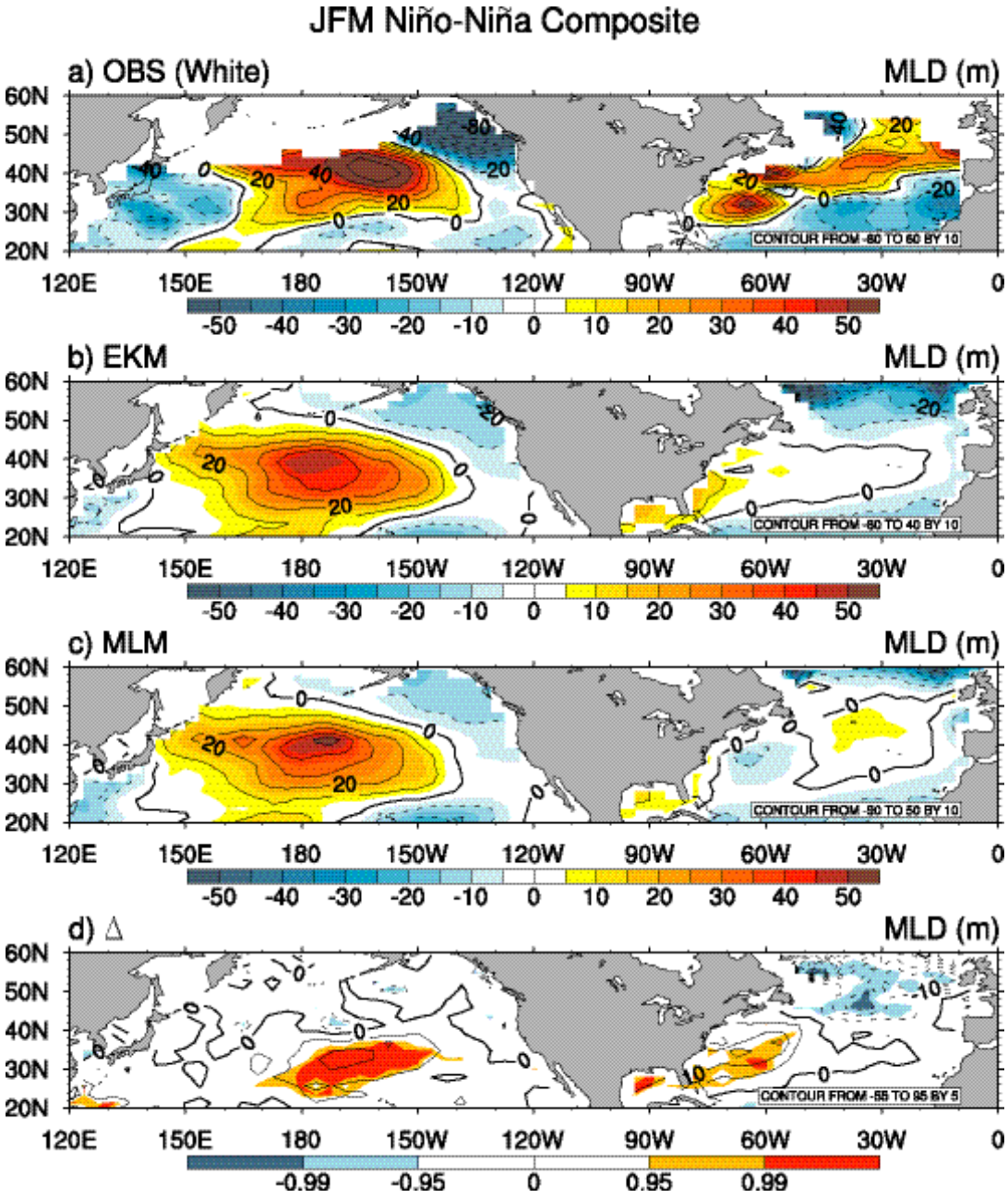

FIG. 4. MLD* (m) during JFM(1) for (a) observations (1956-1999), (b) EKM, (c) MLM, and (d) Δ. The shading (contour) interval is 5 (10) m in (a)-(c). In panel (d), the shading indicates 95% and 99% confidence limits for the ΔMLD (contour interval 5 m).

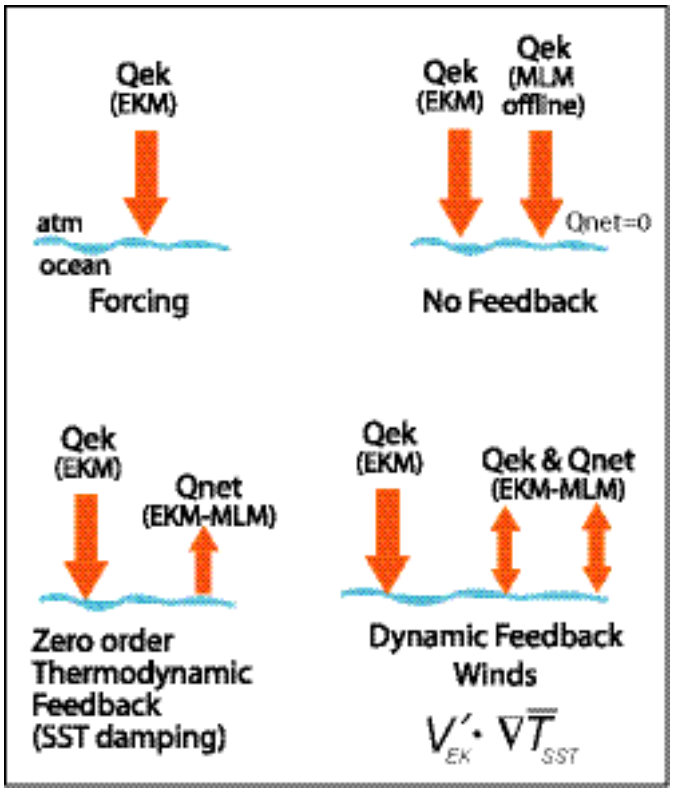

FIG. 5. Schematic for the possible types of air-sea interaction in the EKM and MLM experiments.

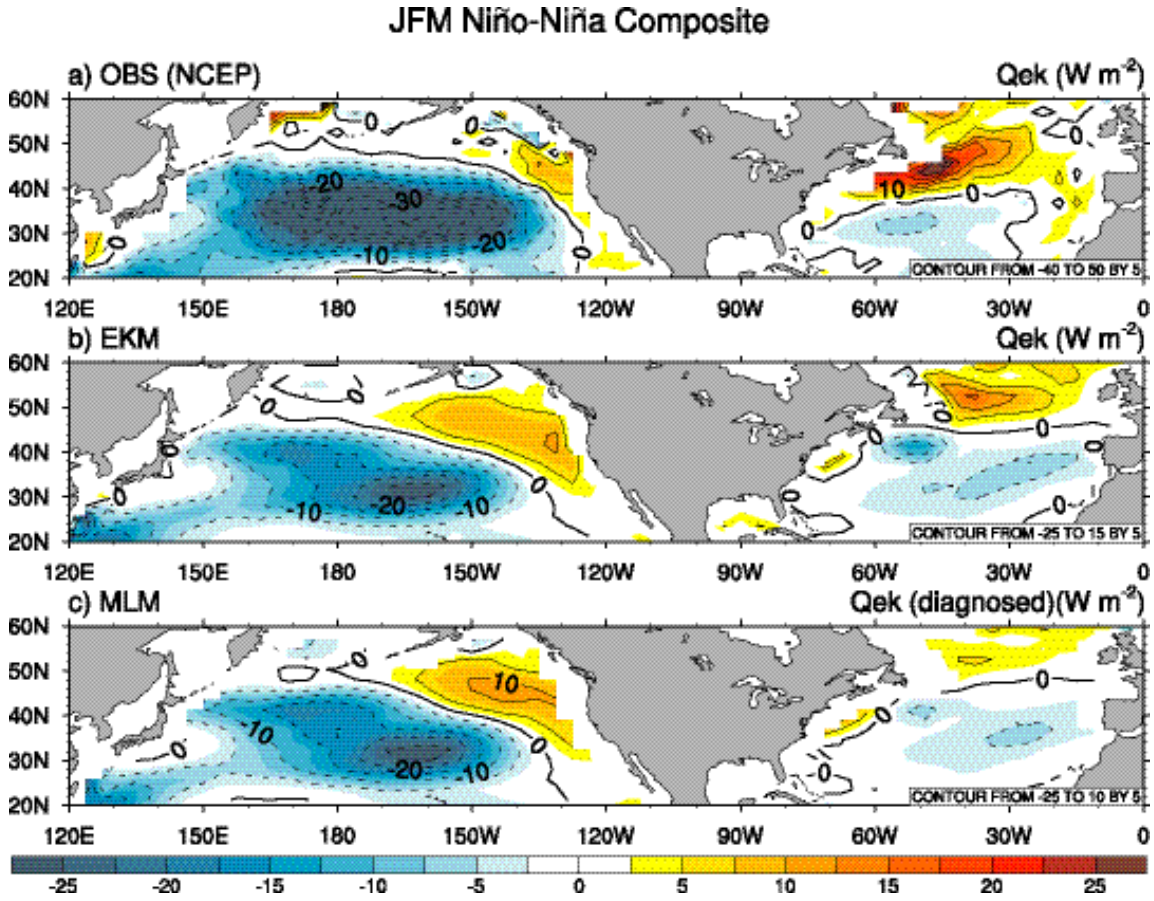

FIG. 6. El Niño-La Niña (Q^*_{ek} Wm^{-2}) during JFM(1) for (a) NCEP reanalysis, (b) EKM and (c) MLM (diagnosed from archived values of the winds and SSTs but does not impact the ocean model). The shading (contour) interval is 2.5 (5) Wm^{-2}.

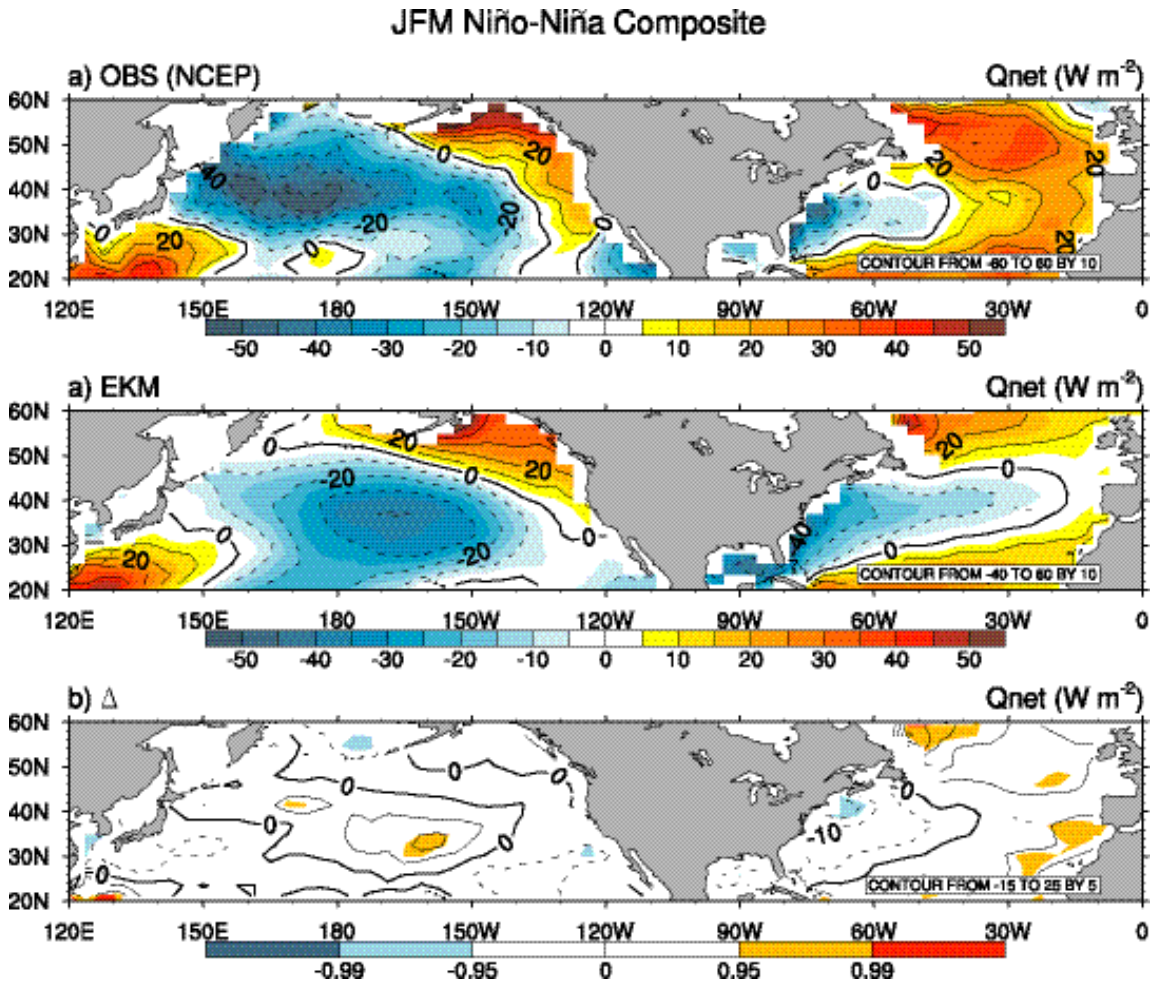

FIG. 7. El Niño-La Niña net surface heat flux (Q^*_{net} in W m^{-2}) during JFM(1) for (a)NCEP reanalysis (a) EKM, and (c) EKM-MLM(Δ). The shading (contour) interval in (a) is 5 (10) Wm^{-2}. In panel (b), the shading indicates 95% and 99% confidence limits for the ΔQ_{net} (contour interval 5 W m^{-2}). Positive values indicate ocean warming.

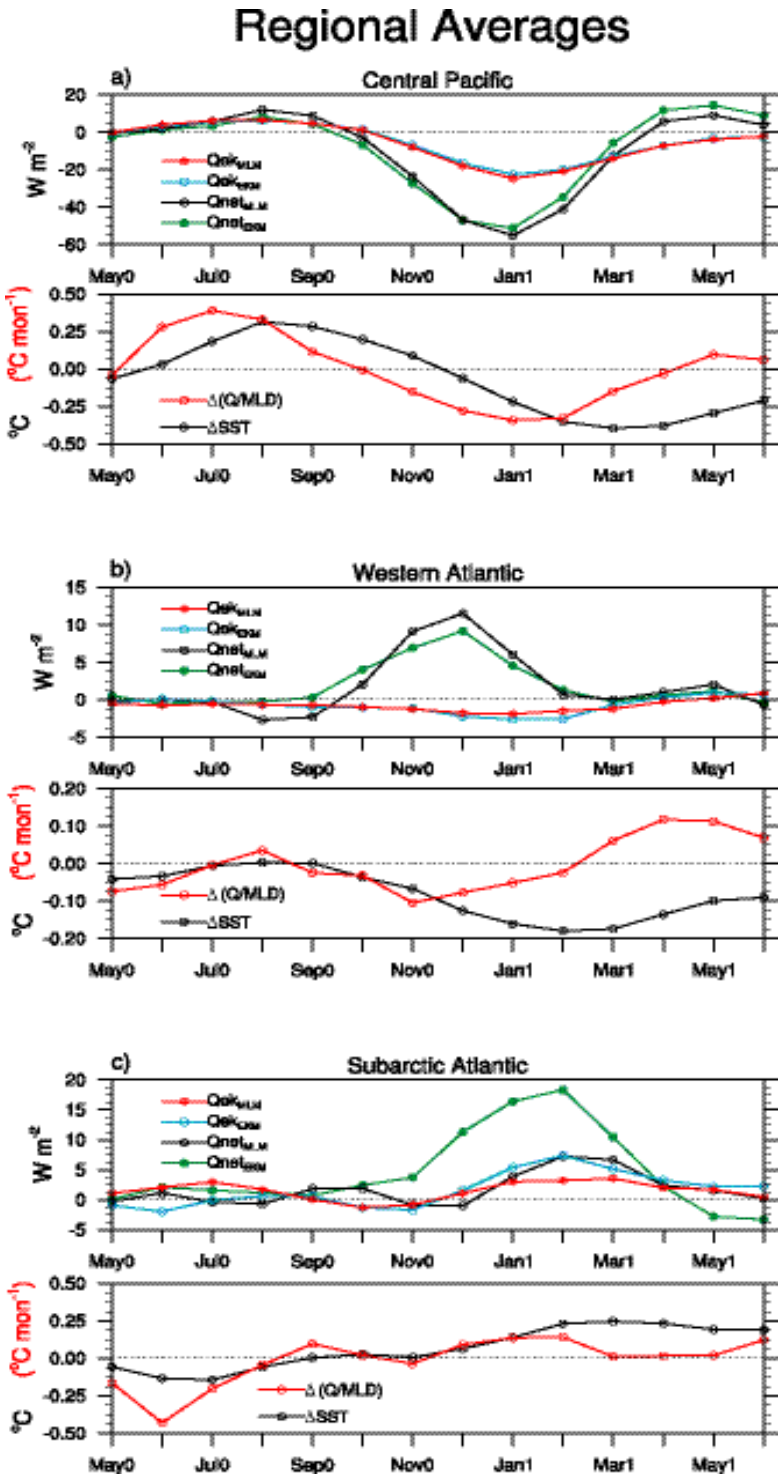

FIG. 8. El Niño – La Niña composite evolution for the (a) central Pacific, (b), western Atlantic, and (c) subarctic Atlantic regions (see FIG. 3d for locations). The top panel for each region shows Q^*_{ek} (W m^{-2}) from the MLM (red) and EKM (blue) and Q^*_{net} (Wm^{-2}) from the MLM (black) and EKM (green). The bottom panel for each region shows ΔQ/MLD (red; ˚C) and ΔSST (black; ˚C). Note the reduced scale in (b).

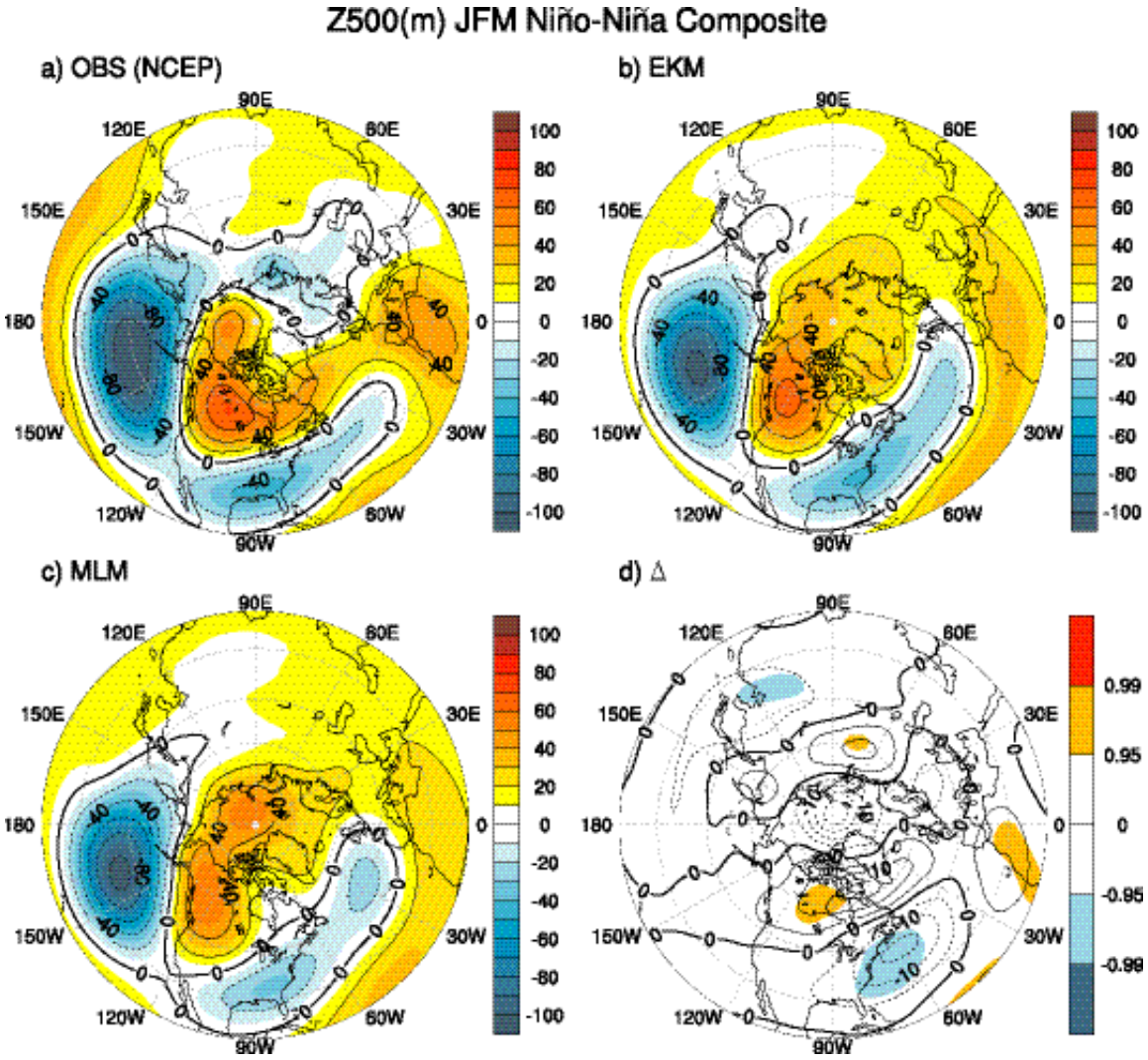

FIG. 9. The El Niño – La Niña composite of Z500 (m) during JFM(1) for (a) observed (1950-1999), (b) EKM, (c) MLM, and (d) Δ. The shading (contour) interval is 5 (10) m in (a)-(c). In panel (d), the shading indicates 95% and 99% confidence limits for the ΔZ500 (contour interval 5 m).

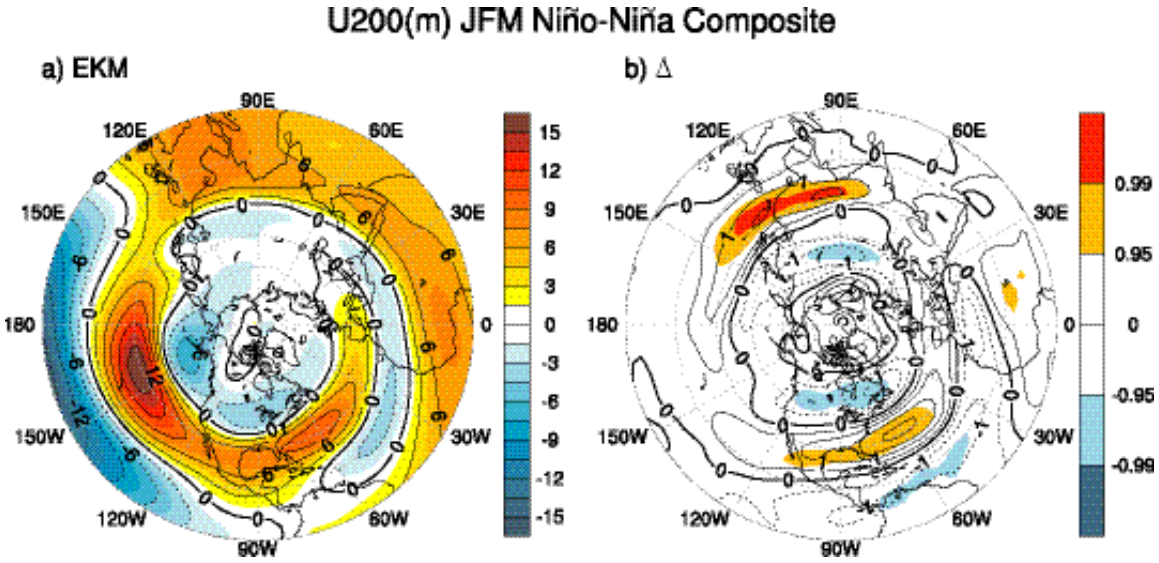

FIG. 10. The El Niño – La Niña composite of U200 (ms^{-1}) during JFM(1) for (a) EKM, and (b) Δ. The shading (contour) interval in (a) is 1.5 (3) ms^{-1}. In panel (b), the shading indicates 95% and 99% confidence limits for the ΔU200 (contour interval 0.5 ms^{-1}).

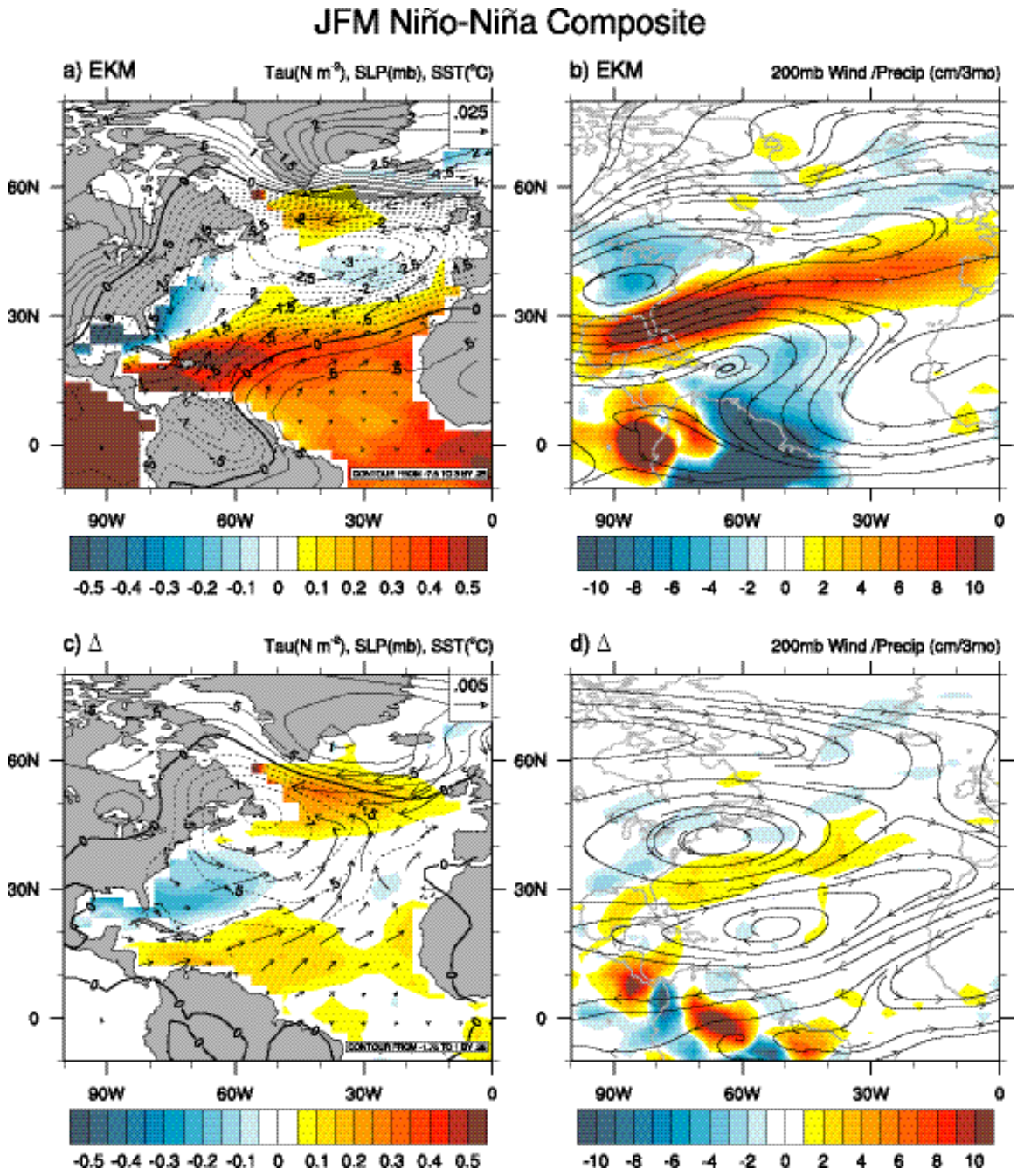

FIG. 11. The El Niño – La Niña composite during JFM(1) for (a) EKM SLP (contour interval 0.25 mb), SST (shading interval 0.05˚C), and surface wind stress (τ, black vectors, N m^{-2}, scale upper right corner), (b) EKM 200mb streamlines and precipiatation (P, shading interval 1 cm/3mo), (c) ΔSLP (contour interval 0.25 mb), ΔSST (shading interval 0.05 ˚K), and $\Delta\tau$ (vectors, N m^{-2}), and (d) 200mb streamlines and ΔP (shading interval 1 cm/3mo).

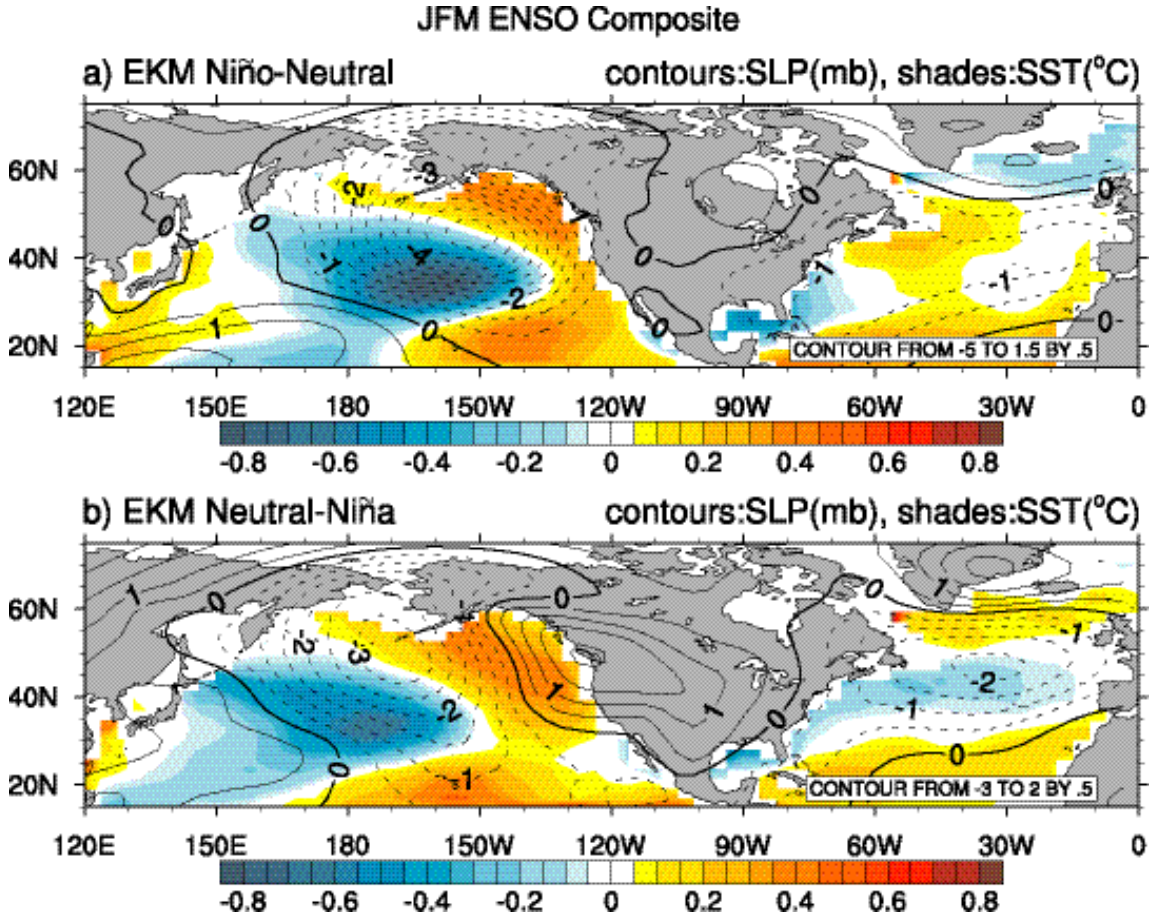

FIG. 12. The EKM a) El Niño – Neutral and b) La Niña – Neutral composites during JFM(1) of SLP (contour interval 0.5 mb) and SST (shading interval 0.05˚C). The La Niña signal was multiplied by -1 to facilitate the comparison with the El Niño composite.

The Role of Ekman Ocean Heat Transport in the Northern Hemisphere Response to ENSO

Michael A. Alexander
NOAA/Earth System Research Laboratory, Boulder, Colorado, USA

James D. Scott
CIRES, University of Colorado, and NOAA/ Earth System Research Laboratory, Boulder, Colorado.

Submitted to the Journal of Climate December 2007
Revised April 2008

Corresponding Author
Michael Alexander
NOAA/Earth System Research Laboratory
Physical Science Division
R/PSD1
325 Broadway
Boulder, Colorado 80305
Michael.Alexander@noaa.gov

Abstract

The influence of oceanic Ekman heat transport (Q_{ek}) on air-sea variability associated with ENSO teleconnections is examined via a pair of atmospheric general circulation model (AGCM) experiments. In the "MLM" experiment, observed sea surface temperatures (SSTs) for the years 1950-1999 are specified over the tropical Pacific, while a grid of mixed layer models is coupled to the AGCM elsewhere over the global oceans. The same experimental design was used in the "EKM" experiment with the addition of Q_{ek} in the mixed layer ocean temperature equation. The ENSO signal was evaluated using differences between composites of El Niño and La Niña events averaged over the 16 ensemble members in each experiment.

In both experiments the Aleutian Low deepened and the resulting surface heat fluxes cooled the central North Pacific and warmed the northeast Pacific during boreal winter in El Niño relative to La Niña events. Including Q_{ek} amplified the ENSO-related SSTs by ~1/3 in the central and northeast North Pacific, producing anomalies comparable to those in nature. Differences between the ENSO-induced atmospheric circulation anomalies in the EKM and MLM experiments were not significant over the North Pacific. The sea level pressure (SLP) and SST response to ENSO over the Atlantic strongly projects on the North Atlantic Oscillation (NAO) and the SST tripole pattern in observations and both model experiments. The La Niña anomalies, which are stronger than during El Niño, include high pressure and positive SSTs in the central North Atlantic. Including Ekman transport enhanced the Atlantic SST anomalies, which in contrast to the Pacific, appeared to strengthen the overlying atmospheric circulation.

1. Introduction

Even though the wind-driven Ekman transport is confined to a thin surface layer in the ocean, it plays a critical role in the global heat balance. Ekman transport is responsible for a large fraction of the mean ocean heat transport within ~25º of the equator (Kraus and Levitus 1986; Levitus 1987). It is especially effective in the tropics due to the strong trade winds, low value of the Coriolis parameter and the large difference between the surface temperature and the temperature of the return flow at depth (when one considers the ocean column as a whole). The transport exhibits significant interannual and decadal variability (Adamec et al. 1993, Dong and Sutton 2001; Sato et al. 2002) where the former is tied to fluctuations in large-scale climate variability including the North Atlantic Oscillation (NAO) and El Niño/Southern Oscillation (ENSO).

In contrast to the column integrated heat budget, the greatest impact of Ekman transport (Q_{ek}) on sea surface temperature (SST) anomalies occurs in midlatitudes, where strong and variable winds coupled with large temperature gradients can generate large SST anomalies (e.g. Frankignoul and Reynolds 1983; Frankignoul 1985). The surface currents respond nearly instantaneously to the winds, and thus Ekman heat transport can influence SSTs on sub-monthly time scales. Early studies of the extratropical ocean heat budget found that Q_{ek}, and specifically the anomalous meridional advection across the mean temperature gradient, was the dominant term in the formation of seasonal midlatitude SST anomalies (Namias 1959, 1965, 1972; Jacob 1967; Adem 1970, 1975; Clark 1972). These initial studies may have overestimated the impact of Q_{ek} on SSTs as they used the value for the Ekman current at the surface, which is substantially larger

than the transport averaged over the well-mixed surface layer (Frankignoul 1985). More recent analyses suggest that while anomalous Ekman heat transport is important for interannual extratropical SST variability, its contribution is generally smaller than the forcing associated with the net surface heat fluxes (Q_{net}; Frankignoul and Reynolds 1983; Haney 1985; Luksch and von Storch 1992; Qiu 2000; Sterl and Hazeleger 2003). In midlatitudes, Q_{net} and Q_{ek} often work in tandem to create SST anomalies; stronger westerly winds enhance the upward latent and sensible heat flux and the equatorward advection of cold water by anomalous Ekman currents, thereby cooling the underlying ocean. While the large-scale patterns of SST variability are generally set by the surface fluxes, Ekman heat transport is necessary to obtain the detailed structure and correct magnitude of these patterns (Luksch 1996; Seager et al. 2000; Haarsma et al. 2005).

Under some circumstances Ekman transport may play a pivotal role in the evolution of SST anomalies. Ocean general circulation models (OGCMs) driven by observed surface observations indicate that the transition from warm to cold conditions in the central North Pacific during the winter of 1976-77 was driven in part by Ekman transport (Haney 1980; Miller et al. 1994). Seager et al. (2001) found that the post 1976 cooling due to Q_{ek} was so strong that even though the wind speed increased, the SST decreased more than the air temperature and thus Q_{net} heated the underlying ocean damping the negative SST anomaly. In addition, the associated wind stress curl changes that began in 1976 over the central Pacific created westward propagating baroclinic Rossby waves that subsequently reduced SSTs in the western Pacific Ocean about 5 years later (e.g. Deser et al. 1999; Schneider and Miller 2001; Seager et al. 2001). Following the Rossby wave

adjustment, Ekman transport enhanced this cooling to the east of Japan, reinforcing the decadal ocean signal (Seager et al. 2001; Kwon and Deser 2007).

Global atmospheric teleconnection patterns associated with SST anomalies in the tropical Pacific influence air-sea heat fluxes and Ekman transport, and thus the atmosphere acts like a "bridge" between the equatorial Pacific and much of the world's oceans during ENSO events (as reviewed by Alexander et al. 2002). In El Niño winters, the enhanced cyclonic circulation around a deepened Aleutian low results in anomalous northwesterly winds that advect relatively cold dry air over the western North Pacific, anomalous southerly winds that advect warm moist air along the west coast of North America, and enhanced surface westerlies over the central North Pacific (Fig. 1). The associated Q_{net} and Q_{ek} anomalies cool the ocean between 30ºN-50ºN west of ~150ºW and warm the ocean in the eastern ~1/3 of the North Pacific (Park et al. 2006; Liu and Alexander 2007). ENSO teleconnections also extend to the North Atlantic where the circulation around the anomalous low in the midlatitudes reduces the trade winds, warming the tropics and enhances the westerlies, which cools the ocean along the east coast of the United States (e.g. Curtis and Hastenrath 1995; Enfield and Mayer 1997; Lau and Nath 2001).

Alexander (1990) used output from an AGCM, with ENSO-related SSTs specified as boundary conditions in the tropical Pacific, to drive a variable-depth ocean mixed layer model (MLM) over the North Pacific, while Alexander (1992a) examined the coupled response of the AGCM-MLM system to ENSO. Both studies established that changes in the near surface circulation associated with El Niño induced a fairly realistic North Pacific SST anomaly pattern during boreal fall and winter. Using model experiments with

a similar design, Lau and Nath (1994, 1996, 2001) found that these bridge-induced SST anomalies could be fairly well simulated by a 50 m slab model driven by surface heat fluxes. Alexander et al. (2002), revisited this issue with a more comprehensive set of AGCM-MLM experiments and found that the ENSO-induced SST anomalies were relatively well simulated by the model, although the amplitude of the North Pacific anomalies were smaller than observed during winter. They suggested that the weaker anomalies could have resulted from the absence of dynamical ocean processes in the model. A potentially important process missing from the aforementioned studies was Ekman heat transport, although Alexander et al. (2002) computed the ENSO-driven Q_{ek} as a diagnostic, i.e. it did not influence SST in the ocean model. The diagnosed Q_{ek} values were generally in phase with Q_{net} but approximately 1/2 as large over the North Pacific Ocean in boreal winter.

Studies using AGCM-mixed layer ocean models have reached different conclusions on the impact of the bridge-related North Pacific and North Atlantic SST anomalies on the atmosphere (Alexander 1992b; Bladé 1999; Lau and Nath 1996, 2001). More recent model experiments suggest that atmosphere-ocean coupling outside of the tropical Pacific modifies the extratropical atmospheric circulation anomalies but these changes are of modest amplitude and depend on the seasonal cycle and air-sea interactions both within and beyond the Northern Hemisphere Oceans (Alexander et al., 2002).

In the Atlantic, Peng et al. (2005) found that imposed tropical SST anomalies induced an extratropical response in late winter in an AGCM coupled to a slab ocean model. The response, consisting of the NAO and the North Atlantic "SST tripole", developed one to two months later in the model than in observations. In a follow-on experiment, Peng et al.

(2006) included Ekman heat transport in the ocean model. Mutual reinforcement between the anomalous Q_{ek} and Q_{net} induced extratropical SST anomalies in early winter that were twice as strong as when no Ekman transport was included. In turn, the larger extratropical SST anomalies led to the development of an NAO response by November-December-January (NDJ). By February-March-April (FMA), the sign of the Q_{net} reversed in the Gulf Stream region so that it opposed the anomalous Q_{ek} and the magnitude of the SST and atmospheric circulation anomalies were similar in the simulations with and without Ekman forcing. Thus, the response developed more rapidly and was also more consistent with the observed evolution of the dominant patterns of atmosphere-ocean variability when Q_{ek} was included in the ocean model.

To what extent does Ekman heat transport impact the ENSO-driven SST anomalies in both the North Pacific and North Atlantic as part of the coupled atmosphere-ocean system? Does Q_{ek} alter the role of surface fluxes in the temperature tendency as suggested by the studies Seager et al. (2001) and Peng et al. (2006)? Do the Ekman-induced SST differences feedback on the atmospheric circulation? We address these questions using an AGCM with specified SSTs in the tropical Pacific and a mixed layer model over the remainder of the global oceans. Experiments are conducted with and without Ekman heat transport added to the SST equation in the ocean model. The experiment design is described in section 2. The results, including the influence of ENSO on SST and mixed layer depth (MLD) anomalies, the role of Q_{ek} and Q_{net} in generating these anomalies and the impact of ENSO plus air-sea feedback on the atmospheric circulation, is presented in section 3. The findings are summarized and discussed in section 4.

2. Experiment design

We have conducted two sets of model experiments to examine how ENSO-related Ekman heat transport anomalies influence the upper ocean, air-sea interaction and the atmospheric circulation. In both experiments, SSTs in the eastern tropical Pacific Ocean (15°S-15°N, 172°E-South American Coast) are prescribed to evolve as observed over the period 1950-1999. In the mixed layer model ("**MLM**") experiment, the ocean model is coupled to the AGCM at gridpoints in ice-free regions that are outside of the tropical east Pacific (Fig. 2). The SST is not smoothed along the boundary between the region with specified SSTs and the MLM. Sea ice is prescribed to repeat the climatological seasonal cycle and the ocean model is not active beneath the ice. The model includes local atmosphere-ocean fluxes, penetrating solar radiation and the turbulent entrainment of water into the mixed layer from below, but not mean vertical motions or horizontal processes. The temperature and salinity in all model layers are damped toward their monthly mean climatological values on a 10-year timescale to crudely represent vertically varying processes, such as the mean geostrophic heat transport, in order to retain a stable density profile.

Due to the absence of ocean currents and errors in the atmosphere and ocean model, surface heat and salt flux corrections are applied to maintain realistic seasonal cycles of SST and surface salinity. The surface heat and salt flux corrections are obtained from a 20-year MLM simulation using surface fluxes from a GFDL AGCM simulation with observed climatological SSTs as boundary conditions. Prior to each time step, the SST is set to the observed climatological value on that day. The MLM is then run for one time step where the difference between the model and observed SST is used to compute the

heat flux correction necessary for the model to match observations at each grid point. A similar method is used to obtain the salt flux correction. This procedure is repeated to obtain 20 years of daily correction values. Long-term monthly mean corrections are computed and then linearly interpolated to daily values, which are added to the temperature and salinity tendency equations. The heat flux corrections primarily compensate for the absence of ocean heat flux convergence and errors in the surface shortwave radiation (Alexander et al. 2000).

While the observed vertical structure of wind-induced currents is more complex than Ekman's original theory, the vertically integrated Ekman heat transport appears to be a more robust quantity (e.g. Weller and Plueddeman 1996). Here we assume that the Ekman heat transport is distributed over the MLD (e.g. see Frankignoul 1985) and its impact on the mixed layer temperature (or equivalently the SST) tendency is given by $Q_{ek}/(\rho C\text{MLD})$, where ρ, the density of seawater, is assumed to have a constant value of 1024.5 kgm^{-3}. The direct effect Ekman pumping on interannual mixed layer temperature, salinity and depth anomalies is generally small compared to turbulent entrainment (White et al. 1980, Frankignoul 1985, Alexander 1992a) and thus is not included here.

The Ekman transport/mixed layer model ("**EKM"**) experiment is identical to the MLM experiment except that Q_{ek} anomalies are added to the mixed layer temperature equation at most ocean model grid points (Fig. 2). Q_{ek} is not added to the ocean model at gridpoints immediately adjacent to the coast and from 6°S - 6°N to avoid singularities and to focus on the direct impact of Q_{ek} on SST rather than on Ekman-driven upwelling along the coast or the equator. The heat flux due to Ekman advection (Wm^{-2}) is computed using

$$Q_{ek} = C/f\left[-\tau_y \frac{\partial SST}{\partial x} + \tau_x \frac{\partial SST}{\partial y}\right], \quad (1)$$

where C is the specific heat capacity of seawater, f the Coriolis parameter, τ_x and τ_y are the zonal and meridional wind stress, and ∂SST/∂x and ∂SST/∂y are the zonal and meridional sea surface temperature gradients. The difference between long-term mean SST in the MLM and EKM experiments is < ±0.2ºC at nearly all model grid points. Likewise, the mean surface winds are nearly identical in the two experiments, with differences of < ±0.25 ms^{-1} at nearly all Northern Hemisphere Ocean grid points. Thus, the climatological Q_{ek} fields, derived using Eq. 1, are very similar in the two experiments.

Q_{ek} anomalies are added to the ocean model in the EKM simulations rather than the total Ekman transport so that the same flux correction could be used in the two experiments while maintaining a similar mean SST state. The Q_{ek} anomalies were obtained as follows. First daily Q_{ek} values in the MLM simulations were computed using Eq. 1. They were subsequently averaged over time and across ensemble members to form long-term monthly means. The monthly means were interpolated to daily Q_{ek} values and then subtracted from the total Ekman transport on the corresponding Julian day in the EKM simulations.

The model integrations have been performed with the GFDL R30 AGCM (Gordon and Stern 1982; Broccoli and Manabe 1992), which has an equivalent horizontal resolution of ~2.25° latitude by 3.75° longitude and 14 vertical sigma levels. The MLM consists of a grid of independent column models that include a bulk mixed layer atop a multi-layer system. The bulk model, based on the formulation of Gaspar (1988),

simulates the mixed layer temperature (equivalent to SST), salinity and depth. Beneath the mixed layer, heat is redistributed via convective overturning, vertical diffusion, and penetrating solar radiation. The bottom of each column is 1000 m or the actual depth of the ocean, which ever is shallower. For open-ocean points there are 31 levels from the surface to 1000 m with 15 layers in the upper 100 m. All layers completely within the mixed layer are set to the bulk model values. The ocean model and the method used to couple it to the R30 AGCM are described in more detail in Alexander et al. (2000).

Both experiments consist of an ensemble of sixteen 50-year simulations, where each member within an experiment is initiated from a different atmospheric state obtained from a long AGCM simulation. The results are presented for the difference between the ensemble average of the MLM and EKM simulations, and the spread among the members is used to assess statistical significance based on the t-test. The findings are presented using composite analyses (e.g. Rasmusson and Carpenter 1982, Harrison and Larkin 1998), which are constructed based on 9 El Niño (warm) events beginning in: 1957, 1965, 1969, 1972, 1976, 1982, 1987, 1991 and 1997 and 9 La Niña (cold) events: 1950, 1954, 1955, 1964, 1970, 1973, 1975, 1988 and 1998. The first 8 El Niño and La Niña events were identified by Trenberth (1997), to which we added the 1997 El Niño and 1998 La Niña events. The year in which ENSO peaks and the following year are designated by (0) and (1), respectively.

We originally planned to use the MLM simulations described in Alexander et al. (2002), which were performed on the GFDL computer system. However, the model's climate was altered when the AGCM was integrated on Earth System Research Laboratory (ESRL) computers, where we performed the EKM simulations. Even after

extensive diagnostic tests the cause of this divergence in climates was unclear, although it was likely due to differences in the compilers.[1] Thus, the MLM simulations used here were performed on ESRL computers, so that differences between the EKM and MLM experiments isolated the impact of Ekman heat transport. The mean differences between the GFDL and ESRL MLM simulations were strongest in high latitudes in the stratosphere, where the latter had a cold bias. The difference between the two systems for ENSO composites reached a maximum of ~20 m at 500 mb, approximately 20% of the overall response to tropical SST anomalies. The Aleutian low was deeper in the ESRL simulations in better agreement with observations.

Several of the model fields are compared to those obtained from the National Center for Environmental Prediction (NCEP) reanalysis (Kalnay et al. 1996; Kistler et al. 2001). Some ("A") variables, such as SLP or geopotential heights, are closer to the true state, than other ("C"), such as the surface wind stress or heat flux, which have greater dependence on the model used in the reanalysis system. The reanalysis and other data-based fields presented here have been interpolated to the R30 AGCM grid.

3. Results

a. SST and MLD

We primarily focus on the atmospheric bridge to the Northern Hemisphere Oceans during boreal winter when the impact of Ekman transport in the model is the most robust. Composite El Niño – La Niña differences, also referred to as anomalies, are indicted by a

[1] The simulations conducted at GFDL were performed on a CRAY computer which is no longer in operation and whose complier was specific to that system. Thus, it was not possible to run the EKM experiments at GFDL or port the CRAY compiler to ESRL's computer systems.

, while the ENSO anomalies in the EKM minus MLM experiments are denoted by a Δ. The SST (°C) composite during January-February-March (JFM) in the year after ENSO peaks (Yr 1) for observations (Smith et al. 1996) and the EKM and MLM experiments are shown in Fig. 3. The observed atmospheric bridge includes negative SST* in the central North Pacific and positive SST* along the coast of North America, both of which exceed 1°C in magnitude. In the Atlantic, negative anomalies on the order of 0.5-1.0°C occur in the Gulf of Mexico and along the east coast of the United States, while positive anomalies of this magnitude are located in the tropics north of the equator. Warming also occurs across the Indian Ocean. Many of these anomalies are well simulated in both the EKM and MLM, although the model values are less than observed along the west coast of the United States, over portions of the Atlantic, and in the equatorial Indian Ocean.

Including Ekman heat transport (diagnosed from the difference between the EKM and MLM experiments) alters the amplitude of several bridge-generated SST signals (Fig. 3d), which generally improves the simulation of SST anomalies over the Northern Hemisphere Oceans. The largest change occurs in the central North Pacific, where including Q_{ek} results in ΔSST of ~-0.4°C, leading to SST* < -1.0°C in the EKM experiment (Fig. 3b), similar to the observed signal (Fig. 3a). Including Q_{ek} further warms the ocean around 45°N in the eastern North Pacific and near 10°N, 150°E. In the Atlantic, the ΔSST field resembles the SST tripole pattern (e.g. Cayan 1992; Venzke et al. 1999; Sutton et al. 2001) with negative values east of Florida flanked by positive values near 15°N and 55°N. The magnitude of these changes reach 0.2°-0.3°C for JFM(1) and amplify the warm ENSO-related SST anomalies in the tropical Atlantic, increase the amplitude and eastward extent of the cold SSTs along the east coast of the United States,

and create small positive anomalies in the subarctic Atlantic where the overall bridge signal is weak. The ΔSST is positive (negative) in the northern (southern) Indian Ocean but of modest amplitude (~ 0.1°C).

The mixed layer depth anomalies (m) during JFM(1) from observations (White 1995), the EKM and MLM experiments and ΔMLD are shown in Fig. 4. The observed MLD, obtained from the Joint Environmental Data Analysis Center (JEDAC 2008), is defined as the depth at which the temperature is 1.0°C cooler than at the surface based on bathythermograph (BT) temperature measurements for the years 1956-1999. The MLD was not estimated by JEDAC at high latitudes where it is primarily controlled by salinity. The MLD in the MLM is computed explicitly from the turbulent kinetic energy equation and depends on both temperature and salinity (see Alexander et al. 2000). Both the EKM and MLM simulations reproduce the general pattern of the observed ENSO-related anomalies with positive values in the central North Pacific ringed by negative values. The maximum MLD*, on the order of 50 m in both experiments, is just slightly less than observed. The model underestimates the MLD* shoaling in the northeast Pacific, although the observed anomalies are likely to be overestimated, since salinity and vertical movements of the halocline, not measured by BTs, regulate MLD in the Gulf of Alaska (Whitney and Freeland 1999; Alexander et al. 2008). Including Q_{ek} increases the MLD* by ~10 m near 30°N, 170°W (significant at the 99% level; Fig. 4d), which enhances the southern portion of the bridge-related signal in the central Pacific.

In the North Atlantic, the mixed layer is observed to be shallower during El Niño than La Niña events (MLD*< 0) in southeast portion of the domain and deeper in midlatitudes, with the separation between the two extending diagonally across the basin

from Florida to Spain (Fig. 4a). This structure is better represented in the EKM than in the MLM simulations, due to the positive ΔMLD located at ~35°N, 70°W, but the MLD anomalies are still much smaller than in observations. The MLD* shoals in the northern North Atlantic in both experiments, but the anomalies have significantly greater amplitude in the EKM experiment. The model and observations also differ in the northeast portion of the basin but it is unclear whether this is due to model error, variability in this region not associated with ENSO, or the difficulty in estimating MLD from BTs. Consistent with previous studies (e.g. Deser et al. 1996), there is a strong inverse relationship between ΔSST (Fig. 3d) and ΔMLD (Fig. 4d) in midlatitudes of the Pacific and Atlantic, since cold dense water enables the mixed layer to penetrate deeper into the ocean.

b. SST forcing and feedback: Q_{ek} and Q_{net} anomalies

When Ekman heat transport is introduced into the coupled model it affects the local SST and MLD, but its full impact depends on the subsequent air-sea interactions (as shown schematically in Fig. 5). In the extreme case of no feedback, Q_{ek} in the EKM experiment would be identical to the value diagnosed (but not applied) in the MLM experiment and there would be no change in Q_{net} between the two. It is possible for Q_{ek} to be balanced by terms other than the net heat flux, such as entrainment at the base of the mixed layer, but these terms tend to be small in winter (Alexander et al. 2000). The response could also consist of a basic thermodynamic feedback, where the Q_{ek} forcing creates an SST anomaly that is damped by the net heat flux without significantly altering the atmospheric circulation. The damping is analogous to its counterpart in the stochastic

model for SST anomalies (e.g. Frankignoul and Hassleman 1977): after high frequency atmospheric forcing creates SST anomalies the "slow" response relaxes the SSTs towards climatology, since positive (negative) SST anomalies lose more (less) heat to the atmosphere. Finally, the air-sea interaction can be dynamic, where the atmospheric circulation changes in response to either local or remote SST anomalies, altering Q_{ek} and/or Q_{net}, which in turn can feed back on the ocean below. We explore the nature of the forcing and feedback by comparing Q_{ek} and Q_{net} in the EKM and MLM simulations.

The anomalous Ekman heat transport during JFM (1) derived from NCEP reanalysis and the EKM experiment are shown in Figs. 6a and 6b, respectively. In both reanalysis and the model, the ENSO signal includes stronger surface westerlies over the central and western North Pacific, resulting in anomalous southward Ekman transport that cools the underlying ocean. The cooling is greatest (Q_{ek}^{*}<-20 Wm^{-2}) in the vicinity of 32°N, 165°W, where the anomalous westerlies are strongest. A secondary maximum occurs along ~40°N from 150°E-170°W where modest westerly winds overlay a strong mean meridional SST gradient (Fig. 1). The amplitude of the negative anomalies are smaller in the EKM, but this may not be solely due to errors in the model: Millif et al. (1999) found that the extratropical winds in reanalysis were stronger than those derived from scatterometer measurements and Q_{ek}^{*} computed from in situ observations (Da Silva 1994) are of similar amplitude to those in the EKM experiment (not shown). Along the west coast of North America, southeasterly winds warm the underlying ocean with a maximum Q_{ek}^{*} of ~10 Wm^{-2} from 40°N-50°N. In the Atlantic, Q_{ek}^{*} indicates warming (cooling) at most locations north (south) of ~40°N in reanalysis and ~45°N in the EKM.

Previous analyses have indicated that Ekman heat transport anomalies are primarily associated with anomalous meridional currents, as given by $c/f\left(\tau_x^{'}\partial\overline{\mathrm{SST}}/\partial y\right)$, where ($\bar{}$) denotes the time mean and ($'$) the departure from the time mean. This is also true in the EKM response to ENSO, where stronger than normal westerlies ($\tau_x^{'} > 0$) and colder temperatures towards the poles ($\partial\overline{\mathrm{SST}}/\partial y < 0$) resulted in cooling ($c/f\left(\tau_x^{'}\partial\overline{\mathrm{SST}}/\partial y\right)^{*} < 0$) of the central North Pacific during El Niño relative to La Niña events. There is a compensating warming by $c/f\left(\bar{\tau}_x\partial\mathrm{SST}'/\partial y\right)^{*}$, as the mean westerlies drive southward Ekman flow across the anomalous negative SST gradient between 35°N-50°N. The magnitude of the latter term is ~1/3 of $c/f\left(\tau_x^{'}\partial\overline{\mathrm{SST}}/\partial y\right)^{*}$. To the south of the SST anomaly, northward advection driven by the mean trade winds also weakly warms the ocean between 20°N-25°N, 180°-140°W. The other components of $\left(Q_{ek}^{'}\right)^{*}$ have a negligible impact on SST*.

Q_{ek}^{*} diagnosed from the winds and SST gradient in the MLM experiment (but not included in the MLM SST equation) are shown in Fig. 6c. The pattern and values of Q_{ek}^{*} in the MLM are very similar to those in the EKM experiment over the Pacific. Allowing Q_{ek} to impact the coupled system (determined by comparing Fig. 6b and 6c) slightly reduces the positive Q_{ek}^{*} values in the northeast Pacific. The difference between Q_{ek}^{*} in the two experiments, however, is < 5 Wm^{-2} at nearly all Pacific grid points (not shown), indicating that air-sea feedback has a modest impact on the surface winds and thus Q_{ek}^{*} over the basin. While the Atlantic Q_{ek}^{*} pattern is similar in the MLM and EKM experiments, the amplitude is greater in the EKM, particularly north of ~40°N where Q_{ek}^{*}

is approximately 2-3 times larger than in the MLM. Thus, allowing Ekman heat transport to impact the coupled system has a positive feedback on Q_{ek}^{*} in the Atlantic.

The anomalous net heat flux (positive into the ocean), obtained from NCEP reanalysis (Fig. 7a) and the EKM experiment (Fig. 7b) are fairly similar over the Northern Hemisphere Oceans in JFM(1). Consistent with previous studies, Q_{net}^{*} strongly cools the central North Pacific and warms the northeast Pacific in reanalysis and the EKM experiment, although the maximum cooling is stronger and further west in reanalysis. However, the pattern of Q_{net}^{*} in the EKM, with the strongest cooling in the central Pacific, is consistent with ship-based estimates (Park et al. 2006). In the Atlantic, $|Q_{net}^{*}| > 30$ Wm^{-2} along the south east coast of the United States, and northeast of Newfoundland (~56°N, 55°W), on par with the ENSO-driven heat fluxes in the North Pacific.

Comparing Figs. 6 and 7 indicates that Q_{ek}^{*} is of relatively large amplitude and coincident with Q_{net}^{*} over the central and northeast Pacific and the subarctic Atlantic enhancing the SST forcing during late winter in these regions. The Q_{ek}^{*} minima in the central Pacific, however, is 50-80% as large and displaced to the southeast of the Q_{net}^{*} minima. In the EKM experiment, Q_{ek}^{*} and Q_{net}^{*} are of opposite sign south of Japan (20°N-30°N, 120°E-140°E), in a small region east of the mid Atlantic states (70°W, 35°N) and in the subtropical Atlantic (20°N-30°N, 30°W-60°W)

Including Ekman transport indirectly affects the surface heat flux as indicated by the difference between the ENSO-related net flux anomalies in the two experiments (ΔQ_{net}, Fig. 7c). ΔQ_{net} is quite small over the Pacific, with positive values on the order of 10 Wm^{-}

[2] centered on 30°N, 160°W, indicative of reduced cooling of the central North Pacific Ocean in the EKM relative to the MLM experiment. Since the EKM-MLM surface circulation changes are negligible over the North Pacific (|ΔSLP| < 0.6 mb at nearly all grid points, not shown), these positive ΔQ_{net} values represent thermodynamic damping of the negative SST anomalies (Fig. 5, bottom left panel). The air-sea interaction is quite different in the Atlantic, where ΔQ_{net} and Q^*_{net} have the same sign over most of the basin indicating a dynamic feedback that acts to amplify the ENSO heat flux signal. This feedback is relatively large, i.e. ΔQ_{net} is on the order of 25% to 50% of Q^*_{net}, but is statistically significant only in small regions to the northeast and southwest of Newfoundland and off the west African coast.

The relationship between Q_{net}, Q_{ek} and SST over the ENSO cycle in the EKM and MLM experiments is explored further in Fig. 8 for the central North Pacific (27°N-37°N, 155°W-175°W), western Atlantic (25°N-32°N, 60°W-78°W) and Subarctic Atlantic (50°N-55°N, 30°W-50°W) regions (boxes in Fig. 3d). For each region, the upper panels show Q^*_{ek} and Q^*_{net} in both experiments, while the bottom panels show ΔSST and the difference in the flux-induced SST tendency, denoted by $\Delta(Q/\mathrm{MLD})$. The latter is given by $([Q_{ek}+Q_{net}+Q_{cor}]/\mathrm{MLD})^*$ in the EKM minus $([Q_{net}+Q_{cor}]/\mathrm{MLD})^*$ in the MLM experiment, since Δ in the other mixed layer heat budget terms, including the entrainment heat flux (Q_{we}), are generally small. The surface heat flux correction, Q_{cor}, is the same in the EKM and MLM experiments but can impact the SST* via differences in MLD between experiments. The anomalous SST tendency is also influenced by the mean seasonal cycle of MLD, which ranges from 20-30 m during summer for all three regions to approximately 70-90 m (105-125 m) in the midlatitude (subarctic) regions during

winter in both experiments (not shown). Thus, SSTs will change more rapidly in summer than in winter for the same forcing.

In the central Pacific (Fig. 8a), Q^*_{ek} is nearly identical in the EKM and as diagnosed from the MLM simulations over the course of the ENSO cycle. Q^*_{net} is also similar in the two experiments, but it is slightly more negative from Aug(0)-Nov(0) and positive from Jan(1)-Jul(1) in the EKM. This difference in Q^*_{net} coincides with slightly warmer ΔSSTs during summer and colder ΔSSTs in the following winter/spring, suggesting weak thermodynamic damping of the ΔSST by the surface fluxes over the full ENSO cycle. In the central Pacific, Δ(Q/MLD) primarily results from the inclusion of Q^*_{ek} and begins to generate negative ΔSST by Dec(0), although ΔQ_{we} also cools the ocean between Aug(0) and Jan(1) (not shown). The general relationship between Q_{ek}, Q_{net}, and SST in the northeast Pacific is similar to the central Pacific in that Q^*_{ek} enhances the ENSO driven SST anomalies that are weakly damped by ΔQ_{net} (not shown).

In the western Atlantic region, Q_{ek} anomalies slightly cool the ocean from Aug(0) – Feb(1) in the EKM experiment, similar to the values diagnosed from the MLM (Fig. 8b). In both experiments, Q^*_{net} warms the ocean in the fall and winter but the heat fluxes are roughly 5 Wm^{-2} lower in the EKM from Nov(0)-Jan (1). So, while air-sea coupling does not greatly alter Q^*_{ek} in the western Atlantic, there is positive feedback between the surface heat flux and SST in fall and winter, as both ΔQ_{net} and ΔSST are negative. The combined cooling of ΔQ_{net} and Q^*_{ek} (Δ[Q/MLD] < 0) result in negative ΔSSTs after October(0) that decrease to ~-0.2°C by Feb(1). In the subarctic Atlantic region, a slight rise in ΔSST in summer and early fall occurs despite negative ΔQ/MLD (Fig. 8c), partly

due to positive ΔQ_{we} from Jul(0) – Sep(0) (not shown). Large differences between experiments occur in this region during winter when ΔQ_{we} is negligible. During Jan(1)-Mar(1) Q^*_{ek} is slightly larger in the EKM than in the MLM experiment while Q^*_{net} is substantially greater in EKM from Nov(0)-Mar(1), resulting in positive ΔQ/MLD in winter and ΔSST of ~0.25°C that persist through spring. The shallower mixed layer in the subarctic Atlantic in the EKM experiment (Fig. 4), decreases the thermal inertia, which increases the positive ΔSST tendency during winter. These findings suggest that changes in the ENSO-driven atmospheric circulation over the North Atlantic induce positive air-sea interaction when Ekman heat transport is included in the coupled system.

c) Atmospheric response

The wintertime atmospheric response to ENSO, indicated by the composite El Niño – La Niña 500 mb geopotential height (z500*), from NCEP reanalysis and the EKM and MLM experiments are shown in Fig. 9. The EKM and MLM model simulations reproduce the observed ENSO signal remarkably well both in terms of the pattern and amplitude of the anomalies (the pattern correlation between both experiments and observations is ~0.8). The two are nearly identical over the Pacific, but the difference between them (Δz500, Fig. 9d), includes a ridge over Canada, trough over the eastern US/West Atlantic and ridge above the subtropical east Atlantic/northwest Africa (all significant at the 95% level). The inclusion of Q_{ek} augments ENSO teleconnections over North America, the North Atlantic and western North Africa by approximately 20% to 40%, as well as improving the correspondence between the model and nature. Indeed, the pattern correlations between z500* in observations with the ensemble mean in the EKM

and MLM over the North America-Atlantic Sector (20°N-90°N, 120°W-0°) are 0.75 and 0.66 respectively, which are significantly different from each other at the 95% level as indicated by a t-test using the spread in the pattern correlations across the 16 MLM and EKM ensemble members. The circulation anomalies have an equivalent barotropic structure where the height anomalies at 200 mb (not shown) are stronger and in the same location as the anomalies at 500 mb.

The atmospheric circulation anomalies during ENSO are explored further in Fig. 10a, which displays the anomalous zonal winds (ms^{-1}) at 200 m (U200*) in the EKM experiment. Anomalous westerlies (U200* > 0) extend across the central North Pacific, the United States and the North Atlantic in midlatitudes. They are flanked by anomalous easterlies in the tropics and high latitudes that are strongest and most extensive in the Pacific sector. The inclusion of Q_{ek} enhances U200 anomalies over most of the Northern Hemisphere, i.e. ΔU200 (Fig. 10b) and U200* have the same sign and pattern. The Ekman induced changes are on the order of 1-2 ms^{-1} over eastern Asia/West Pacific and North America/western Atlantic, significant at 99% and 95% levels, respectively. The former may be in response to the positive ΔSST in the tropical northwest Pacific Ocean and/or the positive (negative) ΔSST to the north (south) of the equator in the Indian Ocean (Fig. 3). Like the ΔSST, the Ekman-induced change in precipitation (ΔP) has a complex structure over the tropical west Pacific and Indian Oceans (not shown), and thus it is difficult to relate the atmospheric circulation changes over Asia to a specific diabatic heat source/sink.

d. Atlantic Air-sea Interaction

Figs. 6-10 indicate that Ekman heat transport significantly enhances air-sea interaction and the response to ENSO over the North Atlantic. To examine these interactions in greater detail, the SST/SLP/$\vec{\tau}$ and 200 mb streamlines/P anomalies are presented for the Atlantic sector in the EKM (Fig. 11 top) and for the EKM-MLM (Fig. 11 bottom). SLP* in the EKM bears a strong resemblance to the negative phase of the NAO, with a low in the central North Atlantic and a high centered over southeast Greenland. High pressure also extends across the tropical Atlantic. The anomalous surface winds oppose the mean trade winds and westerlies at ~20°N and 50°N, respectively, warming the underlying ocean via the surface heat fluxes (Fig. 7) by reducing the wind speed. The anomalous easterlies between 45°N and 60°N also warm the ocean by enhancing the poleward Ekman heat transport (Fig. 6), while anomalous northerly winds advect cold continental air over the Gulf of Mexico and along the east coast of the United States, resulting in negative Q_{net} and SST anomalies. In the upper troposphere, cyclonic circulation in midlatitudes and anticyclonic circulation over the Caribbean are associated with enhanced winds and precipitation extending from Mexico to Western Europe and decreased precipitation over northeastern South America (Fig 11b). Overall, the EKM experiment is consistent with previous observational and modeling studies of the response to ENSO in the Atlantic sector (van Loon and Madden 1981; Van Loon and Rogers 1981; Lau and Nath 2001; Pozo-Vázquez et al., 2001).

The impact of including Q_{ek} resembles the overall response to ENSO over much of the Atlantic (compare top and bottom panels of Fig. 11), including the aforementioned ΔSST tripole with positive (negative) values at 10°N and 50°N (30°N), and a negative NAO-like pattern, although the ΔSLP center in midlatitudes is shifted west relative to the

overall ENSO response. The Ekman-induced increase in the atmospheric circulation can reach 40% of the overall signal, e.g. the ΔSLP is ~1.0 mb, while SLP* is ~2.5 mb in the EKM over Greenland. Likewise including Ekman transport increases the strength of the upper-level circulation and precipitation over the storm track region. While ΔP is negligible over the positive ΔSST in the tropical Atlantic, there are substantial but localized changes over South America, e.g. ΔP > 0 near 0°, 65°W and 8°S, 45°W, and ΔP < 0 further south and west. These precipitation changes appear to influence the circulation over the Amazon (5°S, 40°-70°W) and may impact the broader circulation over the North Atlantic (e.g. Peng et al. 2005).

4. Summary and Discussion

The role of anomalous Ekman heat transport in the ocean on ENSO teleconnections was explored using coupled model experiments. In the MLM experiment, observed SSTs were specified in the tropical Pacific, while a variable depth mixed layer model was employed elsewhere over the global oceans. The same experimental design was used in the EKM simulations with the addition of Q_{ek} in the mixed layer temperature equation. In both the MLM and EKM experiments the ENSO response during winter included a deeper Aleutian Low with the associated cyclonic circulation that cooled the central Pacific and warmed the northeastern Pacific via the surface heat fluxes. In the EKM experiment, including Q_{ek} enhanced the ENSO forcing in the central and northeast North Pacific, increasing the magnitude of the SST anomalies by ~1/3 in these regions. As a result, the amplitude of the SST anomalies exceeded 1.0°C in the central North Pacific in the EKM experiment, on par with the observed ENSO signal. Differences between the

EKM and MLM simulations indicated that Q_{net} weakly opposed the North Pacific SST anomalies in the EKM experiment indicative of thermodynamic damping. This may explain why the ratio of Q_{ek} to Q_{net} was lower in the EKM experiment than as diagnosed from the MLM simulations here and in Alexander et al. (2002). These Ekman-induced changes in Q_{net} did not significantly impact the free troposphere, as only minor differences arose between the atmospheric circulation anomalies in the two experiments over the North Pacific.

While the atmospheric response to ENSO over the Atlantic is weaker than in the Pacific, it appears to be robust. The ENSO teleconnections in the MLM and EKM experiments resemble observations, including low pressure and negative SSTs off the east coast of the United States, similar to negative phase of the NAO and SST tripole patterns (c.f. van Loon and Madden 1981; Pozo-Vázquez et al. 2001). The AGCM experiments of Lau and Nath (2001) also showed that ENSO induced the negative phase of the NAO/SST tripole patterns and that the resulting Atlantic SST anomalies appeared to enhance the local atmospheric circulation. In our study, including Ekman transport further enhanced the Atlantic Ocean temperature anomalies and the overlying atmospheric circulation, including the upper-level height anomalies, jet stream and storm track.

The extent to which the bridge-related Atlantic SST anomalies feed back on the atmosphere is uncertain here as well as in Lau and Nath (2001), since in both studies SST anomalies over the global ocean can impact air-sea interaction in the Atlantic. In our study, the Ekman-induced response over the Atlantic may be caused or augmented by a wavetrain that propagates across eastern Asia, over the pole and into eastern North

America/Western Atlantic (Figs. 9d and 10d). Such features occur in idealized models as atmospheric Rossby waves driven by tropical diabatic heat sources (e.g. Hoskins and Karoly 1981; Ting and Sardeshmukh 1993) and in AGCMs with SST anomalies specified in the Indian and/or West Pacific Oceans (Hoerling et al. 2001b, 2004; Li et al. 2006; Annamalai et al. 2007). However, these studies mainly find that the circulation anomalies develop in the North Pacific as well as the North Atlantic, whereas in our experiments the Ekman-driven response is negligible over most of the North Pacific.

In contrast, Mathieu et al. (2004) concluded that the bridge-related SSTs in the Atlantic influenced the overlying atmospheric circulation based on AGCM experiments during ENSO years with and without Atlantic SST anomalies. In addition, observations (Czaja and Frankignoul 2002; Frankignoul and Kestenare 2005), AGCM experiments with specified Atlantic SST anomalies (Rodwell et al. 1999; Sutton et al. 2001; Peng et al. 2003), AGCM-slab ocean models (Watanabe and Kimoto 2000; Peng et al. 2005) and AGCM-MLM experiments (Cassou et al. 2007) all indicate positive feedback between the NAO and SST tripole during winter.

Why does there appear to be relatively strong air-sea feedback in the Atlantic but not the Pacific, even though the largest Ekman induced SST anomalies occur in the Pacific? The answer may lie in the proximity of the SST anomalies to the storm track. A stronger meridional SST gradient enhances the low-level baroclinicity, which is conducive to cyclogenesis (e.g. Hoskins and Valdez 1990). The Ekman-induced SST anomalies, located between 20°N-30°N in the western half of the Atlantic, enhance the SST gradient slightly south of the mean storm track entrance region. The equatorward position of the anomalous SST gradient relative to the upper-level storm track may lead to positive

feedbacks between the two due to the poleward tilt of baroclinic waves with height (Yin and Battisti 2004). In the Pacific, the largest anomalies are in the eastern half of the basin far from the storm track entrance region. Alternatively, the Ekman-induced changes in diabatic heating over South America (Fig. 11d) may excite a Rossby wave train that emanates into the extratropical Atlantic (Drevillion et al. 2003, Cassou et al. 2004), which may also alter the storm track (Peng et al. 2003, 2005).

Observational analyses indicate that during summer and fall the "North Atlantic horseshoe" SST pattern, which resembles the tripole shifted northeast by roughly 10°-20°, influences the NAO in the subsequent winter (Czaja and Frankignoul 2002; Frankignoul and Kestenare 2005). The EKM-MLM SST difference in summer/fall is similar to the horseshoe pattern, with positive SST centers near Europe and northwest Africa (not shown) and thus may influence the model's NAO in winter. However, it is unclear whether the extratropical horseshoe anomalies influence the atmosphere or are driven by the atmospheric response to SSTs in the tropical Atlantic with little feedback on the atmosphere, as suggested by the modeling studies of Cassou and Terray (2001), Drevillion et al. (2003), and Peng et al. (2005, 2006).

In the present study, we have examined the linear symmetrical response to ENSO by presenting the composite difference between El Niño and La Niña events. The SLP and SSTs for El Niño - neutral years and neutral - La Niña years in the EKM experiment are presented in Fig. 12 (La Niña values were multiplied by -1 to facilitate comparison with El Niño). The El Niño and La Niña anomalies are fairly similar (equal and opposite) over the North Pacific except that the amplitude is somewhat stronger and located ~20° further east during El Niño relative to La Niña events, in general agreement with the data

analyses and AGCM experiments of Hoerling et al. (1997, 2001a). In contrast, the response over the Atlantic is stronger during La Niña than El Niño events, especially when Ekman transport is included (not shown). This asymmetry appears to occur in nature as well, e.g. Pozo-Vázquez et al. (2001) identified the positive phase of the NAO as the response to La Niña but no significant signal during El Niño events. Using cluster analyses, Cassou et al. (2004) found a significant association between La Niña and the "Atlantic Ridge" regime, but no significant link with regimes during El Niño events. However, the Ridge regime, features a high at ~50ºN over the Central North Atlantic, ~15º south of its position found here and by Pozo-Vasquez et al. (2001). In addition, the apparent nonlinear response to ENSO in nature may not be statistical significant over the Atlantic (Sardeshmukh et al. 2000), and may be influenced by decadal fluctuations in the background flow (Deweaver and Nigam 2002). Thus, the asymmetrical response to ENSO, particularly over the Atlantic, warrants further study.

Acknowledgements

We thank Matt Newman, Clara Deser and three anonymous reviewers for their comments and suggestions. This research was supported by NOAA's Climate Variability and Prediction program.

References

Adamec, D., M. M. Rienecker, and J. M. Vukovich, 1993: The time varying characteristics of the meridional Ekman heat transport of the world ocean. *J. Phys. Oceanog.*, **23,** 2704-2716.

Adem, J., 1970: On the prediction of mean monthly ocean temperature. *Tellus*, **22,** 410-430.

Adem, J., 1975: Numerical-thermodynamical prediction of monthly ocean temperature. *Tellus*, **27,** 541-551.

Alexander, M. A., 1990: Simulation of the response of the North Pacific Ocean to the anomalous atmospheric circulation associated with El Niño. *Climate Dyn.*, **5,** 53-65.

Alexander, M. A., 1992a: Midlatitude atmosphere-ocean interaction during El Niño. Part I: the North Pacific Ocean. *J. Climate*, **5,** 944-958.

Alexander, M. A., 1992b: Midlatitude atmosphere-ocean interaction during El Niño. Part II: the Northern Hemisphere atmosphere. *J. Climate*, **5,** 959-972.

Alexander, M. A., J. D. Scott, and C. Deser, 2000: Processes that influence sea surface temperature and ocean mixed layer depth variability in a coupled model. *J. Geophys. Res.*, **105,** 16,823-16,842.

Alexander, M. A., I. Bladé, M. Newman, J. R. Lanzante, N.-C. Lau, and J. D. Scott, 2002: The atmospheric bridge: the influence of ENSO teleconnections on air-sea interaction over the global oceans. *J. Climate*, **15,** 2205-2231.

Alexander, M., A. Capotondi, A. Miller, F. Chai, R. Brodeur and C. Deser, 2008: Decadal variability in the Northeast Pacific in a physical-ecosystem model: The role of mixed layer depth and trophic interactions. *J. Geophys. Res.*, **113**, C02017, doi:10.1029/2007JC004359.

Annamalai, H., H. Okajima, and M. Watanabe, 2007: Possible Impact of the Indian Ocean SST on the Northern Hemisphere Circulation during El Niño**.** *J. Climate*, **20**, 3164–3189.

Bladé, I., 1999: The influence of midlatitude ocean-atmosphere coupling on the low-frequency variability of a GCM. Part II: Interannual variability induced by tropical SST forcing. *J. Climate*, **12,** 21-45.

Broccoli, A. J. and S. Manabe, 1992: The effects of orography on midlatitude Northern Hemisphere dry climates. *J. Climate*, **5,** 1181-1201.

Cassou, C., and L. Terray, 2001: Oceanic forcing of the wintertime low-frequency atmospheric variability in the North Atlantic European sector. A study with the ARPEGE model. *J. Climate*, **14,** 4266-4291.

Cassou, C., C. Deser and M. A. Alexander, 2007: Investigating the impact of reemerging sea surface temperature anomalies on the winter atmospheric circulation over the North Atlantic. *J. Climate*, **20**, 3510-3526.

Cassou, C., C. Deser, L. Terray, J. W. Hurrell, and M. Drévillon, 2004: Summer sea surface temperature conditions in the North Atlantic and their impact upon the atmospheric circulation in early winter. *J. Climate*, **17,** 3349–3363.

Cayan, D. R., 1992: Latent and sensible heat flux anomalies over the northern oceans: the connection to monthly atmospheric circulation. *J. Climate*, **5,** 354-369.

Clark, N. E., 1972: Specification of sea surface temperature anomaly patterns in the

eastern North Pacific. *J. Phys. Oceanogr.*, **2,** 391-404.

Curtis, S. and S. Hastenrath, 1995: Forcing of anomalous sea surface temperature evolution in the tropical Atlantic during Pacific warm events. *J. Geophys. Res.*, **100,** 15835-15847.

Czaja, A. and C. Frankignoul, 2002: Observed impact of Atlantic SST anomalies on the North Atlantic Oscillation. *J. Climate*, **15,** 606-623.

da Silva, A. M., C. C. Young and S. Levitus, 1994: Atlas of Surface Marine Data 1994, Volume 3: Anomalies of Heat and Momentum Fluxes. NOAA Atlas NESDIS 8, U.S. Department of Commerce, NOAA, NESDIS.

Deser, C., M. A. Alexander, and M. S. Timlin, 1996: Upper ocean thermal variations in the North Pacific during 1970 - 1991. *J. Climate*, **9,** 1841-1855.

——, 1999: Evidence for wind-driven intensification of the Kuroshio Current Extension from the 1970s to the 1980s. *J. Climate*, **12,** 1697-1706.

DeWeaver, E., and S. Nigam, 2002: Linearity in ENSO's atmospheric response. *J. Clim.*, **15**, 2446–2461.

Dong, B.-W. and R. T. Sutton, 2001: The dominant mechanism of variability in Atlantic ocean heat transport in a coupled ocean-atmosphere GCM. *Geophys. Res. Lett.*, **28,** 2445-2448.

Drevillon, M., C. Cassou, and L. Terray, 2003: Model study of the North Atlantic region atmospheric response to autumn tropical Atlantic sea-surface-temperature anomalies.

Quart. J. Roy. Meteor. Soc., **129,** 2591-2611.

Enfield, D. B. and D. A. Mayer, 1997: Tropical Atlantic sea surface temperature variability and its relation to El Niño-Southern Oscillation. *J. Geophys. Res.*, **102,** 929-945.

Frankignoul, C., 1985: Sea surface temperature anomalies, planetary waves, and air-sea feedback in the middle latitudes. *Rev. Geophys.*, **23,** 357-390.

Frankignoul, C. and K. Hasselmann, 1977: Stochastic climate models. Part 2. Application to sea-surface temperature variability and thermocline variability. *Tellus*, **29,** 284-305.

Frankignoul, C. and R. W. Reynolds, 1983: Testing a dynamical model for mid-latitude sea surface temperature anomalies. *J. Phys. Oceanogr.*, **13,** 1131-1145.

Frankignoul, C. and E. Kestenare, 2005: Observed Atlantic SST anomaly impact on the NAO: an update. *J. Climate*, **18,** 4089-4094.

Gaspar, P., 1988: Modeling the seasonal cycle of the upper ocean. *J. Phys. Ocean*, **18,** 161-180.

Gordon, C. T. and W. Stern, 1982: A description of the GFDL global spectral model. *Mon. Wea. Rev.*, **110,** 625-644.

Haarsma, R. J., E. J. D. Campos, W. Hazeleger, C. Severijns, A. R. Piola, and F. Molteni, 2005: Dominant modes of variability in the South Atlantic: study with a hierarchy of ocean–atmosphere models. *J. Climate*, **18,** 1719–1735.

Haney, R. L., 1980: A numerical case study of the development of large-scale thermal anomalies in the central North Pacific Ocean. *J. Phys. Oceanogr.*, **10,** 541-556.

——, 1985: Midlatitude sea surface temperature anomalies: a numerical hindcast. *J.Phys. Oceanogr.*, **15,** 787-799.

Harrison, D. E. and N. K. Larkin, 1998: El Niño-Southern Oscillation sea surface temperature and wind anomalies. *Rev. of Geophys.*, **36,** 353-399.

Hoerling, M. P., A. Kumar, and M. Zhong, 1997: El Niño, La Niña, and the nonlinearity of their teleconnections. *J. Clim.*, **10**, 1769–1786.

Hoerling, M. P., A. Kumar, and T.-Y. Xu 2001a: Robustness of the nonlinear atmospheric response to opposite phases of ENSO. *J. Clim.*, **14**, 1277–1293.

Hoerling, M. P., J. W. Hurrell, and T. Xu, 2001b: Tropical origins for recent North Atlantic climate change. *Science*, **292**, 90–92.

Hoerling, M. P., J. W. Hurrell, T. Xu, G.T. Bates, and A.S. Phillips, 2004: Twentieth Century North Atlantic Climate Change. Part II: Understanding the Effect of Indian Ocean Warming. *Climate Dyn.*, **23,** 391-405.

Hoskins, B. J., and D. J. Karoly 1981: The steady linear response of a spherical atmosphere to thermal and orographic forcing, *J. Atmos. Sci*., **38**, 1179 – 1196.

Hoskins, B. J. and P. J. Valdes, 1990: On the existence of storm tracks. *J. Atmos. Sci.*, **47,** 1854-1864.

Jacob, W. J., 1967: Numerical semiprediction of monthly mean sea surface temperature. *J. Geophys. Res.*, **72,** 1681-1689.

JEDAC, cited, 2008: Joint Environmental Data Analysis Center, mixed layer depth. [Available online at http://jedac.ucsd.edu/DATA_IMAGES/index.html].

Kalnay, E. and Coauthors, 1996: The NCEP/NCAR 40-year reanalysis project. *Bull. Amer. Meteor. Soc.*, **77,** 437-471.

Kistler, R., E. Kalnay, W. Collins, S. Saha, G. White, J. Woollen, M. Chelliah, W. Ebisuzaki, M. Canamitsu, V. Kousky, H. van den Dool, R. Jenne, and M. Fiorinio, 2001: The NCEP-NCAR 50-year reanalysis: Monthly Means CD-ROM and documentation. *Bull. Amer. Met. Soc.*, **82,** 247-267.

Kraus, E. B. and S. Levitus, 1986: Annual heat fluctuations across the Tropic Circles. *J. Phys. Oceanog*, **16,** 1479-1486.

Kwon, Y. O. and C. Deser, 2007: North Pacific decadal variability in the Community Climate System Model Version 2. *J. Climate*, **20,** 2416-2433.

Lau, N. C. and M. J. Nath, 1994: A modeling study of the relative roles of tropical and extratropical SST anomalies in the variability of the global atmosphere-ocean system. *J. Climate*, **7,** 1184-1207.

Lau, N.-C. and M. J. Nath, 1996: The role of the 'atmospheric bridge' in linking tropical Pacific ENSO events to extratropical SST anomalies. *J. Climate*, **9,** 2036-2057.

Lau, N.-C. and M. J. Nath, 2001: Impact of ENSO on SST variability in the North

Pacific and North Atlantic: seasonal dependence and role of extratropical air-sea coupling. *J. Climate*, **14,** 2846-2866.

Levitus, S., 1987: Meridional Ekman heat fluxes for the world ocean and individual ocean basins. *J. Phys. Oceanog.*, **17,** 1484-1492.

Li, S., M. P. Hoerling, S. Peng, and K. M. Weickmann, 2006: The Annular Response to Tropical Pacific SST Forcing. *J. Climate*, **19**, 1802-1819.

Liu, Z. and M. A. Alexander, 2007: Atmospheric Bridge, Oceanic Tunnel and Global Climatic Teleconnections. *Rev. Geophys.*, **45,** RG2005, doi:10.1029/2005RG000172.

Luksch, U., 1996: Simulation of North Atlantic low frequency variability. *J. Climate*, **9,** 2083-2092.

Luksch, U. and H. v. Storch, 1992: Modeling the low-frequency sea surface temperature variability in the North Pacific. *J. Climate*, **5,** 893-906.

Mathieu, P.-P., R.T. Sutton, B. Dong, and M. Collins, 2004: Predictability of winter climate over the North Atlantic European region during ENSO events. *J. Climate*, **17,** 1953-1974.

Miller, A. J., D. R. Cayan, T. P. Barnett, N. E. Graham, and J. M. Oberhuber, 1994: Interdecadal variability of the Pacific Ocean: model response to observed heat flux and wind stress anomalies. *Climate Dyn.*, **10,** 287-302.

Millif, R. F., W. G. Large, J. Morzel, G. Danabasoglu, T. M. Chin, 1999: Ocean general circulation model sensitivity to forcing from scatterometer winds. *J.*

Geophys. Res., **104**, 11,337-11,358.

Namias, J., 1959: Recent seasonal interactions between North Pacific waters and the overlying atmospheric circulation. *J. Geophys. Res.*, **64,** 631-646.

Namias, J., 1965: Macroscopic association between mean monthly sea surface temperature and the overlying winds. *J. Geophys. Res.*, **70,** 2307-2318.

Namias, J., 1972: Experiments in objectively predicting some atmospheric and oceanic variables for the winter of 1971-1972. *J. Appl. Meteor.*, **11,** 1164-1174.

Park, S., M. A. Alexander, and C. Deser, 2006: The impact of cloud radiative feedback, remote ENSO forcing, and entrainment on the persistence of North Pacific sea surface temperature anomalies. *J. Climate*, **19,** 6243-6261.

Peng, S., W.A. Robinson, and S. Li, 2003: Mechanisms for the NAO responses to the North Atlantic SST tripole. *J. Climate*, **16,** 1987-2004.

Peng, S., W. A. Robinson, S. Li, and M. P. Hoerling, 2005: Tropical Atlantic SST forcing of coupled North Atlantic seasonal responses. *J. Climate*, **18,** 480-496.

Peng, S., W.A. Robinson, S. Li, and M.A. Alexander, 2006: Effects of Ekman transport on the NAO response to a tropical Atlantic SST anomaly. *J. Climate*, **19,** 4803-4818.

Pozo-Vázquez, D., M. J. Esteban-Parra, F. S. Rodrigo, and Y. Castro-Díez, 2001: The association between ENSO and winter atmospheric circulation and temperature in the North Atlantic region. *J. Climate*, **14,** 3408–3420.

Qiu, Bo, 2000: Interannual variability of the Kuroshio Extension and its impact on the

wintertime SST field. *J. Phys. Oceanogr.*, **30**, 1486-1502.

Rasmusson, E. M. and T. H. Carpenter, 1982: Variations in tropical sea surface temperature and surface wind fields associated with the Southern Oscillation/El Niño. *Mon. Wea. Rev.*, **110,** 354-384.

Rodwell, M. J., D. P. Rowell, and C. K. Folland, 1999: Oceanic forcing of the wintertime North Atlantic Oscillation and European climate. *Nature*, **398,** 320-323.

Sardeshmukh, P. D., G. P. Compo, and C. Penland, 2000: Changes of probability associated with El Niño, *J. Clim.*, **13**, 4268–4286.

Sato, O. T., P. S. Polito, and W. T. Liu, 2002: Intradecadal variability in the Ekman heat flux from scatterometer winds. *Geophys. Res. Lett.*, **29,** 1831, doi:10.1029/2002GL014775.

Schneider, N. and A. J. Miller, 2001: Predicting North Pacific Ocean climate. *J. Climate*, **14,** 3997-4002.

Seager, R., Y. Kushnir, N. H. Naik, M. A. Cane, and J. Miller, 2001: Wind-Driven Shifts in the Latitude of the Kuroshio–Oyashio Extension and Generation of SST Anomalies on Decadal Timescales. *J. Climate*, **14,** 4249–4265.

Seager, R., Y. Kushnir, M. Visbeck, N. Naik, J. Miller, G. Krahmann, and H. Cullen, 2000: Causes of Atlantic Ocean climate variability between 1958 and 1998. *J. Climate*, **13,** 2845-2862.

Smith, T. M., R. W. Reynolds, R. E. Livezey, and D. C. Stokes, 1996: Reconstruction of historical sea surface temperatures using empirical orthogonal functions. *J. Climate*, **9,** 1403-1420.

Sterl, A. and W. Hazeleger, 2003: Coupled variability and air-sea interaction in the South Atlantic Ocean. *Climate Dyn.*, **21,** 559-571.

Sutton, R. T., W. A. Norton, and S. P. Jewson, 2001: The North Atlantic Oscillation - what role for the ocean? *Atmosph. Sci. Let.*, **1,** 89-100.

Ting, M. and P. D. Sardeshmukh, 1993: Factors determining the extratropical response to equatorial diabatic heating anomalies. *J. Atmos. Sci.*, **50,** 907-918.

Trenberth, K. E., 1997: The Definition of El Niño. *Bull. Amer. Meteor. Soc.*, **78,** 2562-2584.

van Loon, H. and R. A. Madden, 1981: The Southern Oscillation. Part I. Global associations with pressure and temperature in northern winter. *Mon. Wea. Rev.*, **109,** 1150-1162.

van Loon, H. and J. C. Rogers, 1981: The Southern Oscillation. Part II: Associations with changes in the middle troposphere in the northern winter. *Mon. Wea. Rev.*, **109,** 1163-1168.

Venzke, S., M. R. Allen, R. T. Sutton, D. P. Rowell, 1999: The atmospheric response over the North Atlantic to decadal sea surface temperature changes. *J. Climate*, **12,** 2562-2584.

Watanabe, M. and M. Kimoto, 2000: On the Persistence of Decadal SST Anomalies in the North Atlantic. *J. Climate*, **13,** 3017-3028.

Weller, R. A. and A. J. Plueddemann, 1996: Observations of the vertical structure of the oceanic boundary layer. *J. Geophys. Res. - Oceans*, **101,** 8789-8806.

White, W., B., R. Bernstein, G. McNally, S. Pazan, and R. Dickson, 1980: The thermocline response to transient atmospheric forcing in the interior midlatitude North Pacific 1976-1978. *J. Phys. Oceanogr.*, **10,** 372-384.

White, W. B., 1995: Design of a global observing system for gyre-scale upper ocean temperature variability. *Prog. Oceanogr.*, **36,** 169-217.

Whitney, F. A. and H. J. Freeland, 1999: Variability in upper-ocean water properties in the NE Pacific Ocean. *Deep-Sea Res Pt II*, **46,** 2351-2370.

Yin, J. H. and D. S. Battisti, 2004: Why do baroclinic waves tilt poleward with height. *J. Atmos. Sci.*, **61,** 1454-1460.

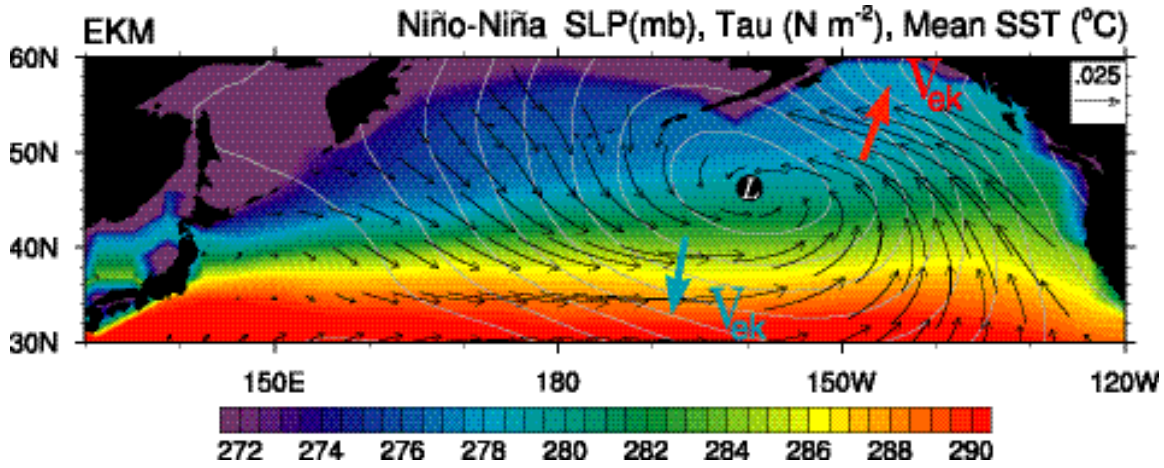

FIG. 1. The El Niño – La Niña composite of SLP (contours, interval 1 mb), surface wind stress (τ, black vectors, N m^{-2}, scale in upper right corner), and mean SST (color shading, interval 0.5 ˚C) during JFM(1) from the EKM, the model that includes Q_{ek}. Colored vectors indicate the direction of anomalous Ekman heat advection.

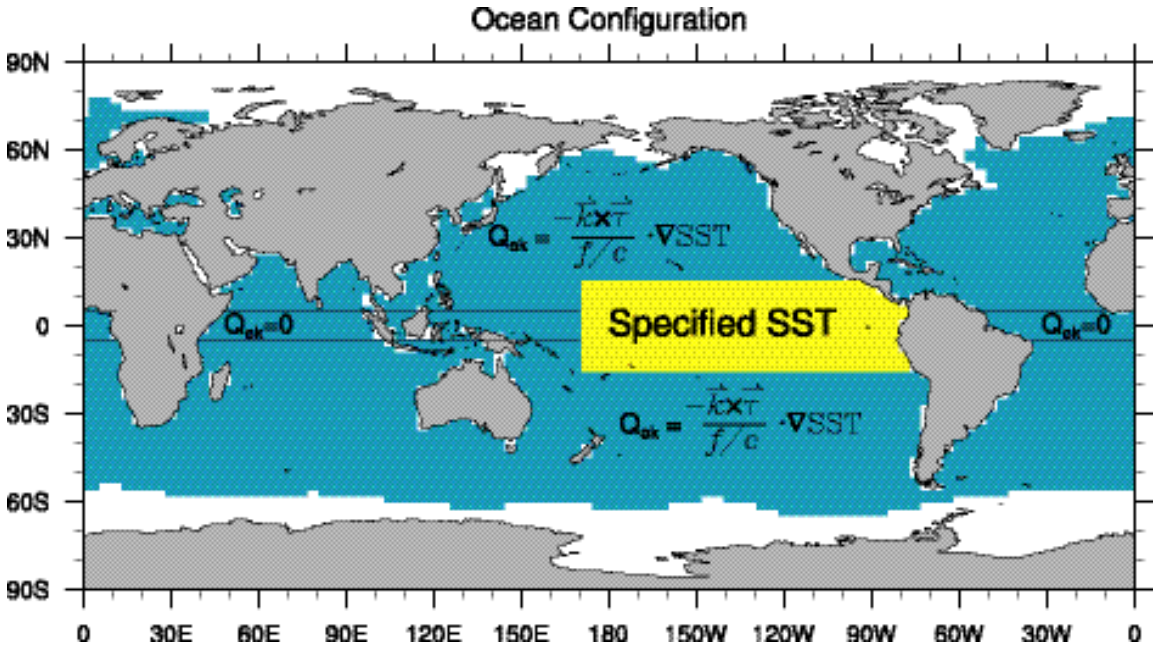

FIG. 2. Schematic of the ocean configuration for the MLM and EKM experiments. In both experiments SST anomalies are specified in the equatorial Pacific (yellow) for the years 1950-1999 and the ocean mixed layer model, MLM, is active over the remainder of the ice-free ocean (blue). Anomalous Ekman forcing is added to the MLM poleward of 5˚N-5˚S in ice-free regions of all ocean basins in the EKM simulations.

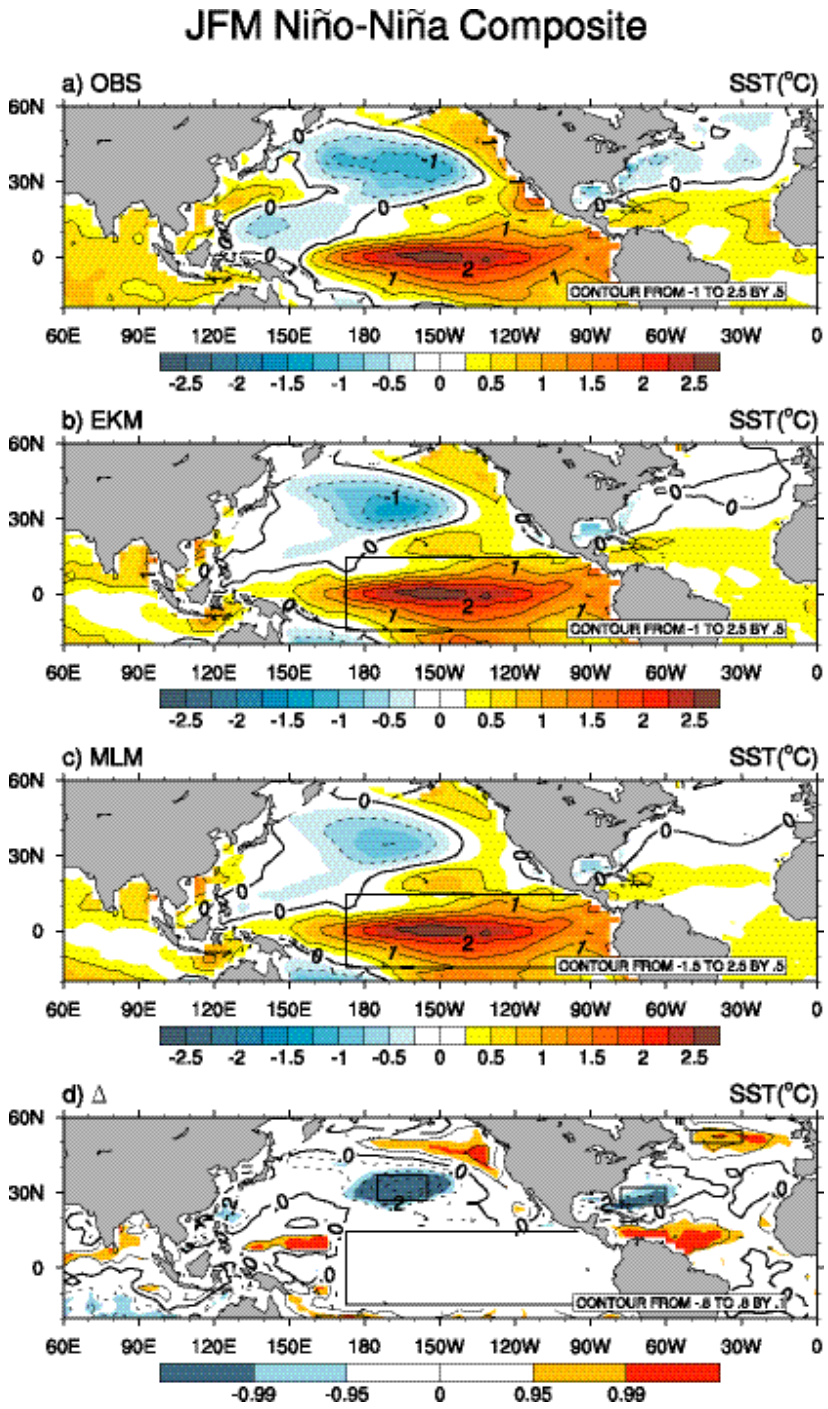

FIG. 3. The composite El Niño – La Niña (*) SST (˚C) during JFM (Yr 1) for (a) observations over 1950-1999, (b) EKM, (c) MLM, and (d) EKM-MLM (Δ). The shading (contour) interval is 0.25 (0.5) ˚C in (a)-(c). The shading in (d) indicates where the t-test exceeds the 95% and 99% confidence levels for ΔSST (contour interval 0.1˚C). The large box in (b)-(d) indicates the region of prescribed SST forcing and the smaller boxes in (d) indicate the regions used in Fig. 8.

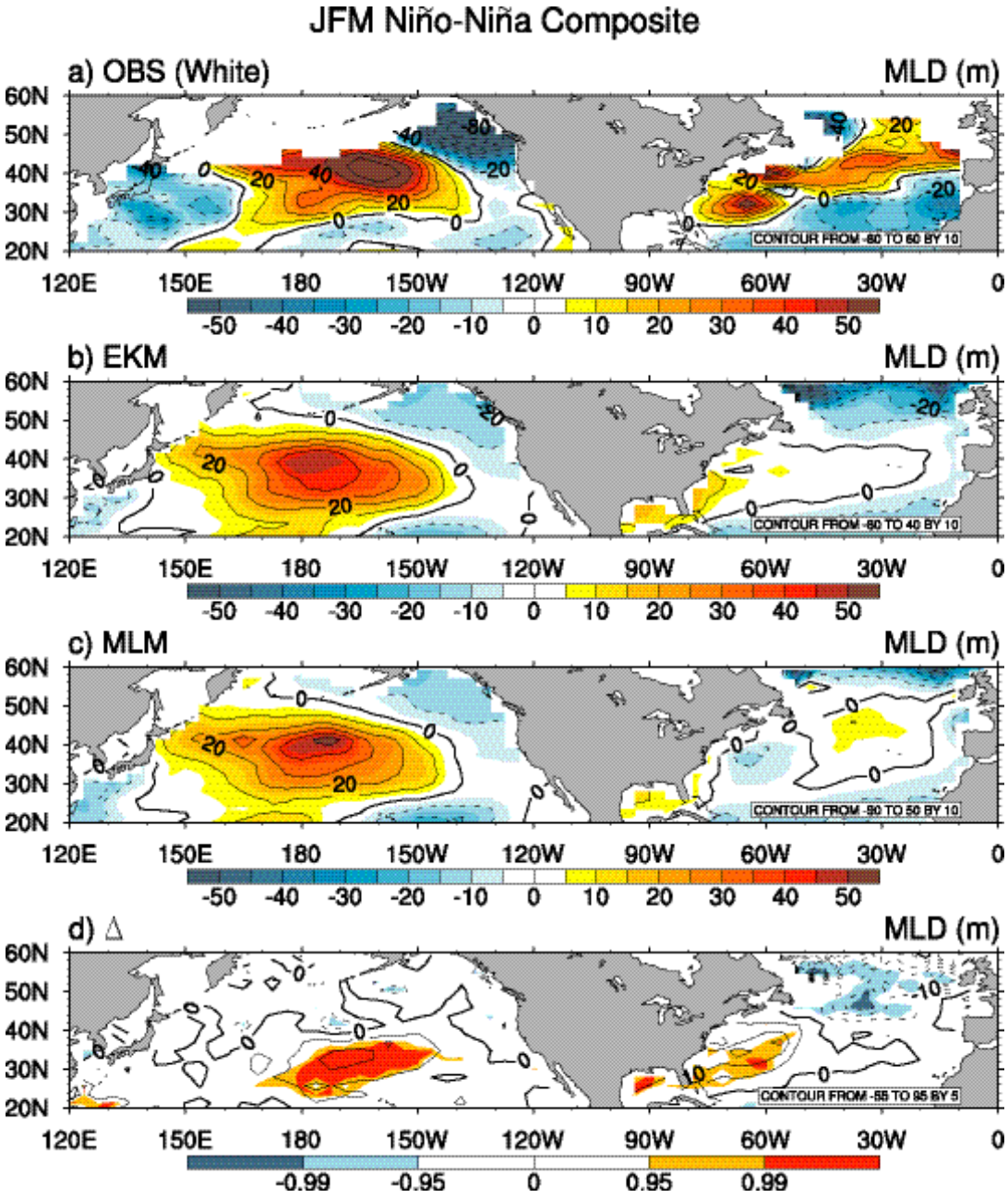

FIG. 4. MLD* (m) during JFM(1) for (a) observations (1956-1999), (b) EKM, (c) MLM, and (d) Δ. The shading (contour) interval is 5 (10) m in (a)-(c). In panel (d), the shading indicates 95% and 99% confidence limits for the ΔMLD (contour interval 5 m).

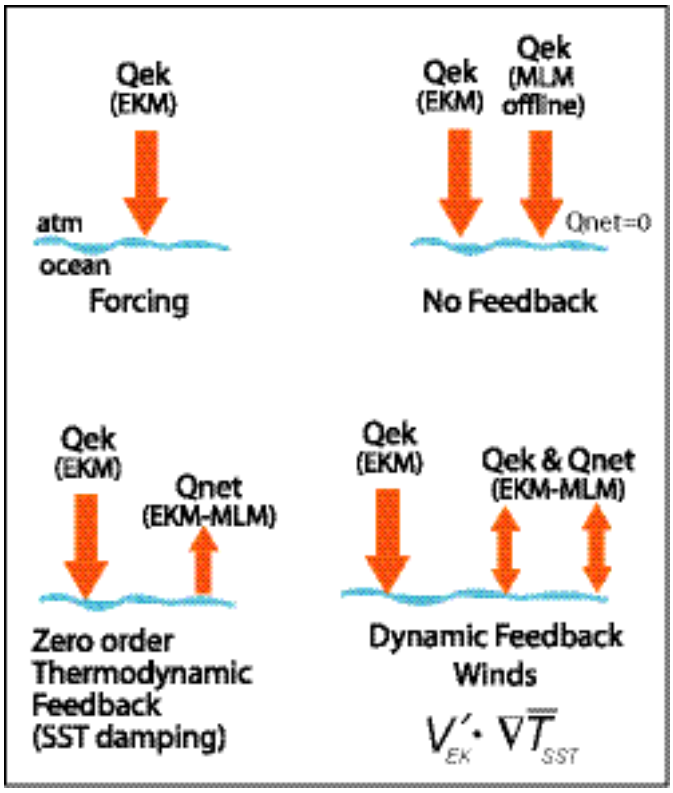

FIG. 5. Schematic for the possible types of air-sea interaction in the EKM and MLM experiments.

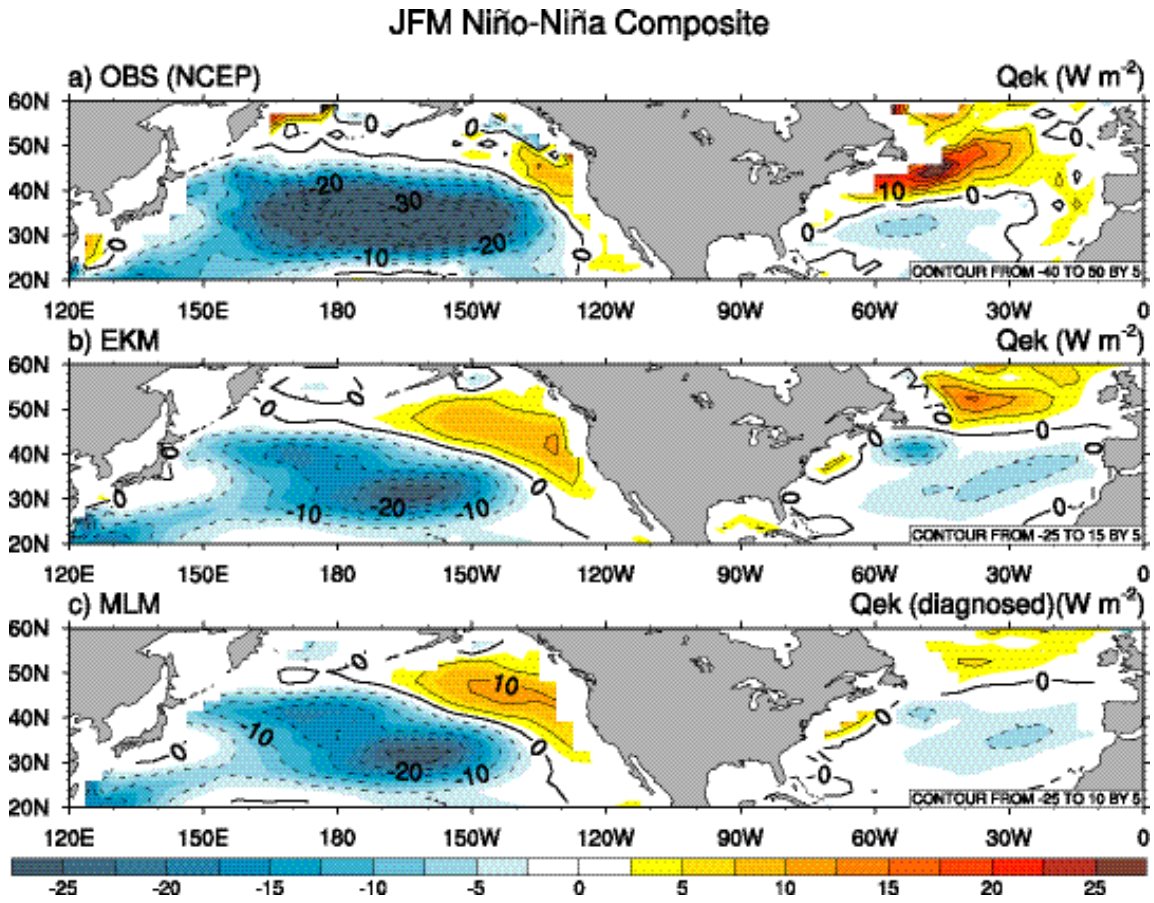

FIG. 6. El Niño-La Niña (Q_{ek}^{*} Wm^{-2}) during JFM(1) for (a) NCEP reanalysis, (b) EKM and (c) MLM (diagnosed from archived values of the winds and SSTs but does not impact the ocean model). The shading (contour) interval is 2.5 (5) Wm^{-2}.

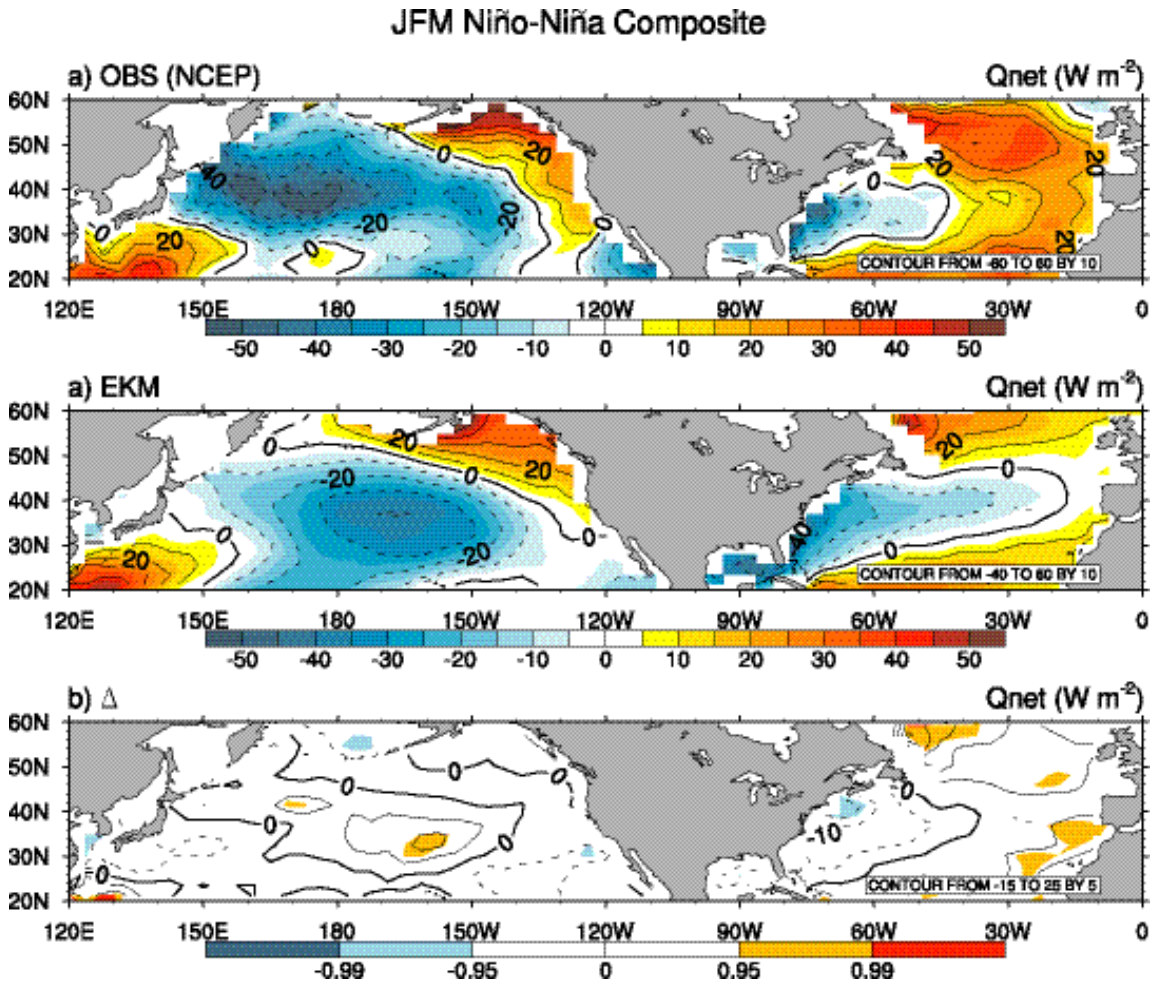

FIG. 7. El Niño-La Niña net surface heat flux (Q^*_{net} in W m^{-2}) during JFM(1) for (a)NCEP reanalysis (a) EKM, and (c) EKM-MLM(Δ). The shading (contour) interval in (a) is 5 (10) Wm^{-2}. In panel (b), the shading indicates 95% and 99% confidence limits for the ΔQ_{net} (contour interval 5 W m^{-2}). Positive values indicate ocean warming.

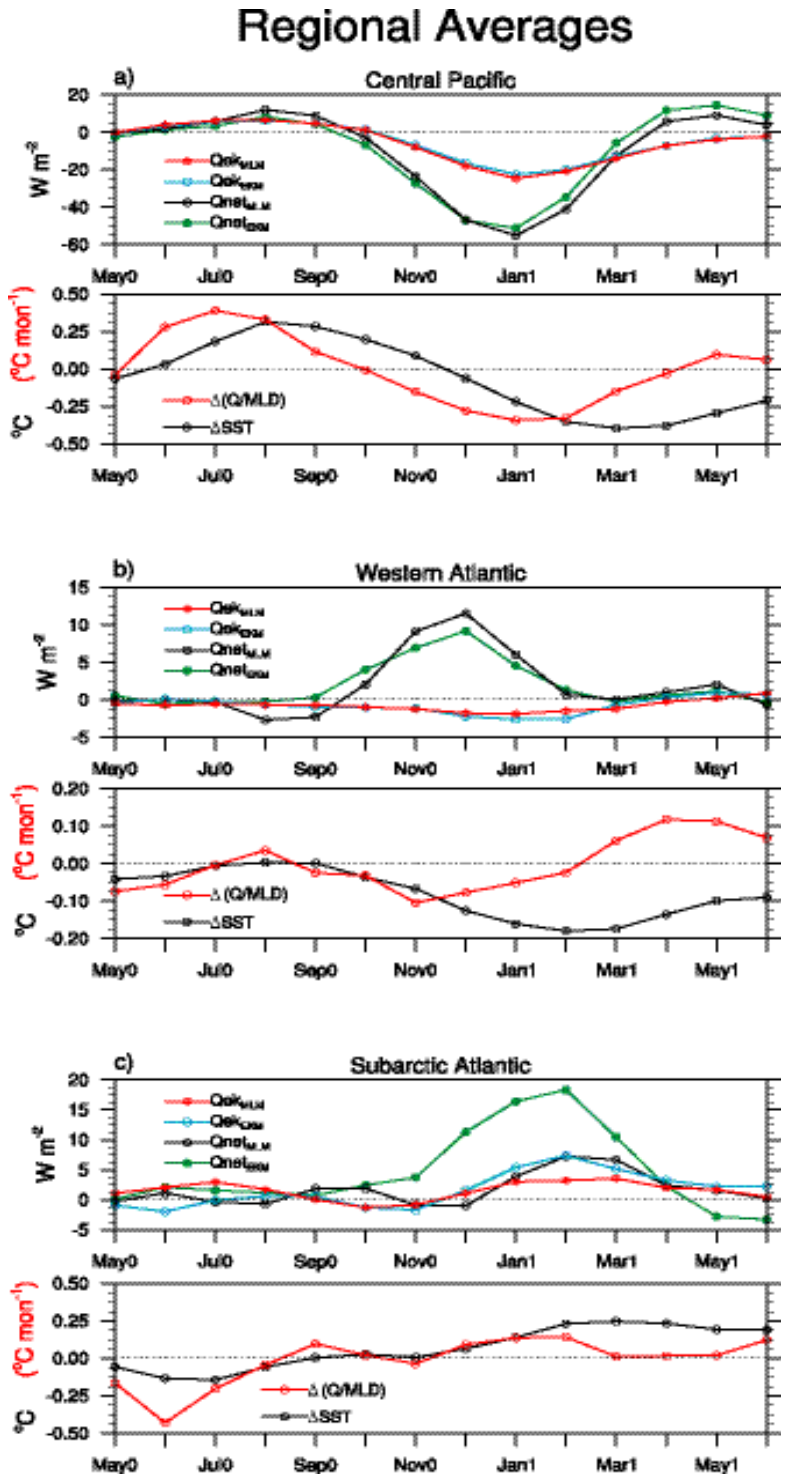

FIG. 8. El Niño – La Niña composite evolution for the (a) central Pacific, (b), western Atlantic, and (c) subarctic Atlantic regions (see FIG. 3d for locations). The top panel for each region shows Q^*_{ek} (W m^{-2}) from the MLM (red) and EKM (blue) and Q^*_{net} (Wm^{-2}) from the MLM (black) and EKM (green). The bottom panel for each region shows ΔQ/MLD (red; ˚C) and ΔSST (black; ˚C). Note the reduced scale in (b).

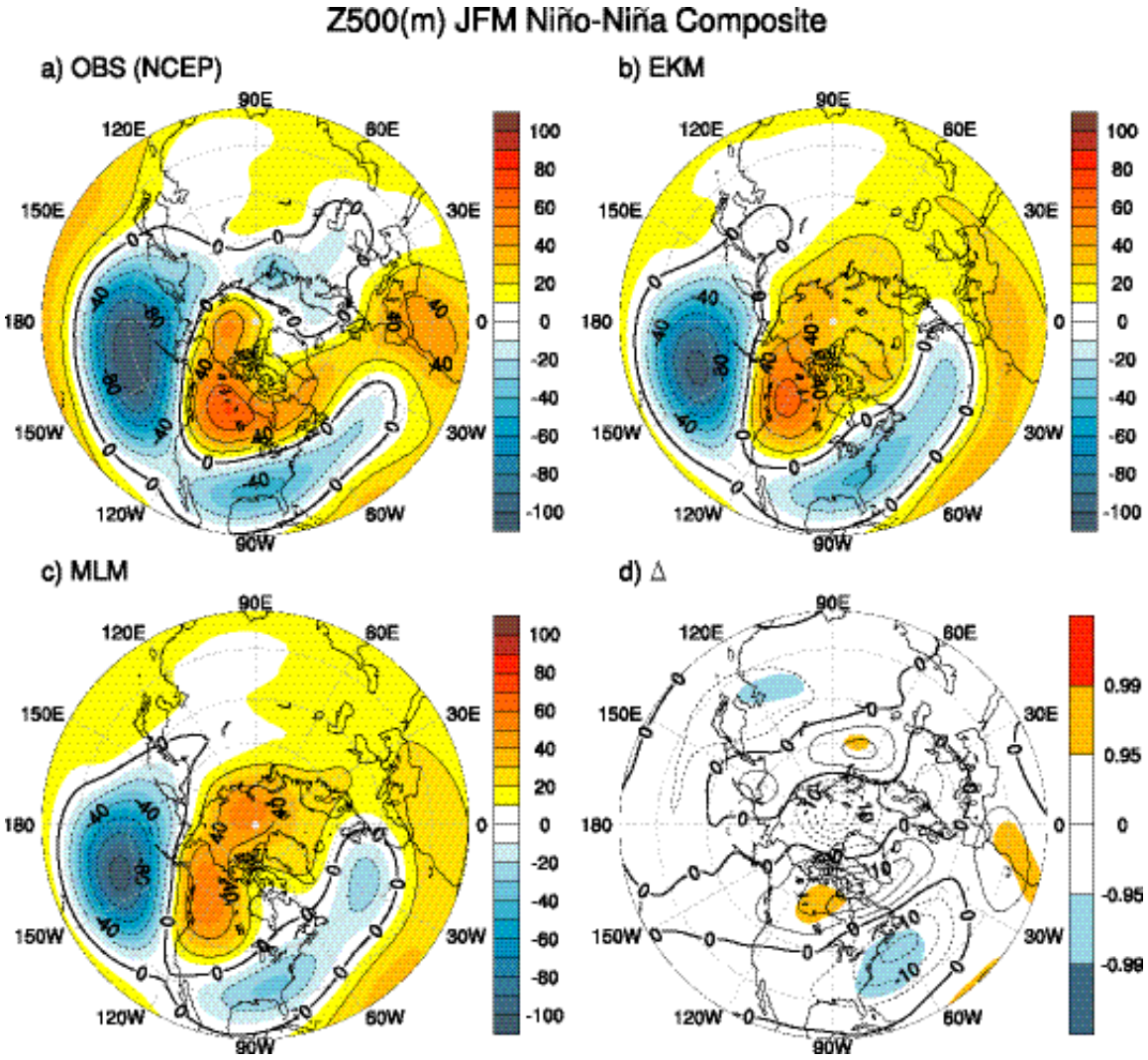

FIG. 9. The El Niño – La Niña composite of Z500 (m) during JFM(1) for (a) observed (1950-1999), (b) EKM, (c) MLM, and (d) Δ. The shading (contour) interval is 5 (10) m in (a)-(c). In panel (d), the shading indicates 95% and 99% confidence limits for the ΔZ500 (contour interval 5 m).

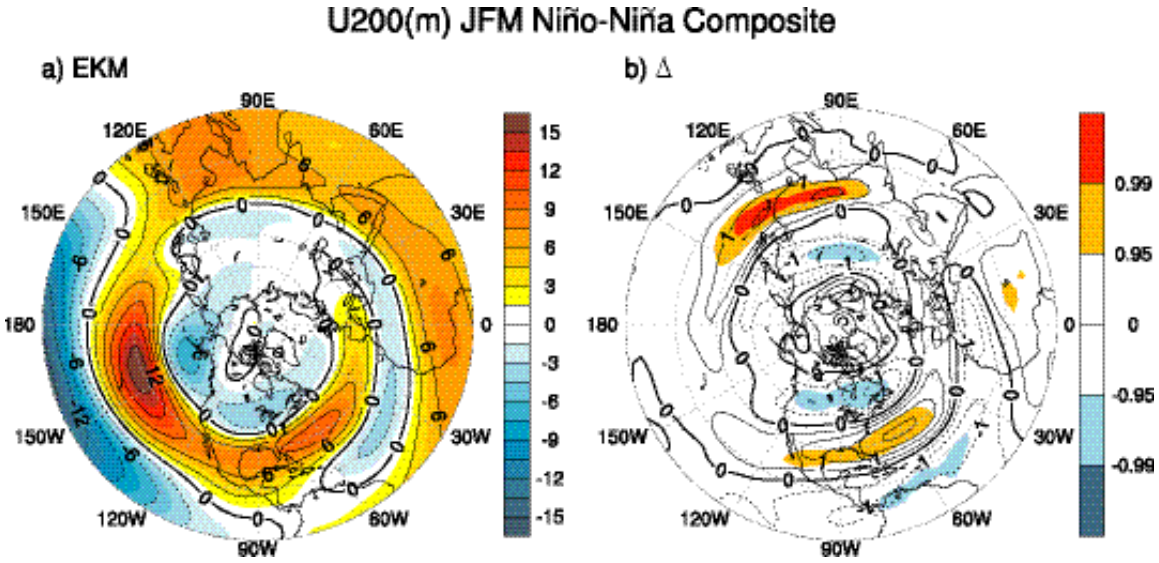

FIG. 10. The El Niño – La Niña composite of U200 (ms^{-1}) during JFM(1) for (a) EKM, and (b) Δ. The shading (contour) interval in (a) is 1.5 (3) ms^{-1}. In panel (b), the shading indicates 95% and 99% confidence limits for the ΔU200 (contour interval 0.5 ms^{-1}).

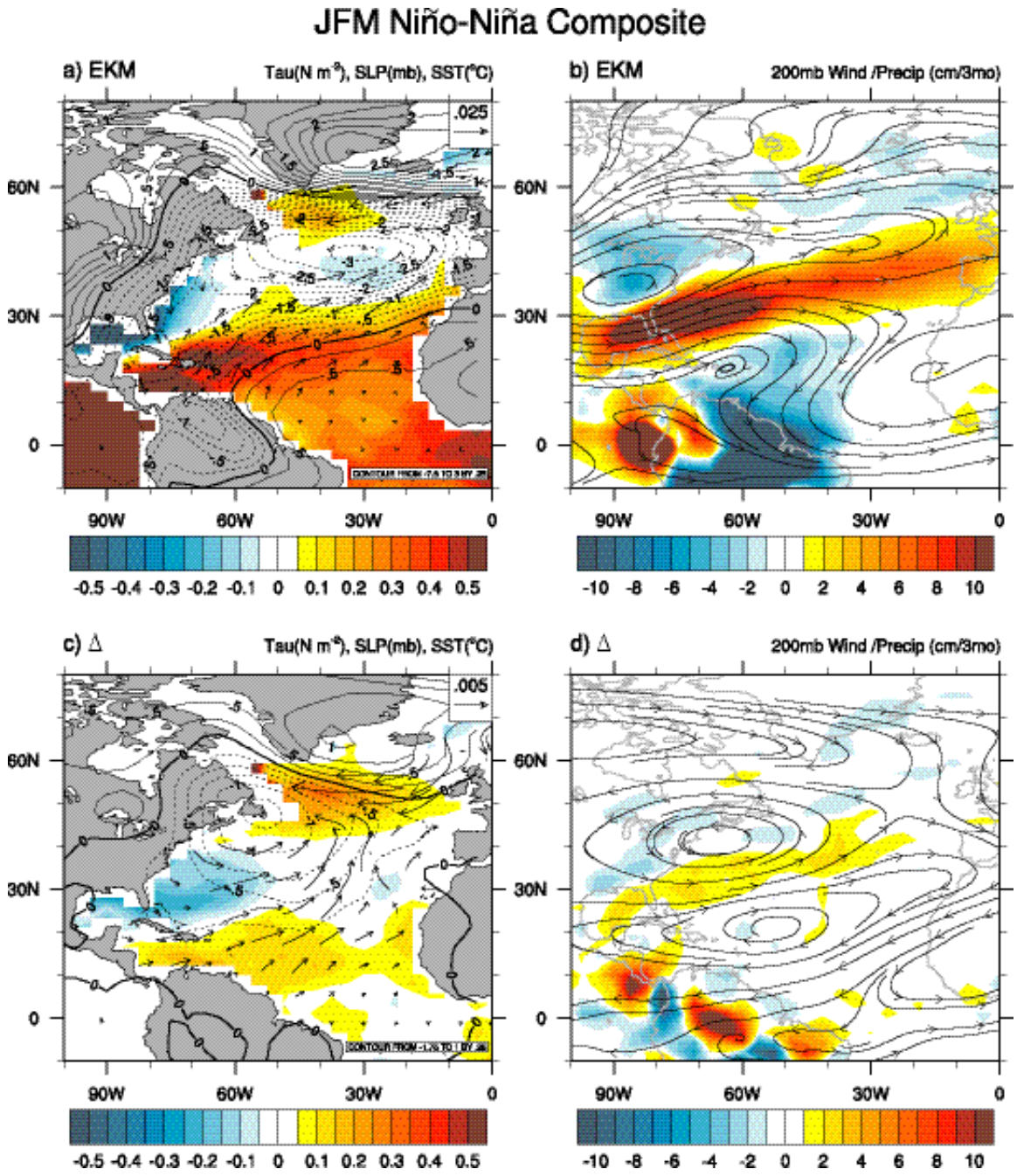

FIG. 11. The El Niño – La Niña composite during JFM(1) for (a) EKM SLP (contour interval 0.25 mb), SST (shading interval 0.05˚C), and surface wind stress (τ, black vectors, N m^{-2}, scale upper right corner), (b) EKM 200mb streamlines and precipiatation (P, shading interval 1 cm/3mo), (c) ΔSLP (contour interval 0.25 mb), ΔSST (shading interval 0.05 ˚K), and $\Delta\tau$ (vectors, N m^{-2}), and (d) 200mb streamlines and ΔP (shading interval 1 cm/3mo).

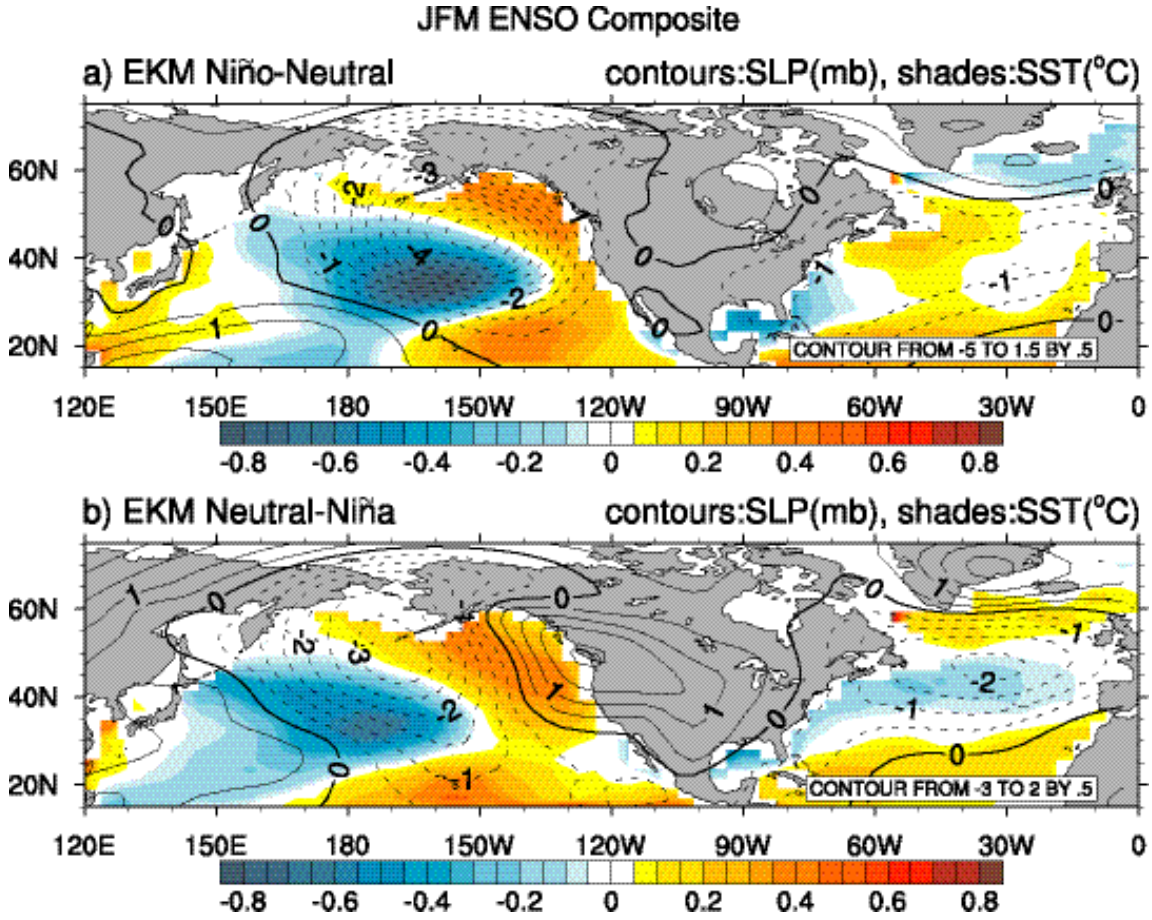

FIG. 12. The EKM a) El Niño – Neutral and b) La Niña – Neutral composites during JFM(1) of SLP (contour interval 0.5 mb) and SST (shading interval 0.05˚C). The La Niña signal was multiplied by -1 to facilitate the comparison with the El Niño composite.